Front. Mater. Sci. 2022, 16(3): 220604
https://doi.org/10.1007/s11706-022-0604-x

REVIEW ARTICLE

Strategies to assemble therapeutic and imaging molecules into inorganic nanocarriers

Sheikh Tanzina HAQUE[1], Mark M. BANASZAK HOLL[2], and Ezharul Hoque CHOWDHURY (✉)[1,3]

1 Jeffrey Cheah School of Medicine and Health Sciences, Monash University Malaysia, Jalan Lagoon Selatan, Bandar Sunway, 47500 Subang Jaya, Selangor, Malaysia
2 Department of Chemical and Biological Engineering, Monash University, Clayton, Victoria 3800, Australia
3 Health and Wellbeing Cluster, Global Asia in the 21st Century (GA21) Platform, Jeffrey Cheah School of Medicine and Health Sciences, Monash University Malaysia, Jalan Lagoon Selatan, Bandar Sunway, 47500 Subang Jaya, Selangor, Malaysia

ABSTRACT: Inorganic nanocarriers are potent candidates for delivering conventional anticancer drugs, nucleic acid-based therapeutics, and imaging agents, influencing their blood half-lives, tumor targetability, and bioactivity. In addition to the high surface area-to-volume ratio, they exhibit excellent scalability in synthesis, controllable shape and size, facile surface modification, inertness, stability, and unique optical and magnetic properties. However, only a limited number of inorganic nanocarriers have been so far approved for clinical applications due to burst drug release, poor target specificity, and toxicity. To overcome these barriers, understanding the principles involved in loading therapeutic and imaging molecules into these nanoparticles (NPs) and the strategies employed in enhancing sustainability and targetability of the resultant complexes and ensuring the release of the payloads in extracellular and intracellular compartments of the target site is of paramount importance. Therefore, we will shed light on various loading mechanisms harnessed for different inorganic NPs, particularly involving physical entrapment into porous/hollow nanostructures, ionic interactions with native and surface-modified NPs, covalent bonding to surface-functionalized nanomaterials, hydrophobic binding, affinity-based interactions, and intercalation through co-precipitation or anion exchange reaction.

KEYWORDS: inorganic nanoparticle; cancer; ionic interaction; covalent bonding; affinity interaction; intercalation

Contents

Received February 23, 2022; accepted April 17, 2022

E-mail: md.ezharul.hoque@monash.edu

1 Introduction

Chemotherapy, the most common cancer treatment paradigm, is not only effective against metastatic lesions but also causes adverse effects on rapidly growing healthy tissues. Researchers have dedicated significant efforts to improve the limitations of cancer chemotherapeutics, including short half-life, broad tissue distribution and lack of targetability [1], responsible for weak therapeutic (anticancer) activities and significant adverse effects. In addition, these drawbacks necessitate the administration of large quantities of drugs to achieve the desired therapeutic efficacy, which is not cost-effective and often renders undesired toxic effects on healthy tissues [2]. The dose-limiting solubility of chemotherapeutic drugs presents a challenge. Oral and intravenous drug delivery are the two most prevalent methods. These approaches do, however, have some drawbacks. For instance, oral administration of these drugs can disrupt pharmacokinetics due to their interaction with metabolic pathways in the body [3]. Consequently, higher pharmacological dosages may be utilized than necessary, which can lead to greater toxicity [4]. Usually, the formulation of hydrophobic drugs requires the use of solvents (due to their poor solubility), which intensifies their toxic effects [5]. For optimal drug concentrations in the bloodstream and adequate pharmacological effects, the solubility of the drug is critical [6]. For example, the oral administration of poorly water-soluble drugs requires substantial doses to achieve therapeutic plasma levels. The discovery and development of drugs are affected by their low aqueous solubility. Any drug that needs to be absorbed by the body must be in an aqueous form to ensure complete absorption. Traditional intravenous (i.v.) routes come with their own set of difficulties. Some traditional i.v. drugs have low specificity. This non-specific drug distribution

restricts the therapeutic effects within cancer cells while causing considerable toxicity in healthy cells, tissues, and organs, resulting in a variety of negative side effects, including hair loss, weakness, nausea, vomiting, and organ dysfunction, all of which contribute to cancer patients' poor quality of life [6]. Moreover, the multidrug resistance-associated protein (MRP) or P-glycoprotein (P-gp) overexpressed in cancer cells' membranes provides a path for removing chemotherapeutic drugs from the cells, thereby inducing multidrug resistance (MDR) and rendering insufficient drugs in the cytosol for the desired therapeutic effect [6]. These limitations associated with chemotherapeutic drugs have led to the growing interest in using nanoparticles (NPs) as carriers for various therapeutics, including small molecule anticancer drugs, siRNA, miRNA, mRNA, plasmids, and proteins. Nanocarriers offer enhanced therapeutic efficacy as a result of their prolonged blood circulation half-life and improved biocompatibility, coupled with improved off-target distribution and higher accumulation in the tumor, thus significantly reducing the adverse effects of drugs [7]. While the too small nanocarriers (i.e., < 5 nm) are excreted by the kidneys, the larger ones (250 nm–3 μm) are often recognized by the mononuclear phagocytic system (MPS) [8–9], which activates a critical defense mechanism and eliminates the NPs from the body. The MPS in the spleen, liver and lymph nodes tend to eliminate and degrade foreign materials in the blood [10].

Inorganic NPs have attracted significant attention since their large surface area-to-volume ratio enables effective loading of the therapeutics [11]. Additionally, other distinctive characteristics of inorganic NPs, including their facile surface modification, inertness, tunable size and morphology, high stability, porosity, and ability to mitigate chemotherapy-related side effects and drug degradation, make them promising candidates to deliver therapeutic cargos for treating malignant cells [12–13]. Inorganic nanocarriers that apparently adopt some of these features are in clinical trials [14], while others are being extensively studied for their potential clinical applications. However, among the approved nanocarriers for clinical studies, only a few showed positive results due to the underexplored heterogeneity of cancer cells, which alters the uptake and localization of NPs, thereby compromising their therapeutic efficacy [14]. Moreover, the insufficient knowledge of the physiological and pathological variations in animal and human studies necessitates the careful screening of patients to determine which patients are most likely to respond to the nanotherapy. In this sense, the treatments are comparable to the therapies approved or under development to treat specific groups of patients based on biomarkers. Thus, there are substantial complexities in the biological foundations of malignancy as well as within patients, which affect the distribution and efficacy of NPs [15]. Therefore, the translational gaps between animal models and human studies [8] pose a serious problem to drug delivery systems in targeted therapies [15].

Inorganic NPs as drug carriers have benefits over organic nanocarriers. Listed below are some of the advantages of inorganic NPs:

• **Surface modification:** Most modifications applied to inorganic NPs offer protection to biomolecules against enzymic degradation. This is true even for modifications involving sodium chloride [16]. For example, layered double hydroxide (LDH) NPs was found to progressively dissolve in a slightly acidic compartment (pH = 4.5–6.0) [17–18]. The disintegration of LDH NPs might raise the pH, causing subsequent dissolution to be slowed. This allows for the controlled release of DNA and other biomolecules into the cell. Surface modification options for inorganic nanocarriers are more diverse than those for organic nanocarriers. A variety of methods for combining therapeutic agents with inorganic NPs have been explored owing to the easy surface functionalization and distinct physicochemical characteristics. To enable responsive release, therapeutic agents most commonly bind to inorganic NPs via hydrophobic and covalent interaction with particular functional groups that can be cleaved by enzymes or other stimuli [19].

• **Stability:** The majority of inorganic NPs exhibit chemical stability, with LDHs being the exception [17]. This is an excellent characteristic since it ensures that their physicochemical properties remain unaltered throughout the delivery of the therapeutics to the target site. As long as the NPs have high chemical stability, they will not degrade in the human plasma and cytoplasm. Consequently, these NPs will either build up in cells, circulate in the blood, or be metabolised [17]. The stability and extended circulation time of inorganic NPs in the blood can be increased by modifying their surfaces with polymers, like polyethylene glycol (PEG) [20]. Additionally, antibodies, ligands, and other molecules can also be attached to inorganic NP surfaces for active targeting [21]. Targeted delivery of inorganic nanocarriers can maximize their therapeutic effectiveness based on

prolonged circulation time in blood and active targeting of nanocarriers. Furthermore, numerous approaches have been applied to inorganic nanocarriers for the release of drugs triggered by external stimuli [22–23]. In contrast, organic NPs, such as polymeric micelles, are prone to distortion and disassembly as a result of severe dilutions by blood following intravenous injection of the micellar solution, potentially causing leakage and subsequent discharge of loaded drugs. Currently, this limitation can be addressed by chemical conjugation or cross-linking of the micelles' shell to improve drug-polymer interactions [24–25]. Moreover, the stability of organic NPs decreases at high temperatures [26]. These suggest that inorganic NPs are a better option to treat cancer.

• **Toxicity:** The biocompatibility and low cytotoxicity of inorganic NPs make them excellent delivery vehicles. Biocompatible inorganic NPs include Au (1–100 nm), carbon nanotube (CNT; 1–100 nm), LDH (30–200 nm), and Fe_3O_4 (1–50 nm) [17]. Their LD_{50} (or LD_{80}) is incredibly high at a concentration of around 1 $mg \cdot mL^{-1}$ compared to cationic organic carriers (10 $\mu g \cdot mL^{-1}$) which display LD_{50} (or LD_{80}) at around 10 $\mu g \cdot mL^{-1}$ concentration [17]. Researchers found that lactoferrin, ceruloplasmin, pullulan, dextran, and albumin-modified magnetite NPs [27–29] adhere strongly to human fibroblast cells and prevent their internalization into the cells, thereby enhancing cell viability. As a result, appropriate modifications on inorganic NPs can restore cell viability to normal levels. Most organic polymeric NPs are composed of polymers such as polystyrene (PS), polymethyl methacrylate (PMMA), and polyacrylamide (PAA), which are non-biodegradable [30]. As a result of difficulty excreting these polymeric NPs from the systemic circulation, they tend to accumulate in the body and cause toxicity. Liposomes can induce toxicity based on their composition, average diameter, or surface potential. Cationic liposomes, for instance, can interact with serum proteins, lipoproteins, and the extracellular matrix (ECM), causing aggregate formation and releasing the drug cargo prior to reaching the target site, thus causing severe undesirable toxicity due to their off-target interactions with different tissues in the body [31]. In one study, it was shown that zoledronic acid (ZOL) encapsulated in PEGylated liposomes caused undesired toxicity *in vivo* [32].

• **Optical and magnetic properties:** Some inorganic nanocarriers have imaging, magnetic and optical properties, making them ideal for cancer treatment. It was reported that pure antibody-conjugated iron oxide NPs (10 nm core size) targeted the epidermal growth factor receptor deletion mutant vIII (EGFRvIII) in glioblastoma multiforme (GBM) cells for targeted therapy and to enhance magnetic resonance imaging (MRI) contrast in experimental glioblastoma. After treatment with the nanocarrier, the glioblastoma cell survival was significantly reduced. Moreover, the human astrocytes showed no toxicity on treatment with the NP conjugate. The MRI-guided convection-enhanced delivery (CED) of magnetic NPs was found to elevate the survival rates in tumorigenic glioblastoma xenografts (U87DeltaEGFRvIII) [33]. Using anti-EGFR antibodies-conjugated Au NPs, another study was conducted to explore the optical and electronic properties of Au NPs for biological imaging. Images were obtained under white-light illumination using a conventional microscope under optimum surface plasmon scattering conditions, which yielded colored images of the Au NPs on dark background [34]. Additionally, inorganic NPs exhibit a higher quantum yield, a longer shelf life, and excellent photostability than organic NPs [35].

Apart from the complex biological system, the accumulation of chemotherapeutic drugs at desirable therapeutic quantities in metastatic tumors depends on their interactions with the carrier, influencing the stability of the resultant complex in the biological system before reaching the target site and the subsequent release of the therapeutic payloads from it. Therefore, it is crucial to understand the different approaches to loading or encapsulating therapeutics and imaging molecules into inorganic nano-carrier for maximizing drug loading efficacy, prolonging the plasma half-life of the drug and enhancing its distribution and delivery at the target site. Drug loading into the NPs can change the size, morphology, and surface property of the complex, and thus its pharmacokinetics, with effects on plasma clearance and tumor targeting. In addition, drug release from the nanocarrier in the target site could depend on the various strategies used to assemble the drugs into the particle. These emerging topics need to be addressed to achieve a milestone for the clinical translation of inorganic nano-carriers in precision cancer therapies. This review focuses on various loading mechanisms harnessed for different inorganic NPs, particularly involving physical entrapment into porous/hollow nanostructures, ionic interactions with native and surface-modified NPs, covalent bonding to surface-functionalized nanomaterials, hydrophobic binding, affinity-based interactions, and

intercalation through co-precipitation or anion exchange reaction.

2 Principles involved in loading of therapeutic and imaging molecules into inorganic NPs

Various strategies and interactions are employed to load therapeutics and imaging agents in different types of inorganic NPs, modulating the pharmacokinetic profiles of the loaded molecules by increasing their solubility, stability and blood circulation time (plasma half-life). The major classes of the interactions include:

- Entrapment or encapsulation of small molecule drugs
- Affinity interaction
- Intercalation via co-precipitation or anion-exchange reaction
- Covalent bond linkages
- Ionic interaction

Figure 1 highlights the different strategies undertaken to load drugs into inorganic NPs.

3 Accommodation of small molecule drugs inside the cavity of porous nanomaterials

The design of chemically stable nanocarriers to protect encapsulated drugs during their transport to the target site is of prime importance. The strength and nature of NP-drug interactions also influence the pace at which a drug is released. In addition, stimuli-responsive linkers or surface-functionalized pores, which attach drugs to their cores, can be used to modify release rates [36]. Pore engineering facilitates the generation of defined porous structures capable of encasing drugs with a defined chemical structure. Mostly, mesoporous silica nanoparticles (MSNs), porous calcium phosphate (CaP), and calcium carbonate ($CaCO_3$), hollow manganese oxide (HMnO) and hollow gold nanoparticles (HGNPs) are gaining interest as drug encapsulated nanocarrier systems. Importantly, for porous nanomaterials, the cavity structure's design and synthesis are crucial for their functionalization, as they help regulate mutual atom–molecule and molecule–molecule interactions, thermal/statistical forces between atoms and molecules, and harmonize the actions of atom or molecules within and between the cavity units.

3.1 MSNs

The ability of MSNs to encapsulate nucleic acids and drugs is due to their unique porous structure, large internal and external surface area, increased pore volume, tunable pore diameter, flexible surface modification, negligible toxicity, excellent biocompatibility, and narrow size-distribution [37]. Selective surface functionalization of MSNs enables them to achieve particular drug interactions, which in turn allows them to control the release of drugs [38]. In most cases, these are the leading factors in determining the type and quantity of drugs eligible for delivery by MSNs. As a precaution against premature releases, the pore size range for therapeutic drugs must be defined [39]. Conversely, mesoscale channels can prevent drugs from crystallizing, thereby enhancing their release [40]. Ideally, the ratio between pore diameter and molecular drug size must be more than 1 for optimal drug loading. Due to increased diffusion, the loading rate of the drug increases as this ratio rises [39]. The size of the pores can be modified by adjusting the concentration of surfactants. The pore size of MSNs is influenced by the parameters of the experiment, such as concentration of catalyst, silica precursor, and temperature/time of reaction [41]. Furthermore, differing pore geometries, whether two-dimensional (2D) or three-dimensional (3D) structures, have a notable effect on drug loading and release. The large surface area of mesopores can affect interactions between particles and their surroundings *in vivo*. Further, MSNs can speed up epinephrine oxidation, resulting in reactive oxygen species (ROS) on the pores' surface. Consequently, mesoporous structures with increased porosity are less toxic [42–43]. Importantly, the encapsulation of drugs in MSNs through surface loading, matrix loading, and cavity loading mechanisms [44] is not yet achieved by other particle formulations. The release of the payloads from MSNs can be initiated by a cap structure that only opens in response to external stimuli [45] and can be regulated using the "gatekeeper" strategy or modifying the pores' inner surface to control the binding affinity of drugs (Fig. 2) [46]. Figure 2 depicts a diagrammatic representation of various MSN drug delivery approaches.

In the targeted MSNs drug delivery, premature drug release presents a significant challenge [47]. The most typical drug loading approach is adsorption of the drug to the pores, followed by drug dissolution, which releases the cargo at the desired location. In this regard, several

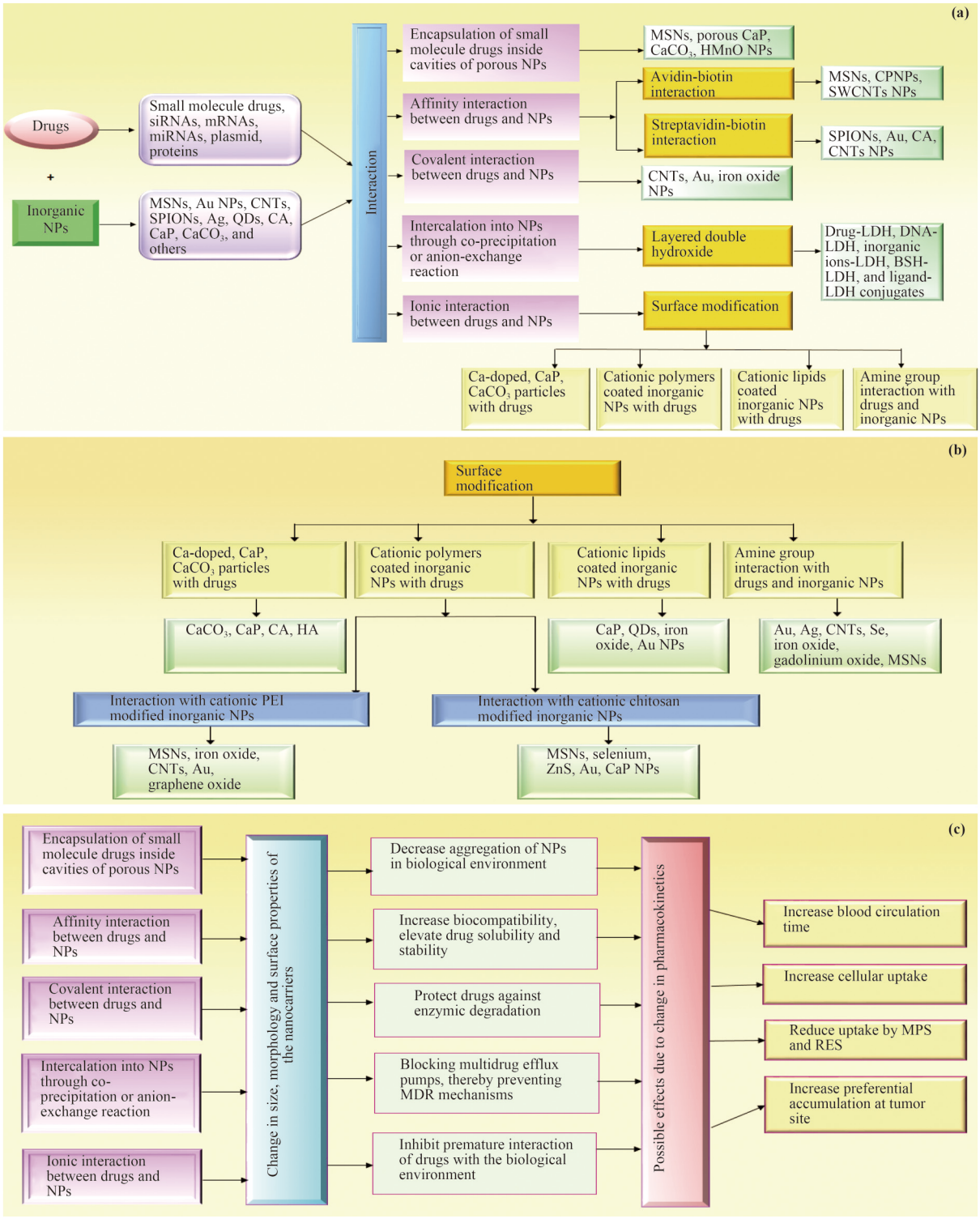

Fig. 1 (**a**) Schematic illustration of different strategies to assemble therapeutics and imaging molecules into inorganic NPs. (**b**) Different surface modification approaches between inorganic NPs and drugs. (**c**) Change in size, morphologies, and surface properties of the inorganic nanocarriers due to their interaction (via different approaches) with drugs, highlighting their possible effect on pharmacokinetics. Note: Ag, silver; Au, gold; CA, carbonate apatite; $CaCO_3$, calcium carbonate; CaP, calcium phosphate; CNT, carbon nanotube; CPNP, calcium phosphosilicate nanoparticle; HA, hydroxyapatite; HMnO, hollow manganese oxide; LDH, layered double hydroxide; MDR, multidrug resistance; MPS, mononuclear phagocytic system; MSN, mesoporous silica nanoparticle; QD, quantum dot; RES, reticuloendothelial system; SPION, superparamagnetic iron oxide nanoparticle; SWCNT, single-wall carbon nanotube; ZnS, zinc sulfide.

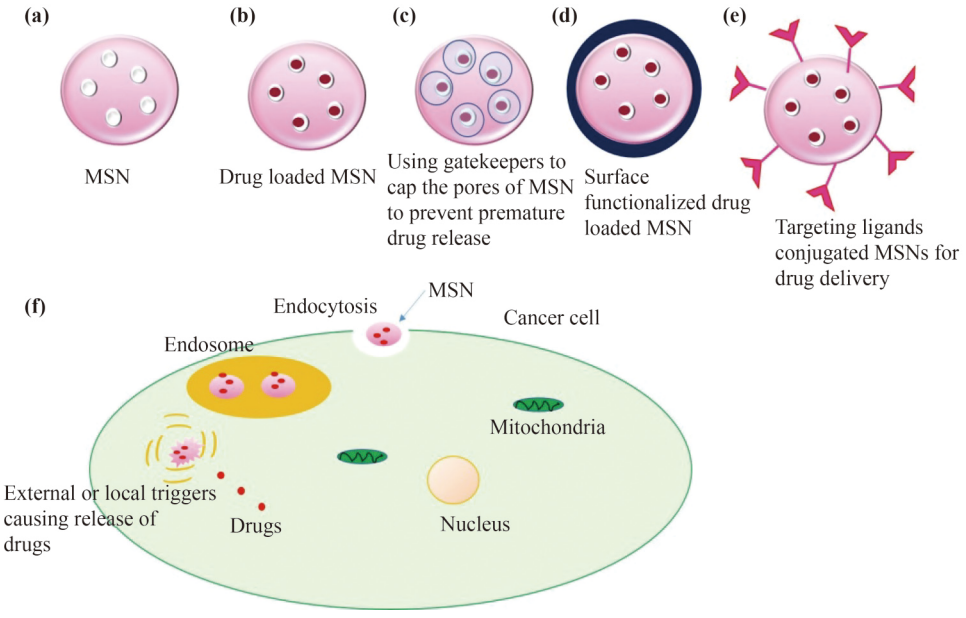

Fig. 2 Schematic illustration: (**a**) MSN; (**b**) Drug-loaded MSN; (**c**) Gatekeepers are employed to cap the pores on the MSN in order to prevent drug release prematurely; (**d**) Drug-loaded MSNs which has been surface-functionalized to decrease off-target interactions and boost site-specific characteristics; (**e**) Ligand-conjugated MSNs which can facilitate effective cellular internalization via endocytosis for the delivery of drugs at the targeted site; (**f**) MSNs enter cancer cells via endocytosis and release the drugs when triggered by external or local stimuli.

MSN drug delivery systems (DDSs) have been designed with gatekeepers of pores. Polymeric supramolecular constructs, DNA constructs, and proteins are examples of gatekeepers [48]. Various stimuli, including enzymes, photoirradiation, magnetic fields, pH, redox chemistry, and competitive binding, elicit the release of these drugs [49–50]. MSNs are mostly coated with polyethyleneimine (PEI) to cap the opening of the pores to enhance cargo retention through "molecular gatekeeping" and facilitate cellular uptake of NPs via endocytosis (Fig. 3) [51–52]. Interestingly, one research group found that functionalizing the surface of MSNs with PEI by non-covalent attachment dramatically increased the cellular uptake and formed a positively charged body for DNA or small interfering RNA (siRNA) to bind. It was observed that coating with 10 kD PEI effectively knocked down green fluorescent protein (GFP) expression by transducing HEPA-1 cells with a siRNA [53]. Another group conjugated PEI/PEG/MSNs with Trastuzumab [an anti-human epidermal growth factor receptor 2 (anti-HER2) monoclonal antibody] to efficiently transport siRNA. The NPs had a hydrodynamic diameter of ~100 nm (with three uniform-sized core materials of MSNs) and 200 nm (non-uniform-sized core materials of MSNs). Importantly, the PEI in the formulation contributed to the positive surface charge due to its cationic nature. The PEI/PEG/MSNs/siRNA construct was successful in inducing apoptosis in HER2-positive cells *in vitro*. Consequently, multiple intravenous injections of PEI/PEG/MSNs/siRNA construct inhibited tumor development in orthotopic HCC1954 tumor-bearing mice for three weeks. When subjected to human mononuclear cells from the peripheral blood, the PEI/PEG/MSNs/siRNA construct posed low cytokine induction and biocompatibility [54]. Thus, PEI-coated MSNs could increase cellular uptake, which, in turn, could result in cancer cell apoptosis. Wang and colleagues grafted the outlets of MSN with poly(acrylic acid) (PAA) via cleavable disulfide linkages. PAA was selected as a gatekeeper to prevent drugs from entering the mesopores of MSN mainly due to its numerous advantages, including the proper molecular mass for obstructing MSN entry points, high biocompatibility, as well as the capability to extend the blood circulation period and make MSN more stable in physiological conditions. In this study, the fluorescent dye, RhB served as a model drug. RhB was found to be significantly restricted in mesopores without glutathione (GSH) or in phosphate buffer saline (PBS) at physiological pH (7.4) based on *in vitro* release kinetics. In contrast, the release of RhB was significantly increased when supplemented with GSH or in PBS at pH 5.0. Furthermore, in the simultaneous presence of GSH and PBS (pH 5.0), the

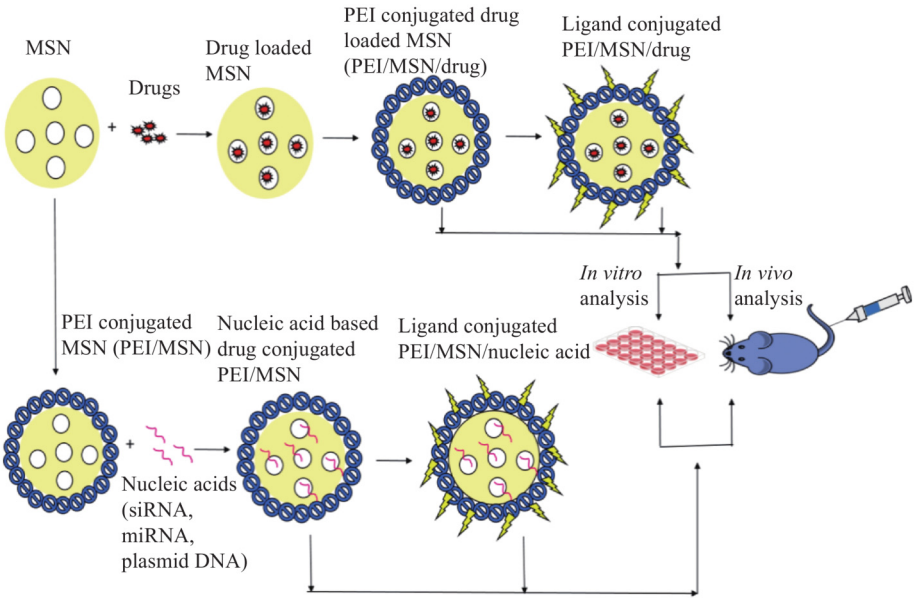

Fig. 3 Schematic representation of PEI-conjugated MSNs loaded with cargos and modified with and without ligands for *in vitro* and *in vivo* analyses.

release of RhB was enhanced even further. These findings showed that this drug delivery approach, which has dual-responsive drug release properties, might be a good choice for cancer therapy [55].

It was reported that cationic polymeric coatings could improve the transfection efficiency and DNA loading onto MSNs. In one study, the poly(amidoamine) (PAMAM) dendrimer coating on MSNs (average size 250 nm, average pore diameter 2.7 nm) allowed the cationic binding for DNA complexation. This approach ensured open pores for loading DNA. In HeLa and CHO cells, confocal fluorescence microscopy (CFM) and transmission electron microscopy (TEM) confirmed the efficient endocytosis of the dendrimer (G2)-MSN-DNA complex. The biocompatibility study validated that proliferation in HeLa cultures with and without G2-MSNs was analogous to each other, suggesting that G2-MSNs did not interfere with cell growth. Thus, MSNs were not toxic *in vitro* and served as a DNA protectant against enzymatic cleavage [56]. In another study, poly-L-arginine (n = 10 and 20) was grafted to the surface of MSNs, as reported by Kar et al. [57], to deliver drugs or plasmid DNA successfully. Surface modification of MSNs with cationic functional groups could bind with the negatively charged nucleic acids and facilitate rapid cell membrane penetration. Both MSN-p(LArg)20 and MSN-p(LArg)10 exhibited a zeta potential of (+32 ± 4) and (+20 ± 2) mV, respectively. Both particles were discrete, and a particle diameter of 17 nm (TEM and scanning electron microscopy (SEM)) and 80 nm (dynamic light scattering (DLS)) were seen for MSN-p(LArg) 20 and 76 nm (TEM and SEM) for MSN-p(LArg)10, respectively. Furthermore, the MSN-p(LArg) particles were used for the intracellular delivery of mCherry DNA plasmid in cells, leading to mCherry protein expression. The MSN-p(LArg) showed higher (85%) cell viability and increased cellular uptake (greater than 90%) with 100 μg·mL^{-1} MSN concentration in both HeLa and A549 cells. The preliminary data using doxorubicin (DOX) revealed that DOX-MSN-p(LArg) could effectively enhance the therapeutic efficacy and result in apoptosis in both HeLa and A549 cells. The MSN pores contained increased levels of DOX, which could improve the therapeutic efficacy significantly. Thus, MSN with a bigger pore size could render a more promising effect. The results with nucleic acids and drugs indicate that MSN conjugates can be important vehicles for delivering genes and drugs to cancer cells.

To develop a pH-dependent intracellular carrier for the distribution of DOX inside the nuclei of the targeted tumor cells, Zou et al. capped MSNs with gelatin (MSN@Gelatin), which was ~8 nm thick [58]. The surface charge of MSN@Gelatin was found to be electronegative (−0.226 mV). At physiological pH, the encapsulated DOX was not released due to the gelatin coating, whereas, under acidic pH, electrostatic repulsion

between the gelatin and MSN uncapped the coating and released the DOX entrapped in the MSN@Gelatin system. This system revealed DOX encapsulation efficacy as high as 47.3 $mmol \cdot g^{-1}$ SiO_2, observed by UV-Vis absorption measurements. Cellular internalization by endocytosis revealed the successful accumulation of DOX/MSN@Gelatin in the lysosomes, followed by an acid-induced uptake of DOX into the nuclei of Hep-G2 hepatoma cells. For DOX/MSN@Gelatin, a dose-dependent cytotoxicity was recorded (IC_{50} = (17.27 ± 0.63) $\mu g \cdot mL^{-1}$). On the contrary, minimal toxicity (IC_{50} > 100 $\mu g \cdot mL^{-1}$) was observed for MSN@Gelatin. In another study, mannosylated polyethylenimine (MP) was coupled with MSNs, generating MPS conjugates, used for *in vitro* plasmid DNA transfection to target macrophages containing mannose receptors. Cytotoxicity studies revealed a high percentage of viable cells for MPS/DNA complexes compared to PEI 25K (vector). The effectiveness of MPS/DNA complexes in transfecting HeLa and Raw 264.7 cell lines was enhanced via receptor-mediated endocytosis [59]. When Dox and P-gp siRNA loaded PEI-PEG-MSNs complex were examined in MCF-7/MDR tumor-bearing xenograft model, an enhanced accumulation in the tumor was observed as a result of prolonged blood circulation, leading to 80% of tumor growth suppression in comparison to free DOX (17%), MSN-DOX (62%) and P-gp siRNA (0%) [60].

Likewise, liposome-encapsulated mesoporous silica-core–shell magnetic NPs, Lipo[MNP@m-SiO_2] (negative zeta potential) was used to conjugate and deliver Trastuzumab (Lipo[MNP@m-SiO_2]-$Her2_{Ab}$) for the *in vitro* targeting of Her2/*neu*-overexpressing breast cancer cells. MRI and CFM were both used to evaluate the targetability of Lipo[MNP@m-SiO_2]-Her2Ab. In Her2/neu-positive cancer cells, Lipo[MNP@m-SiO_2]-Her2Ab was found to accumulate significantly, suggesting their potential for drug delivery and multimodal imaging *in vitro* [61]. Sun et al. showed that gadolinium (Gd)-doped MSNs loaded with DOX and conjugated with thermosensitive liposomes (TSLs) containing indocyanine green (ICG) (DOX@GdMSNs-ICG-TCLs) could serve as triple-modal imaging-guided nanoplatforms. They exhibited an average particle diameter of 233.8 nm and a surface charge of −25.2 mV. In order to prevent DOX leakage and heighten cellular uptake, DOX@GdMSNs were coated with TSLs containing folic acid (FA). In response to near-infrared (NIR) irradiation, ICG generated heat and ruptured ICG-TSLs, releasing DOX efficiently [62]. Needless to say, MSNs' potential for site-specific targeting is likely to boost cancer treatment efficacy, owing to their imaging capabilities.

3.2 $CaCO_3$ and CaP

Notably, other commonly researched nanoporous carriers include $CaCO_3$ and CaP, frequently deployed for gene delivery. $CaCO_3$ NPs, however, are more frequently exploited than CaP NPs due to their more porous structure, larger surface area, biocompatibility, pH sensitivity, and ability to load and release drugs [63–64]. Moreover, the preparation of $CaCO_3$/DNA co-precipitates does not require the addition of buffer solutions to adjust pH, whereas the synthesis of CaP/DNA co-precipitates does [65]. For instance, carboxymethyl chitosan (CMC)-modified $CaCO_3$ micro/nanospheres were used to encapsulate DOX by capillary force and electrostatic attraction between negative and positive charges of CMC and DOX, respectively. Due to the electrostatic interaction between CMC and DOX and the presence of the porous structure, the encapsulation efficiency of DOX greatly improved by more than 60% [66]. Furthermore, researchers have focused on innovative approaches to using CaP NPs as imaging platforms and drug carriers. For example, one study highlighted the encapsulation of CaP with organic molecules (~27 nm) for distribution and imaging within the cells due to their biocompatibility and pH dissolution properties in order to release therapeutic cargos in a regulated manner within the tumor [67].

3.3 HMnO and HGNPs

Another area of interest includes surface modification of inorganic NPs by cationic PEI-3,4-dihydroxy-L-phenylalanine (DOPA) conjugates for complexing therapeutics. In an attempt to facilitate tumor targeting, Bae et al. investigated the effectiveness of HMnO NPs in cancer therapy and imaging via MRI [68]. First, the positively charged HMnOs were prepared using DOPA as an adhesive moiety. Next, cationic PEI-DOPA conjugates were immobilized on HMnO NP surfaces utilizing the vital metal oxide binding affinity of DOPA, confirmed via Fourier transform infrared spectroscopy (FTIR) and X-ray photoelectron spectroscopy (XPS). To transport targeted siRNA into breast and ovarian cancer cells, NPs were conjugated on the surface with Herceptin using maleimide-PEG-succinimidyl carbonate (SC). Confocal microscopy

and MRI displayed that conjugated Herceptin could enhance the uptake of modified HMnOs in SK-BR3 cells (HER2+). This, in turn, played a vital role in detecting cancer cells using T_1-weighted MRI than those in MCF-7 (HER2−) cells, indicating that herceptin-functionalized NPs displayed targetability [68]. Similarly, one study demonstrated the development of DOX-loaded PEGylated multi-functional HGNPs (DOX-HGNPs), which released DOX and generated heat on NIR irradiation, leading to DOX and hyperthermia-induced detrimental effect on lung cancer-bearing A549 xenograft mice [69].

4 Affinity interaction

Recently, the affinity interaction (avidin/biotin or biotin/streptavidin) to load drugs in inorganic NPs has experienced a renaissance in developing suitable drug carriers. Avidin is an essential basic tetrameric glycoprotein present in the eggs of aves, reptiles, and amphibians. Biotin, commonly known as vitamin H, vitamin B7, or coenzyme R, has a ring structure that is a tetrahydrothiophene bonded to a tetrahydroimidizolone. The biotin moiety may prove useful in cancer therapeutics [37] since it is expressed in proliferating cancer cells more frequently than in normal cells [70]. The high positive charge of avidin improves the internalization of biotin-coated NPs into the cells [71–72]. In contrast, bioconjugated avidin incubation with biotinylated cell lines resulted in nearly 100% surface adherence and endocytosis efficacy [73]. Streptavidin has also been shown to accumulate *in vivo* in specific tissues [74–75], particularly in malignancies [76]. As a result, some gene therapy vectors can be targeted to specific tissues using avidin alone, while changing tissue specificity using biochemical changes to the protein. Avidin/biotin interaction has great promise in therapeutic action as it is one of the versatile, specific, and stable high-affinity interactions which is resistant to denaturing chemicals, pH, proteolytic enzymes, temperature, and harsh organic reagents [77–78]. Importantly, imaging agents and targeting ligands are often employed in avidin-NP platforms to deliver drugs to specific sites [79]. These avidin-based platforms have shown lower toxicity to normal tissues while heightened toxicity against malignancies [76]. The biotinylation of ligands or tissues *in vivo* can take advantage of the strong avidin/biotin interaction for targeted delivery [80–81]. Notably, streptavidin is the most common analog of avidin. Streptavidin (originating from *Streptomyces avidinii*) is a 56 kDa non-glycosylated tetrameric protein with an isoelectric point (pI) value of approximately 5–6 [75,82]. It should be noted that the avidin/biotin and biotin/streptavidin system exhibits strong bonds and specificity, allowing them to be modified with biotinylation reagents and biomolecules like DNA oligomers, peptides, fluorescent dyes, and antibodies. Figure 4 demonstrates the avidin/biotin and streptavidin/biotin complex formation and depicts the general interaction between them.

4.1 Superparamagnetic iron oxide nanoparticles (SPIONs)

SPIONs were well-known MRI materials noted for their excellent relaxation properties at T2 (spin–spin). Consequently, the aggregation of their highly hydrophobic surfaces, macrophage absorption, and elimination by the reticuloendothelial system (RES) limit their utilization. To address these limitations, many SPIONs-drug delivery platforms based on affinity interactions were developed. An early study revealed the formation of radiologically active nanoprobes to identify breast cancer cells in preclinical tumor models with soiTrastuzumab loaded into SPIONs through biotin–streptavidin interaction for heightened cellular labeling. In addition, this method successfully detected HER2 receptors [83]. Nevertheless, these probes utilizing the biotin-streptavidin interaction could trigger profound immunological responses in humans. Interestingly, the molecular diameter of superparamagnetic iron oxide particles used in this approach was around 50 nm (molecular weight: 40–50 MD) as stronger relaxivity and reduced molecular size could foster effective drug delivery.

Biomarkers could be pretargeted with NPs in MRI to aid a precise diagnostic approach in soft tissues *in vivo*, offering high contrast imaging with excellent spatial resolution. It was Liu's research team that modified SPIONs into magnetoliposomes with 1,2-distearoyl-sn-glycero-3-phospho-rac-glycerol sodium salt (DSPG), cholesterol, and 1,2-distearoyl-sn-glycero-3-phosphoethanol-amine-N-[biotinyl(polyethylene glycol)2000] (biotin-PEG2000-DSPE). The surface functionalization of biotin moieties enabled the study of angiogenesis in tumors via pretargeting. Liposomal bilayers and PEG modification prevented macrophage uptake of Fe_3O_4 cores. The cell toxicity assay demonstrated that the generated magnetoliposomes were superparamagnetic and biocompatible.

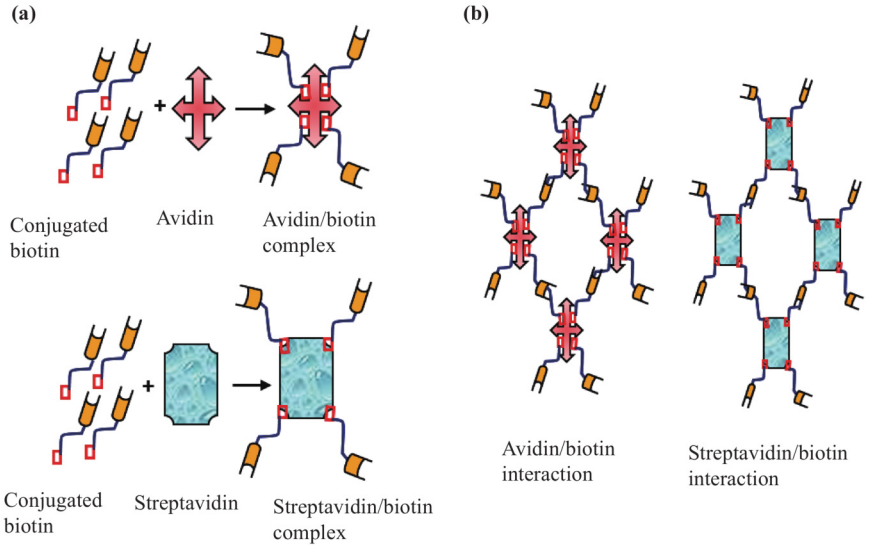

Fig. 4 (**a**) Avidin/biotin and streptavidin/biotin complex formation. For the generation of the resulting avidin/biotin and streptavidin/biotin complex, both avidin and streptavidin can bind with four conjugated biotin (biotin generally conjugated to antibody, protein, peptide, and enzyme) molecules. (**b**) Interaction between avidin/biotin and streptavidin/biotin. One avidin/biotin complex or streptavidin/biotin complex can be linked with another avidin/biotin complex or streptavidin/biotin complex via binding with the conjugated biotin.

The $\alpha_v\beta_3$-integrin, absent on inactive endothelial cells or healthy tissue, was a common hallmark of tumor neovascular endothelial cells. Following the injection of an anti-$\alpha_v\beta_3$ antibody directly into tumors, avidin and streptavidin were incorporated. This magnetoliposome was able to deliver specific anti-$\alpha_v\beta_3$ antibodies targeted at cancer cells. On administration of magnetoliposomes to the targeted group, the effector molecules were found to adhere permanently to tumor pretargeting antibodies due to the high affinity between avidin and biotin. MRI revealed a strong signal intensity surrounding the tumor, amounting to 7% of the tumor area, as opposed to only 2% improvement in the non-targeted group. According to histologic examination, the magnetoliposomes exhibited colocalization with the neovasculature, resulting in a reduction in magnetic resonance signal [84].

4.2 MSNs

Ligand-anchor binding could successfully deliver small molecule drugs with high specificity and target site discrimination [85]. Avidin was evidenced to act as a bridge between receptors and ligands (ligands could be functionally modified or unmodified) [86]. Accordingly, in one study, it was found that by tightly closing the pores of MSNs with biotin and covering MSNs with avidin, the release of cisplatin from the core of MSNs was prevented [87]. A matrix metalloproteinase 9 (MMP9) specific cleavable linker was added to the avidin-capped MSNs, which displayed site-selective drug delivery in tumors expressing high levels of MMP9. The tunable porous structure and high volume enabled the loading of drugs in these NPs. Using this technique, MMP9 was found to stimulate the release of cisplatin into human tumor cells through the MSNs, as well as in 3D lung cell cultures of mice and human lung cancers *ex vivo*. Moreover, apoptotic cell death was only detected in cisplatin-releasing MMP9-positive tumor sites in the lungs of Kras mutant mice. No toxicity was observed in non-tumorous or unaffected areas of the mice [87].

4.3 Au NPs

In another interesting study, Au NPs were synthesized using a supramolecular approach by functionalizing with β-cyclodextrins (β-CDs) and γ-cyclodextrins (γ-CDs) via streptavidin (SA)–biotin-binding [88]. Notably, by varying the cavity dimension or functionalization site, it was possible to synthesize many different CD-coated NPs. These NPs were found to be more stable than the native ones. It was observed that NP@SAγ-CD had a considerably greater DOX loading efficacy compared to NP@SAβ-CD. In contrast, adrenomedullin (ADM) loading efficiency was higher for NP@SAβ-CD. Therefore, NP@SAβ-CD was better suited to load smaller drugs (ADM) than larger drugs (DOX).

4.4 Calcium phosphosilicate nanoparticles (CPNPs)

CPNPs usually accumulate in solid tumors through enhanced permeation and retention (EPR) effects. The effectiveness of these NPs could dramatically augment when they were conjugated with fluorescent dye. ICG was introduced into the amorphous calcium phosphate matrix doped with silicate by Barth et al. to produce a novel CPNP composite (approximately 20 nm diameter) [89]. The CPNP was conjugated to biotinylated diferric transferrin (human holotransferrin), biotinylated anti-CD71 antibody (transferrin receptor-specific), and biotinylated pentagastrin using an avidin–biotin coupling. The interaction of biotinylated human holotransferrin (diferric transferrin) and biotinylated anti-CD71 antibody (anti-transferrin receptor antibody) to avidin-conjugated CPNPs (avidin-CPNPs) allowed for more precise targeting of transferrin receptors, abundant in breast cancer cells. Therefore, theranostic materials based on avidin-CPNP could be used for the treatment of breast cancer and other fast proliferating and transferrin-expressing cancerous cells [89].

4.5 Carbonate apatite (CA)

Recently, Mozar et al. utilized biotin-streptavidin interaction to prepare drug-loaded CA NPs coated with hydrophilic and electrically neutral PEG and a fibronectin-specific ligand to improve the particle drug complex's ability to target and deliver into breast cancer cells via receptor-mediated endocytosis (through the interaction of fibronectin and integrin) [90]. According to the results, the average particle diameter of CA NP is approximately 820 nm, which decreases to 615 nm for PEG-CA, and further to 402 nm for biotinylated PEG-fibronectin-CA. The surface charge of PEG-CA and PEG-fibronectin-CA were more electropositive than the CA NPs. In this study, SA served as a linker between biotinylated PEG and drug-loaded CA complexes as the CO_3^{2-} and PO_4^{3-} (negatively charged domains) bind with the Ca^{2+}-rich domain of the particles. Thus, the SA–biotin interaction facilitated the binding of drugs with the NPs [90]. The uptake of drugs by breast cancer cells was assessed using high-performance liquid chromatography (HPLC), which revealed that the cellular uptake (hydrophobic drugs) was higher for surface-modified NPs than CA and free drugs. In the cytotoxicity study, NPs with surface modifications showed greater substantial toxicity than unmodified CA NPs and free drugs. Additionally, a tumor regression study using surface-modified drug-encapsulated NPs revealed dramatic shrinkage of tumors [90]. Therefore, surface modification using affinity interactions could reduce particle size, increase cellular internalization and retention of drugs in the tumor, as well as prevent opsonization and off-target distribution.

4.6 CNTs

Using Raman-imaging immunoassays, Bajaj et al. reported a biotinylated single-wall carbon nanotube (SWCNT) (typically 0.7–1.5 nm diameter, 10 nm to several centimeters long), which could successfully detect Her2 receptors in BT-474 cells as detected by confocal Raman imaging. NeutrAvidin-fluorescein isothiocyanate (FITC) bridges were found to link the biotinylated secondary antibody and SWCNTs after the monoclonal Her-66 antibody binds to Her2 receptors. Through confocal Raman microscopy and NeutrAvidin-FITC, Her2 receptor expression was visualized by immunofluorescence through the produced complex on BT-474 cells. The Raman signal was reduced by 94% in biotinylated SWCNTs as compared to non-biotinylated SWCNTs. It implied that a biotin-avidin interaction could reduce the nonspecific binding of biotinylated SWCNTs to the primary antibody. The biotinylated nanotubes were found attached to cell surfaces via Her2 receptors, while bare nanotubes were observed within vesicles inside the cells [91].

The use of a disposable immunosensor array with a SA-functionalized CNT/Ag NP was being investigated for ultrasensitive multiplexed tumor marker detection. The CNT/Ag NP nanohybrid was generated by deposition of Ag NPs on carboxylated CNTs *in situ*. The nanohybrid was functionalized with SA through the intrinsic affinity between protein and Ag NPs, enabling the biotinylation of signal antibodies to acquire tagged antibodies. The dispersibility of the nanohybrid in water was considerably improved by the functionalization process. The captured antibodies were covalently immobilized on chitosan-modified screen-printed carbon electrodes to create the immunosensor array.

Numerous Ag NPs were collected onto each immunocomplex via a sandwich-type immunoreaction on the immunosensor array, which was enhanced following Ag NP-induced deposition of Ag by an Ag enhancer

solution generating an electrochemical-stripping signal of Ag NPs. The suggested multiplexed immunoassay approach displayed satisfactory accuracy and a wide range of linearity, with detection limits as low as 0.093 and 0.061 pg·mL^{-1}, respectively, using carcinoembryonic antigen (CEA) and α-fetoprotein (AFP) as model analytes. With the proposed method, the serum assay results with reference values were within acceptable bounds. The newly developed approach and functionalized tag eliminated the cross-talk and the need for deoxygenation in electrochemical immunoassays, indicating that they might be useful in clinical settings [92].

5 Intercalation into NPs through co-precipitation or anion-exchange reaction (e.g., LDHs)

LDHs are naturally occurring, synthetic and layered materials, which are also referred to as anionic clays, hydrotalcite-like (HTI), or hydrotalcite-type (HTt) [93]. The general formula of most LDH materials is as follows: $[MII_{1-x}MIII_x(OH)_2]^{x+}(A^{n-})_{x/n}\cdot mH_2O$ (x = 0.2–0.4; n = 0.5–1), where MII represents a divalent metal cation, MIII a trivalent metal cation, A^{n-} an anion, and m the number of moles of solvent (Fig. 5) [94]. Figure 5 shows the construction of LDH for therapeutic applications. LDHs are effective drug carriers because they are highly biocompatible, have double-layered structures that can be recovered after thermal degradation, are easy to prepare, provide rapid drug delivery, have high drug loading capacities, and are resistant to enzyme degradation [94–95].

Ligand exchange reaction-free intercalation and surface modification are viable strategies to directly load genes, nucleic acids, drugs, aptamers, peptides, antibodies, and proteins into LDHs. Biomolecules like peptides, vitamins, ATPs, and polysaccharides can intercalate into LDHs through co-precipitation or anion exchange reactions [94]. Co-precipitation with drugs provides the most precise and straightforward method of conjugating LDH with drugs due to their less tendency to incorporate CO_3^{2-} and other anions [94]. The drugs utilized must be able to survive post-preparative procedures (e.g., hydrothermal treatment) in order to increase the homogeneity and crystallinity of the materials obtained. Nevertheless, some anions, such as siRNA and antisense oligonucleotides, however, are unable to resist these conditions. As a result, they are integrated into LDH-drug conjugates using the anion-exchange method.

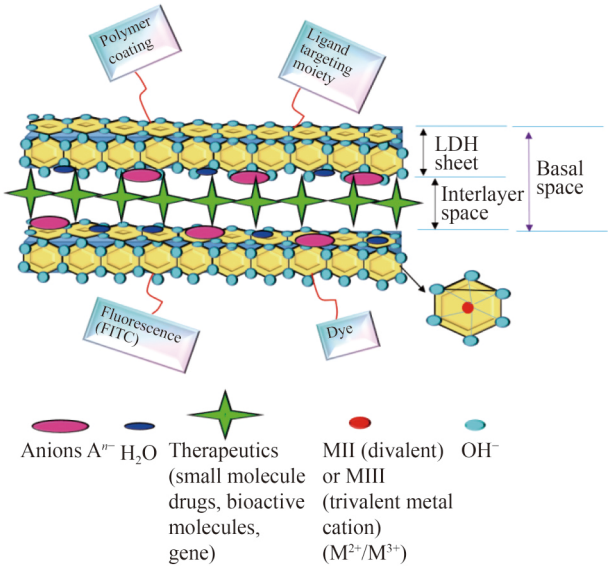

Fig. 5 Schematic illustration of a LDH structure with the general formula $[MII_{1-x}MIII_x(OH)_2]^{x+}(A^{n-})_{x/n}\cdot mH_2O$ (x = 0.2–0.4; n = 0.5–1), used for therapeutic purposes. MII (M^{2+}) represents a divalent metal cation and MIII (M^{3+}) a trivalent metal cation. Here 'x' is a ratio of $M^{3+}/(M^{2+}+M^{3+})$. The M^{2+}/M^{3+} ratios of 2–4 are considered relatively steady. A^{n-} (in the interlamellar region) is an anion. A^{n-} represents any charge compensating organic or inorganic anions, such as oxo-anions (carbonates, nitrates, etc.), halides, oxo- and polyoxo-metallates (dichromates, $(Mo_7O_{24})^{6-}$, $(V_{10}O_{28})^{6-}$, etc.). 'm' represents the number of moles of solvent contained in the interlamellar zone where no anions are present. The LDH can be modified with inorganic ions, fluorescence (FITC), dye, polymer coating, and ligand targeting moieties.

There is evidence that LDHs can efficiently intercalate a wide range of anionic biomolecules, such as nucleotides, siRNA, DNA, and anticancer drugs, allowing for high bioavailability and effectiveness [96–97]. LDH size limits must be defined for utilization as intracellular carriers in order to maximize uptake efficiency. In one study, cellular uptake of various-sized LDH-FITCs was assessed using flow cytometry [98]. It was found that particle size greatly affected the amount of LDH absorbed by cells. The smallest particles, 50 nm, were readily internalized, followed by 200 ⩾ 100 > 350 nm. The fact that only a minimal amount of 350 nm LDH could penetrate the cells suggested that 350 nm is too large to permeate the cell membranes efficiently [98]. All of the findings implied that LDHs ranging in size from 50 to 200 nm selectively entered the cells via clathrin-mediated endocytosis, whereas LDHs greater than 200 nm could not. Thus, there appeared to be a strong correlation between LDHs' size-dependent uptake mechanisms and uptake behaviors [98].

NPs are prone to size-dependent toxicity [99]. One research group investigated the size-dependent toxic effects of LDHs on human lung tissue cultures [100]. It was revealed that LDHs within 100–200 nm size range exhibited mitigated toxicity in cell proliferation, inflammation response, and membrane damage. Furthermore, the *in vivo* study demonstrated that different-sized LDHs did not influence body weight or cause mortality. These studies, therefore, indicated that LDH (within 100–200 nm) could promote biocompatibility and enhance the intracellular delivery of drugs. Mostly, in internal cavities of LDH, negatively-charged oligonucleotides were intercalated via ion exchange reactions. As a result of the intercalation of oligonucleotides into LDH NPs, the loaded nucleotides were protected from DNase attack.

5.1 Drug-LDH conjugates

Due to the subsequent stability of drug-LDH conjugates, the cellular internalization of the drugs could be improved without any noticeable negative consequences [101]. One example of this is 5-fluorouracil-LDH (5-Fu-LDH), which showed sustained release, an extended half-life, and a higher accumulation of 5-Fu in tumors compared to free 5-Fu [96]. In addition, 5-Fu-LDH proved to be biodegradable and does not necessarily get accumulated in healthy organs after administration. This indicated that they were rapidly cleared from the body [102]. Choy et al. reported that methotrexate (MTX)-loaded LDH (MTX-LDH) could facilitate cellular internalization through clathrin-mediated endocytosis [97]. However, no noticeable changes were observed in the conjugate's morphology and functional properties. Later, Oh et al. prepared a similar MTX-LDH via the co-precipitation method. The end result was enhanced toxicity and increased cellular internalization employing clathrin-mediated endocytosis in bone cancer cell lines (Sao-2 and MG-63) as proved by 3-(4,5-dimethylthiazol-2-yl)-2,5-diphenyltetrazolium bromide (MTT) and 5-bromo-2-deoxyuridine (BrdU) assays [103–104].

Choi and colleagues conducted a thorough investigation into the antitumor effects of intact MTX and its nanohybrid, MTX-LDH, using HOS-bearing xenograft mice models [105], in which 48 mice were split between four groups: control (PBS buffer), LDH (45 $mg \cdot kg^{-1}$), free MTX (30 $mg \cdot kg^{-1}$), and MTX-LDH (75 $mg \cdot kg^{-1}$ was equivalent to 30 $mg \cdot kg^{-1}$ MTX). A total of three injections were given intravenously on days 0, 7, and 14. The MTX-LDH treated tumors were found to be considerably smaller than those in the control group. One point to note was that each free MTX-treated group and MTX-LDH group received 30 $mg \cdot kg^{-1}$ of MTX (~LD_{20} value) [105].

One interesting study, investigated by Li et al., displayed the intercalation of Fenbufen (FBF, a nonsteroidal anti-inflammatory drug used in relieving cancer pains [106]) into the interior of the LDH NPs by co-precipitation in the nitrogen medium [107]. X-ray diffraction (XRD) study revealed that following intercalation with FBF, the distance between LDH layers was raised to 1.87 nm, in comparison to the initial gallery height (0.39 nm) and also the brucite-like layer (0.48 nm thick) [108–109]. Changing the pH has a considerable effect on the FBF-LDH intercalation. The FBF changed from a monolayer to a bilayer as pH increased from 8 to 13, while the change in distance (1.87–3.00 nm) pointed towards an intercalated structure. Increasing interlayer spacing enhanced ion diffusion kinetics, particularly ions with large sizes and multiple valencies, by reducing their diffusion barriers and diffusion energy barriers for ion intercalation. Based on Xue et al.'s study on the modification of paclitaxel-LDH (PPT-LDH), it indicated that tyrosine (Tyr) could be co-precipitated with LDH to enhance the PPT loading efficiency [110]. Thus, the interlayer space was pre-opened, creating a conducive environment for drug attraction. Preliminary *in vitro* anticancer investigations verified the inhibitory properties of PPT-LDH hybrids on tumor cell development, with a 34% drug loading efficiency (w/w of drug/material).

5.2 Ligand-LDH conjugates

Researchers in one study incorporated a targeting molecule, FA, onto the LDH NPs' surface, resulting in FA-LDH, in order to investigate the targeting functions of MTX-FA-LDH nanohybrid in both *in vitro* and *in vivo* models. In addition to the EPR effect, clathrin-mediated endocytosis and folate receptor-mediated endocytosis were considered reasons for improved uptake and therapeutic effects. In a siRNA delivery study in which KB cells were transfected with siRNA or mice were injected with siRNA, it was discovered that siRNA(Survivin)-FA-LDH significantly reduced gene expression at the mRNA and protein levels *in vitro* and ultimately mitigated tumor growth by threefold compared to Survivin-LDH *in vivo* without any targeting ligand. In

view of such a result, it seemed more likely that the Survivin gene was targeted more efficiently (1.2-fold) towards tumors than normal cells and other tissues [111].

Cancer treatment usually entails chemotherapy involving two or more complementary drugs. However, combination chemotherapy has yet to be proven safe and effective. An albumin-stabilized LDH (BLDH) system was designed for colorectal cancer treatment to load and deliver two commonly used anti-cancer agents, 5-Fu and albumin-bound paclitaxel (Abraxane, ABX), as delineated by Li and colleagues. The 168.3 nm diameter, a polymer dispersity index (PDI) of 0.181, and 14.0 mV surface potential were the dimensional properties of the produced BDLH/5-Fu-ABX system. An *in vitro* drug release model involving BDLH/5-Fu-ABX showed that the slow LDH neutralization in an acidic environment might cause 5-Fu and ABX to be released into cancer cells' late endosomes/lysosomes. Based on the cellular uptake study, the BLDH/5-Fu-ABX NPs were successfully internalized by the colorectal cancer cell (HCT-116), eliciting apoptosis in colon cancer cells synergistically. An *in vivo* test demonstrated that the BLDH/5-Fu-ABX NPs could effectively reduce tumor development with no apparent side effects following three intravenous injections. The significant increase in treatment effectiveness was attributed to the efficient accumulation of BLDH/5-Fu-ABX in the tumor and acid-sensitive co-loaded drug release. As a result, BLDH/5-Fu-ABX NPs might be used as a new approach for treating colorectal cancer [112].

5.3 Mercaptoundecahydro-closo-dodecaborate (BSH)-LDH conjugates

Choy et al. investigated LDH nanocarrier for boron delivery using boron neutron capture therapy (BNCT). A substantial amount of boron (B-10) was required to successfully deliver BNCT to cancer cells. The cluster of anionic boron molecules, such as BSH, a B-10 compound approved by the Food and Drug Administration (FDA), was intercalated with LDH to generate BSH-LDH and eventually investigated as a boron delivery system. According to biodistribution studies involving a BSH-LDH nanohybrid drug (100 nm) in animal models, the tumor-to-blood (T/B) ratio of BSH in the BSH-LDH-treated group was increased (4.4-fold) compared to the intact BSH-treated group 2 h post-injection, thus supporting its mechanism of targeting by endocytosis via EPR effect and clathrin-mediated pathways [113].

5.4 Inorganic ions-LDH conjugates

Nanotheranostic platforms that respond to the acid microenvironment of tumors are crucial for accurate tumor identification and therapy. One laboratory [114] reported the successful fabrication of a 2D nanotheranostic platform where functional ferrous ions were doped into MgAl-LDH with DOX to form Fe-LDH/DOX NPs, enabling MRI-guided synergistic cancer chemotherapy and photothermal therapy. The incorporation of ferrous ions into Fe-LDH/DOX gave off a strong photothermal effect, with a conversion efficiency of 45.67%, which in conjunction with DOX could render a synergistic killing of cancer cells with both photothermal therapy (PTT) and chemotherapy. Furthermore, Fe-LDH/DOX was found to be susceptible in the tumor's acidic microenvironment, as evidenced by T_2-weighted MRI results and its pH-dependent degradation *in vitro*. Importantly, the growth of tumors in 4T1 bearing mice was efficiently suppressed following treatment of PTT and chemotherapy with Fe-LDH/DOX. According to these findings, doping functional metal ions into LDH NPs could lead to a unique approach for developing a nanotheranostics platform with increased diagnostic and therapeutic capabilities [114].

Likewise, Xu and colleagues modified positively charged Cu-containing LDH NPs conjugated to a pH-sensitive polymer in order to enhance the colloidal stability of particles during blood circulation, prevent off-target accumulation in healthy cells, and promote tumor distribution and internalization within the tumor microenvironment. Based on *in vitro* experiments, the polymer-LDH nanocarrier decreased macrophage capture in blood pH (7.4) but enhanced uptake by cancer cells in weakly acidic pH (6.8) due to the detachment of the polymer coating. *In vivo* pH-responsive MRI verified the charge-convertible nanohybrids' ability to accumulate in the tumor, with an accumulation rate of 4.8% (of the administered dose) 24 h after injection, bolstering their versatility as anticancer nanocarriers [115].

Interestingly, the LDH interlayer was capable of replacing any organic or inorganic ion, whether simple or complex. Consequently, LDH stability was dependent on the nature of the anions in the interlayer. For example, Baek et al. developed Mg-Al-LDH-Cl, which was less toxic than Mg-Al-LDH-CO_3 with regards to apoptosis, membrane damage, and oxidative stress due to their propensity to disintegrate quickly in lysosomes' acidic

compartment (pH 4.5) [116].

5.5 DNA-LDH conjugates

Rapid gene expression/silencing using LDH involved the following steps: (1) The DNA/siRNA loaded LDHs hybrids (50–250 nm, with an overall positive charge) could bind to the negatively charged cell membrane; (2) Following adsorption, the LDH host could internalize into the cytoplasm via the clathrin-mediated endocytosis route, allowing it to permeate the cell membrane; (3) After dissolving the LDH host, the DNA/siRNA was released at or near the nucleus, in which case the plasmids would directly enter the nucleus, resulting in expression or targeting of specific mRNA for gene silencing [117]. One research group showed that FITC as a reporter molecule significantly elevated the uptake in cells treated with DNA/LDH hybrids, which increased proportionally with increasing cell exposure to LDH. The results indicated that c-myc/LDH hybrids could be rapidly absorbed by cells and that antisense oligonucleotides assisted in the metabolic processes of cells. After exposing human leukemia (HL-60) cells to the AS-myc–LDH hybrids (20 $\mu mol \cdot L^{-1}$ concentration) for 4 d, a 65% reduction in cancer cell proliferation resulted, suggesting that the LDH NPs were capable of transferring small nucleic acid to target cells. In addition, this group had reported that cell proliferation was inhibited over time and in a dose-dependent manner [117].

6 Covalent bonding

Covalent attachment offers the advantage of modulating the release of drugs through attachment chemistry (such as the cellular release of thiol-based payloads via GSH [118]). To form a covalent bond between drugs and NPs, the binding sites must be available and free of strong electrostatic repulsion and extremely dense and rigid coatings with tiny pores. The various functional groups available on the nanocarriers and the drugs to be conjugated have led to the development of covalent conjugation strategies (Fig. 6). Certain internal or external stimuli trigger the release of covalently bonded genetic materials. siRNAs can be covalently attached to several cell-penetrating or targeting ligands, including small molecule receptors, peptides, and lipids. However, they are unstable in serum and have a short circulation time, hindering the long-term silencing of the gene. CNTs, Au

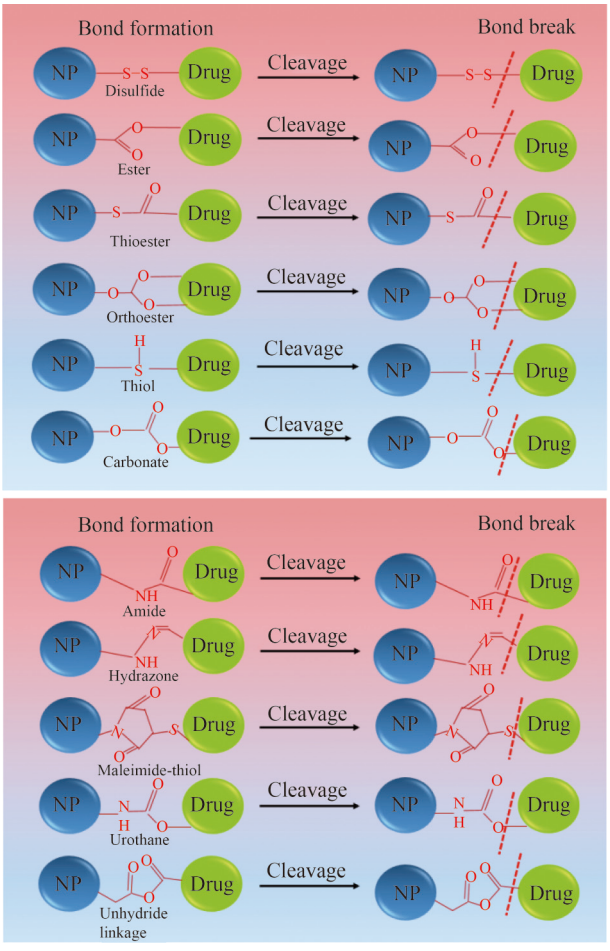

Fig. 6 Schematic illustration of the formation and cleavage of covalent bonds between NPs and drugs. The covalent bonds presented are mostly based on the functional groups (e.g., disulfide, ester, thioester, orthoester, thiol, carbonate, amide, hydrazone, maleimide-thiol, urothane, and unhydride linkage) available on nanocarriers and drugs being conjugated.

NPs, and SPIONs bind small molecules, siRNAs, and plasmids via covalent functionalization or thiol-gold covalent chemistry. In an attempt to induce a humoral immune response within the tumor, CNTs may function as antigen-presenting carriers, which can improve the weak immunogenicity of tumor-based peptides and antigens [119–120].

6.1 CNTs

Chemotherapeutic drug molecules are generally conjugated to the CNTs through 1) surface conjugation to functional groups or 2) generation of CNT polymer coatings by cleavable bonds. Hence, biomolecules, imaging agents, and drugs can covalently bind to the CNT surface by chemically functionalizing them with strong acids such as HNO_3 and H_2SO_4, which introduce

oxygenated groups such as carboxyl and hydroxyl groups at the tips and defect sites of CNTs, or by 1,3-dipolar cycloaddition reaction, providing a covalently coupled functionality [121]. Furthermore, using CNT sidewall modification to incorporate different functional groups allows further derivatization of the nanotube [122]. These covalent functionalization techniques are mainly used to modify CNTs for enhanced siRNA delivery.

Covalent bonds containing acetyl hydrazone, amide, or ester groups are usually used to bind drugs to nanocarriers or polymers covering nanocarriers. PEGylation of CNTs best illustrates the covalent interaction between them in prolonging the blood circulation period and mitigating off-target toxicity. For example, Liu et al. verified that paclitaxel (PTX) could covalently bind to PEG-coated SWCNTs through cleavable ester bonds [123]. The SWCNT-PTX attenuated the proliferation of 4T1 breast cancer cells with greater efficacy than commercial Taxol by leveraging the EPR effect. Thus, extending the blood circulation half-life and increasing PTX accretion in the tumor by tenfold. Additionally, SWCNTs released PTX in the RES, where it was excreted through the bile [123]. Sobhani and colleagues demonstrated that intratumoral injection of PEG-coated CNTs attenuated the growth of melanoma tumors in mice after exposure to a NIR laser for 10 min compared to the group exposed to laser alone [124]. Another similar study revealed that PEGylated SWCNTs conjugated with glucocorticoid-induced tumor necrosis factor receptor (TNFR)-related protein (GITR) ligands on single retro-orbital injection displayed enhanced uptake by regulatory T cells (Treg) residing in a B16 melanoma compared to splenic Treg or intratumor non-Treg via receptor-mediated endocytosis, thus elevating the immune response against cancer [125].

6.2 Au NPs

Thiol-gold covalent chemistry was one of the holistic approaches for conjugating siRNAs on the Au NP surfaces. Nagasaki et al. conjugated siRNAs on the Au NP surface by modifying Au NPs with thiol-PEG5000–PAMA7500 polymer, then self-assembling the thiolated siRNA. The resulting Au NP/siRNA conjugate exhibited 65% gene silencing efficiency with human hepatoma HuH-7 cells [126]. To heighten the intracellular delivery of DNA, Lee et al. modified Au NPs with PEG through disulfide linkages, prior to complexation with poly(β-amino ester)s (PBAEs) [126]. TEM micrographs showed that the core–shell structure of the PBAE-siRNA-Au NPs has an approximate diameter of 100 nm. On conjugation with PBAEs, the surface charge of the siRNA-Au NPs changed from −34 to +13 mV, which facilitated the intracellular delivery by interacting with the negatively charged cell membranes [126]. It was evident that the thiol-Au chemistry improved siRNA delivery to the site of action, as well as promoted the gene silencing effectiveness.

Researchers at Huh's team developed iron oxide/gold NPs and investigated their photoactivity and (*in vitro* and *in vivo*) biological activity. The covalent link between Au and S allowed these NPs to be coated with thiolated heparin-pheophorbide. Following uptake by tumor cells, the photosensitizer's photoactivity was restored by the ablation of Au−S bonds by glutathione. Quenching and dequenching were assessed by measuring the fluorescence of the photosensitizer with or without GSH. After 60 min of incubation, the fluorescence intensity (670 nm) had increased ninefold compared to control without glutathione. In the presence of 9,10-dimethylanthracene ($^1O_2$ trap), the generation of $^1O_2$ was evident. A confocal laser scanning microscope was used to examine the penetration in A549 cells, which revealed a significant photosensitizer signal of the internalized NPs, supporting GSH action in the cytoplasm. Regardless of NPs that were free or released the photosensitizer, exposure to light reduced cell viability. In A459 tumor-bearing nude mice xenograft models, the comparison between free photosensitizer and NPs revealed that NPs had superior tumor selectivity and a more extended stay in the tumor than free pheophorbide, whereas the latter was promptly eliminated from the body. Tumor-induced mice were given saline (control), free photosensitizer, or NPs every 2 d and were accompanied by a light source. On examination of tumor weight and volume, it was apparent that the NP treatment group outperformed the free photosensitizer by 2.5 times [127].

An alternative technique involved using a triggered linker. The study by Chen and coworkers applied an Au−S covalent interaction to couple Au NPs to the Si phthalocyanine Pc 4 [hydrophobic photodynamic therapy (PDT) drug]. Interestingly, photosensitivity distinguishes this ligand, causing hemolytic photocleavage of the Si−C bond following NIR irradiation (660 nm), thus releasing Pc 4 after the exchange of ligands with water on the middle Si atom. The researchers demonstrated that PDT was as efficient as non-covalently bound Pc 4 in HeLa

cells, but that the covalent interaction facilitated a more targeted release of Pc 4 since Au NPs inhibited it during transport [128].

The covalent attachment of oligonucleotides to the Au core resulted in oligonucleotides compactly packed around the Au core, which had evident benefits in modifying how cells would respond to Au NPs. These findings were also applied to HeLa cells more generally based on analyzing genome-wide expression profiles with various Au NPs [129]. With oligonucleotide-functionalized Au NPs (ssDNA, dsNA, and dsRNA), cellular responses were modest in terms of cell cycle regulation, gene expression, and apoptosis. Unmodified citrate-capped Au NPs, on the contrary, were shown to pose a marked negative effect on cells, including the onset of apoptosis, related to the weak attachment of citrate cappings in contrast to the firmly attached, densely oligonucleotide-functionalized NPs. The significance of exerting robust control over surface functionality was highlighted in this study, which explained the prevalence of covalent interactions.

A typical approach for releasing DNA was to use light-responsive NPs such as nanocages, nanoshells, and nanorods. These NPs' diameters could be adjusted to obtain considerable absorption in the NIR transparency window. Photothermal effects and laser-induced electron generation at a suitable frequency can induce DNA release covalently linked to these NPs [130]. Chen et al. used this method of femtosecond laser irradiation at the rods' longitudinal plasmon wavelength to induce the release of plasmid DNA encoding enhanced green fluorescent protein (EGFP) bound to Au nanorods [131]. This approach caused the rods to melt and the DNA to be released simultaneously, allowing up to 80% release of the DNA molecules covalently attached to the surface of the nanorods. Additionally, the presence of EGFP fluorescence in cells suggested that the plasmid had been successfully transfected.

For the intracellular release of platinum(II) ions, the platinum(IV)–NP complex has attracted attention as a drug delivery vehicle and a prodrug [132–133]. The method was advantageous due to the fact that Pt(IV) was less reactive with biological agents than Pt(II), resulting in reduced systemic toxicity and improved bioavailability [134]. Lippard et al. employed traditional carbodiimide coupling chemistry with 1-ethyl-3-(3-dimethylamino-propyl) carbodiimide and N-hydroxysuccinimide to generate oligonucleotide-functionalized Au NPs with a terminal dodecyl amine moiety, linked with a carboxyl-containing Pt(IV) complex [134]. Pt(II) species were generated via intracellular reduction of Pt(IV) in GSH-containing platinum complexes. Following the loss of axial ligands, free cisplatin would be released. The conjugate was absorbed into cells in the same way that conventional DNA-functionalized NPs were. It was demonstrated that these complexes had anticancer efficacy similar or equivalent to cisplatin in various cancer cells, despite the fact that most of the IC_{50} values were similar. Min and coworkers employed a similar approach to link Pt(IV) prodrugs to Au nanorods [135]. Using in situ dithiocarbamate production on one terminal, Au nanorods were first covalently modified with a diamino(polyethylene glycol) before coupling with a carboxyl-containing Pt(IV) molecule (via amino group) [135]. In comparison to free cisplatin, cytotoxicity analyses based on the MTT assay revealed substantially more toxicity for three separate cancer cell lines, with approximately 9 to 65 fold lower IC_{50} values. These results were linked to higher intracellular concentrations of Pt ions in nanorod-treated cells, implying that the NP delivery systems might play a key role in improving drug uptake via different pathways of endocytosis.

6.3 Magnetic NPs

The cleavage of covalent bonds between proteins and drugs was indispensable for drug release. The bond could be either sustained in systemic circulation or breached within tumor cells and released at targeted sites. As an example, Ding et al. demonstrated that 85% of DOX loading was achieved through indirect conjugation of (transferrin)-coated Fe_3O_4@SiO_2 NPs via a multi-armed linker, poly-L-glutamic acid (PLGA) [136]. The PLGA was chemically coupled to transferrin (Tf) and DOX with dual-function magnetic NPs (DMPs). The respective NPs displayed a mean diameter of approximately 90.8 nm, confirmed by DLS and TEM, and a zeta potential of −44.1 mV. These data revealed their tendency to aggregate less. Notably, DOX was linked by the amide bonds to the PLGA-coated layer of the NPs. The TfDMP NPs demonstrated the receptor-targeting function of Tf, along with high DOX loading percentage, pH-sensitive drug release, and improved Tf receptor-expressing tumor cell uptake, suggesting a more significant cytotoxic effect on cancer cells than that of DOX-coupled DMP without Tf modification (DDMP) [136]. Kresse et al. reported the covalent interaction between Tf and SPIONs for *in vivo*

imaging in an SMT/2A tumor-bearing rat (rat breast carcinoma) model [137]. Following 150 min of injection, the conjugates reduced MRI tumor signals by 40% (range 25%–55%), and the signal reduction persisted for 8 h with a half-life of 17 min in normal rats. On the contrary, only a 10% decrease in tumor signal was acquired with identical parent SPIONs or those labeled with human serum albumin (HSA) [137].

Additionally, researchers used covalent cross-linking between drugs and nanocarriers to target cancer cells. For instance, Yu et al. engineered DOX-loaded thermally cross-linked (TCL) SPIONs via covalent cross-linking for targeted delivery and MRI [138]. The DOX@TCL-SPION exhibited an average particle size of (21 ± 6) nm (PDI = 0.13) and a zeta-potential of (−25 ± 2) mV, which was more electronegative than TCL-SPION (−37 ± 2) mV. The more electronegative zeta potential of DOX@TCL-SPION validated that some negative charges of COO^- groups on TCL-SPION were neutralized by DOX (positively charged). *In vivo* studies showed greater tumor growth suppression with DOX@TCL-SPIONs than mice treated with 5% glucose, TCL-SPION, DOX (0.64 $mg \cdot kg^{-1}$), and DOX (5 $mg \cdot kg^{-1}$). Thus, DOX@TCL-SPION allowed passive tumor targeting and detection for MRI. Moreover, they displayed enhanced antitumor efficacy based on drug accumulation within the tumor and subsequent release from the NPs.

7 Ionic interaction

In an attempt to construct nanotherapeutic platforms capable of delivering therapeutics and imaging agents to tumor sites, ionic interactions between drugs and NPs must be considered. Generally, the strategy to modify the NP surfaces with amine groups, cationic macromolecules (polymers, lipids), or Ca-doped, CaP, and $CaCO_3$ particles for complexation with small molecule drugs, siRNAs, and plasmids, stemmed from the observation that many drug delivery platforms exhibit compromised therapeutic efficacy. This notion justifies the need to develop and optimize nanotherapeutics to aggrandize the site-specific drug delivery.

7.1 Interaction of Ca-doped, CaP, and $CaCO_3$ particles with drugs

Needless to say, the strong nucleic acid binding capacity, low toxicity, and enhanced endosomal disruption capacity of CaP/$CaCO_3$ NPs make them promising carriers for DNA/miRNA/siRNA. In addition, the positive charge on Ca ions offers useful binding sites to the negatively charged nucleic acids, thus strengthening their resistance or stability against attack from ribonucleases, RNAse (siRNAs and pDNAs) nucleases. Mostly, Ca ions serve to bind phosphate backbones in antisense oligonucleotides.

7.1.1 $CaCO_3$ NPs

For the purpose of controlling pH in tumor treatment, Som and colleagues generated a monodisperse non-doped vaterite nano-$CaCO_3$. Researchers observed that selectively depositing nano-$CaCO_3$ on tumors elevated the acidity of tumors over time, preventing tumor growth. The diameter of the synthesized NPs was from 20 to 300 nm. In HT1080 tumor-bearing mice, the i.v. delivery of 1 mg bolus doses of nano-$CaCO_3$ raised the tumor pH by different amounts for over 3 h. The 100 nm nano-$CaCO_3$ had the highest pH and the longest-lasting impact. The 20 nm particle diffused faster into and out of a tumor than the 100 nm particle. Moreover, there was no indication that 300 nm nano-$CaCO_3$ could significantly influence the pH of the tumor. Since these particles have a low diffusion rate, they could only penetrate a minimal area of 3D tumor tissue. Thereby, using this research, it might be possible to develop a pH-sensitive nanoplatform capable of modifying cancer's acidic environment [139].

Likewise, $CaCO_3$ nanocrystals were prepared and tested by Kamba et al. to serve as an efficient delivery vehicle for DOX. These nanocrystals induced apoptosis in cancer cells with high levels of selectivity and specificity without causing nonspecific damage. Intercalation of DOX into $CaCO_3$ nanocrystals occurred at high loadings (4.8%) and encapsulation levels (96%), respectively. $CaCO_3$/DOX nanocrystals were extremely stable at physiological pH (7.4), resulting in the delayed release. However, in acidic pH (4.8), nanocrystals dissociate more rapidly, resulting in a quicker release of DOX. The MDA-MB-231 breast cancer cells showed a significant absorption of the $CaCO_3$/DOX nanocrystals, providing evidence of potential DOX delivery. The *in vitro* chemosensitivity test utilizing MTT, modified neutral red/trypan blue assay, and LDH were used to demonstrate that $CaCO_3$/DOX nanocrystals could mitigate tumor cell growth more than free DOX. $CaCO_3$ nanocrystals, according to these findings, could prove helpful for the controlled delivery of

drugs and the treatment of cancer [140]. Similarly, Hammadi et al. created a docetaxel (DTX) nanocarrier loaded with $CaCO_3$ for breast cancer screening. To evaluate the generated NPs for their drug delivery and release ability, they were tested *in vitro* in a physiological environment (pH 7.4) as well as an intracellular lysosome environment (pH 4.8). Physicochemical studies led to the successful fabrication of homogeneous pleomorphic pure aragonite type DTX-$CaCO_3$ NPs (average size 37 nm) with excellent crystallinity and a 96% entrapment efficiency and a sustained release profile at pH 7.4. The average diameter of the prepared NPs was within the range of 5 to 100 nm, which made them less likely to be eliminated by the spleen, kidney, and liver. At 800–1000 $g \cdot mL^{-1}$, free $CaCO_3$ NPs revealed cell viability of 90%, indicating that these nanocrystals were cytocompatible. After 24 h, it was observed that the synthesized drug-loaded NPs had reduced toxic effects against MCF-7 cells than DTX, whereas similar effects were acquired at 48 and 72 h, which was linked to the NPs' sustained-release performance. Thus, it was hypothesized that DTX's long-acting properties would increase bioavailability and less frequent doses [141].

Nanocarriers with a diameter less than 600 nm could improve the internalization of drugs into the tumor by exploiting the EPR at the tumor site [142]. Peng and the research group used a multistage self-assembled approach to prepare pH-sensitive mesoporous $CaCO_3$. The anticancer drug etoposide was encapsulated in a stable form, capable of highly effective drug loading. As demonstrated by the MTT assay, the produced nanostructure inhibited SGC-7901 cells more effectively and lessened the toxic effects of etoposide in HEK-293 T cells compared with free etoposide. According to the research group, these nanocarriers were more efficient at delivering etoposide than free etoposide, causing a more potent inhibition of tumor cell growth. In response to extrinsic or intracellular stimulation, a rapid and stable release of etoposide could be induced at a lower pH than in normal cells through NP distribution in the tumor cells via the EPR effect. Thus, mesoporous $CaCO_3$ nanospheres offered a way to boost the therapeutic effects of drugs, such as etoposide, by overcoming their water-insoluble nature [142].

7.1.2 CaP NPs

The surface modification of carrier constructs composed of CaP could promote the site-specific delivery and release of therapeutics in tumors. One study aimed to achieve tumor-targeting siRNA delivery by employing asymmetric lipid bilayer stabilizing CaP NPs. Additionally, NPs modified with PEG targeting anisamide ligands were shown to significantly improve *in vivo* gene silencing as well as targeted delivery of siRNA in human H460 lung cancer xenograft models. When compared to LPD (lipid/polycation/DNA complex), LCP-II (lipid/calcium/phosphate type II) exhibited greater curvature and smaller particle size that could preferentially accumulate therapeutics at the tumor site. Furthermore, siRNA silencing activity (delivered by LCP-II) was detected after treatment with NPs containing luciferase siRNA through single tail vein injection in the H460 xenograft tumor model [143]. In light of the successful delivery of siRNA, Wu et al. developed two formulations of enzyme-response PEG/lipids/calcium phosphate hybrid (siRNA@NP1 and siRNA@NP2). It was reported that there was no significant effect of the nearly neutrally charged siRNA@NP2 on disintegration caused by serum. Specifically, in SMMC-7721 cell lines and SMMC-7721 bearing mice, siRNA@NP2 was more efficiently delivered than siRNA@NP1, which does not trigger an enzyme response. In addition, the NPs were found to be relatively safe, as demonstrated by in vitro and *in vivo* studies. Therefore, the siRNA@NP2 delivery method might facilitate the distribution of siRNA-based cancer gene therapy *in vivo* [144].

Since triple-negative breast cancer (TNBC) is characterized by heavy DNA repair and negative antigen expression, chemotherapy and endocrine treatments are generally ineffective. A quick solution to this issue is of paramount importance to improve therapeutic outcomes. Dong et al. developed a CaP-based pH-sensitive shell–core platform to administer BRCA1 siRNA and Pt prodrug (Pro-Pt) to TNBC patients in a synergistic manner. During thin-film hydration, the DSPE-PEG (1, 2-distearoyl-sn-glycero-3-phosphoethanolamine-polyethylene glycol), which self-assembled into micelles harboring lipophilic Pro-Pt, caused Pro-Pt to transform to Pt upon intracellular reduction for triggering DNA damage. The micelles form porous shells on their surfaces, with Ca^{2+} and PO_4^{3-} (CaP) binding to negatively charged siRNA via electrical interactions and physical adsorption. Notably, the CaP shell was found to disintegrate in the acidic lysosomes, allowing lysosomal escape and successive release by establishing an ion pair with lysosomal

membranes. This ensured the escape from lysosomes and the release of siRNA and Pro-Pt in a sequential manner, blocking DNA repair by BRCA1 siRNA and reducing Pro-Pt to Pt for irreversible DNA damage. Furthermore, the exposed PEG hydrophilic chain generated a hydrated coating that stabilized the NPs in the blood, preventing them from being precipitated by serum protein or inactivated by nuclease. Moreover, urokinase plasminogen activator analogs (uPA, which have a high affinity for the uPA receptors highly expressed on TNBC cells and tumor-related fibroblast cells but barely found in normal tissues) served as an excellent medium for introducing NPs into tumor cells via dual passive and active tumor targeting ability. In addition to providing augmented encapsulation efficiency and stability, pH-sensitive NPs suppressed the breakdown of siRNA and Pro-Pt throughout the circulation, assuring their activity in tumor tissue [145].

In the study by Qiu and coworkers, the alendronate-hyaluronan graft polymer (AHA) was coated across calcium phosphate-siRNA co-precipitate surfaces to generate hyaluronan (HA)-functionalized calcium phosphate NPs (CaP-AHA/siRNA NPs), suitable for delivering siRNAs to the targeted tissues. The CaP-AHA/siRNA NPs displayed a homogeneous spherical geometry, with an average size and surface potential of about 170 nm and −12 mV, respectively. Since Ca^{2+} and PO_4^{3-} could interact strongly, coating the NPs with hydrophilic HA was found to increase their physical stability over a month. Moreover, *in vitro* investigations showed that CaP-AHA/siRNA NPs were capable of delivering EGFR-targeted siRNA via CD44-mediated endocytosis into A549 cells and could drastically lower EGFR expression. Furthermore, the siRNA's pH-dependent release from internalized CaP-AHA/siRNA NPs indicated lysosomal acidification had contributed to NP disassembly, causing sharply higher internal osmotic pressure and substantially accelerating siRNA release into the cancer cells' cytosol. Furthermore, *in vivo* tumor therapy indicated that when CaP-AHA/siEGFR NPs were injected intravenously to nude mice xenografted with A549 tumor resulted in considerable shrinkage of the tumor accompanied by EGFR gene silencing, as well as minimal weight loss in the mice models. These findings revealed that a systemic siRNA delivery strategy based on CaP-AHA/siRNA NPs might serve as an effective and safe option for targeting cancer cells [146].

7.1.3 CA NPs

Recently, pH-sensitive CA NPs were extensively explored for the effective delivery of drugs, DNA, siRNAs, and proteins [147–149]. Our laboratory demonstrated that surface modification of CA by PEG could significantly improve the delivery and cytotoxicity of gemcitabine (a hydrophilic nucleoside inhibitor), elevate cellular internalization in breast cancer cells, and extend the half-life of drug-particle complexes as validated by measuring gemcitabine levels in plasma, cancer cells and healthy organs in mice bearing breast carcinoma. It should be noted that modified CA NPs are round and appear more solid than non-modified CA NPs. It was reported that on conjugation with gemcitabine, the particle size of CA reduced dramatically to 685 nm, indicating the potential of gemcitabine to mitigate particle size. When modified with biotin-PEG without or with an add-on linker, gemcitabine-loaded CA exhibited particle sizes of 537 and 554 nm, respectively. Data from the protein corona analysis indicated that PEGylation of CA could greatly diminish opsonization. An *in vivo* study in breast tumor-induced mice demonstrated a nearly six-fold rise in the accumulation of gemcitabine in the tumor, reducing off-target distribution in healthy tissues as opposed to the free drug. Moreover, there was evidence of increased blood circulation for PEGylated particles based on high plasma drug concentrations. Thus, modification of CA with PEG was found to successfully enhance their therapeutic effectiveness for targeted drug delivery [149]. Our research group has also developed AZ628 loaded α-ketoglutaric acid-modified CA to decrease the growth of the NPs and improve the cellular internalization and delivery of AZ628 in 4T1 and MCF-7 cell lines. In both cell lines, AZ628 loaded α-ketoglutaric acid-modified CA NPs increased cellular uptake by 21%. The respective NPs might therefore be beneficial in delivering AZ628 to breast cancer cells [150]. Additionally, we evaluated the antitumor efficacy of citrate-modified CA and α-ketoglutaric acid-modified CA in murine breast cancer models. Compared with cyclophosphamide (CYP) alone, the group treated with CYP-loaded α-ketoglutaric acid-modified CA NPs showed a five-fold reduction in tumor growth. In addition, the CYP-loaded NPs accumulated more in the tumor than free CYP. Biodistribution studies showed less accumulation of DOX-loaded NPs in the heart than free DOX, suggesting their effectiveness in attenuating cardiotoxicity in mice. These findings

indicated that both citrate-modified CA and α-ketoglutaric acid-modified CA carriers could prolong the circulation time, increase the antitumor effect, and abate the toxicity of the chemotherapeutic drugs in healthy tissue [148]. In a previous study from our group, Hossain et al. demonstrated that citrate and succinate modified CA NPs could induce more potent delivery of DOX in MCF-7 cells. When compared with succinate modified CA, citrate modified CA exhibited the strongest affinity towards DOX binding. Furthermore, citrate-modified CA improved the cellular internalization in MCF-7 cells and possessed a half-maximal inhibitory concentration, 1000 times lower compared to free DOX [151]. Thus, all these results indicated that the improved pharmacokinetic profile of pH-sensitive CA (through surface modification) might provide a coherent interpretation regarding the enhancement of NP drug delivery.

7.1.4 Hydroxyapatite NPs

One study concerning the surface functionalization of citrate-modified hydroxyapatite (Cit-HA) NPs highlighted the transport of DOX in cancer cells. Due to the electrostatic interaction between DOX's positive charge and Cit-HA's negative charge, DOX encapsulation efficacy increased by approximately 85% (using DOX:Cit-HA ratio = 1:10). Cit-HA NPs showed remarkably low toxicity and improved cellular uptake (substantiated by fluorescence micrographs) in hemolysis and cytotoxicity studies [152]. Likewise, Rodríguez-Ruiz et al. developed citrate-functionalized nanocrystalline apatites (prepared by thermal decomplexation of metastable calcium/citrate/phosphate solutions) in the presence (cAp) or absence (Ap) of carbonate ions to load and deliver DOX. At physiological pH after seven days, cAp-DOX released approximately 42% more DOX than Ap-DOX. Interestingly, in acidic pH, both approaches yielded similar DOX release profiles. The *in vitro* studies displayed the potential of cAp-DOX to selectively internalize, accumulate, and exert significant toxicity in GTL-16 human carcinoma cells. Further, the cAp-DOX was found to be more effective in targeting tumors and enhancing blood circulation time when administered intravenously [153].

7.2 Interaction of drugs, siRNAs, and plasmids with cationic polymer modified inorganic NPs

In cancer therapy, encapsulating NPs with positively charged polymers could improve NP internalization. The coating of hydrophilic molecules like drugs, DNA, and peptides with cationic polymers was expected to aid the encapsulation efficacy and inhibit enzyme degradation of polynucleotides [154].

7.2.1 Interaction with cationic PEI modified NPs

One special cationic polymer is PEI, used primarily to modify inorganic NPs due to their endosomal activity and DNA condensation capacity. In addition, PEI played a crucial role in delivering genes because of their unique buffering capacity (proton sponge effect) to exit the endosomal compartments [155]. Furthermore, PEI's high positive charge density enables the cell membrane's negatively charged components to interact electrostatically with PEI, enabling effective gene delivery through endocytosis [156]. Research, however, shows evidence for different transport mechanisms for cationic PEI, contradicting the hypothesis for the proton sponge effect [157–158]. Various methods have been developed to graft or physically absorb PEI molecules on the surface or into the interior of inorganic NPs. The NPs modified with PEI have many potential functions, enabling the simultaneous delivery of small molecule drugs, nucleic acids (DNA, RNA, and oligonucleotides), and imaging agents to enable effective imaging-guided synergistic drug and gene treatment. Interestingly, gene therapy can be made safer and more effective with this approach [159].

7.2.1.1 MSNs

Inorganic NPs conjugated with PEIhase sparked many research interests in improving cancer treatment. Since PEI have branched structures, facile surface modification is possible, thus making them suitable carriers of siRNAs (*in vitro* and *in vivo*) [160]. Reportedly, in one study, an electrostatic adsorption process was used to load and protect siRNAs inside MSN pores that were modified with hyperbranched polymerized PEI (hbPEI). The PEI-coated siRNA/MSN delivered siRNAs more efficiently and enhanced siRNA uptake in cells compared to unmodified MSNs [155].

Li et al. established siRNA-loaded magnetic MSNs (M-MSNs) with external PEI surface coating, and chemically conjugated fusogenic KALA peptides (contorted as M-MSN_siRNA@PEI-KALA) [161]. Low cytotoxicity was observed for the NPs. Consequently, the NPs could easily

penetrate cells, escape from endolysosomes and release siRNA in the cytosol. The intratumoral injection of M-MSN_VEGFsiRNA@PEI-KALA prevented cancer cell growth *in vivo*, probably by constraining tumor neovascularization [161].

To increase distribution, protect the siRNA, and deliver siRNA to specific sites, a new generation siRNA delivery system was constructed with a PEI-coated MSN core, followed by coating with PEG and an antibody. The construct includes a 47-nm MSN core encased in a crosslinked polyethyleneimine–polyethyleneglycol copolymer containing siRNA targeting the HER2 oncogene in conjunction with trastuzumab (monoclonal antibody against HER2). The construct was designed to extend the half-life of siRNA in the circulation, improve uptake by tumor cells, and enhance siRNA knockdown. However, in HER2+ breast cancer cells, the targeted anti-HER2 NPs trigger cell death, while in HER2− breast cancer cells, they do not. In trastuzumab-resistant HCC1954 xenografts, a single dosage of siHER2-NPs decreased HER2 levels by 60%. Over a three-week period, multiple intravenous doses were found to reduce tumor proliferation significantly. When exposed to human peripheral blood mononuclear cells, the siHER2-NPs exhibited an outstanding safety profile in terms of hemocompatibility and minimal cytokine production. The construct was highly consistent for batch to batch production, and the manufacturing procedures were conducive to large-scale production. Clearly, these siHER2-NPs could be evaluated clinically [54].

One feasible strategy to minimize charge-induced toxicity associated with unmodified PEI was generated by Shen and colleagues, where the MSN pore-functionalized with PEI were grafted on cyclodextrin (CD). The efficacy of CD-PEI-MSNs to release siRNA in MDA-MB-231 breast cancer-bearing xenograft mice models was proven using fluorescently labeled siRNA and *in vivo* imaging. Diffuse fluorescence was observed 6 h after treatment in the targeted cells, possibly due to the release of siRNA from endosomes due to the “proton sponge effect”. The “proton sponge effect” was caused by the polyvalent cationic surface’s ability to buffer, causing salt to influx into the endosomes in an attempt to regulate the correct pH, finally disrupting the endosomal membrane and releasing the siRNA into the cytosol [162].

7.2.1.2 Iron oxide NPs

Tutuianu and coworkers synthesized PEI-coated iron oxide NPs (Fe-PEI) to investigate their antitumor efficacy with cisplatin. Results demonstrated that Fe-PEI NPs loaded with cisplatin could more effectively suppress cancer cell growth (*in vitro* and *in vivo*) than free cisplatin [163]. A similar study reported that coating magnetic iron oxide (MIO) nanoclusters with cationic alkylated PEI (Alkyl-PEI2k) resulted in a biocompatible complex that efficiently delivered siRNAs and silenced the expression of the luciferase gene in 4T1 cells as well as in a fLuc-4T1 xenograft model [164].

Li et al. fabricated PEI-functionalized iron oxide-mesoporous silica yolk–shell nanocapsule (NC) that attached siRNA to the surface electrostatically through interaction with PEI. The vehicle’s “yolk–shell” feature integrated a variety of materials and took advantage of their unique qualities. The mesoporous silica shell’s fluorescence and the iron oxide yolk’s paramagnetism would allow for both fluorescent imaging and magnetic navigation. The PEI-Fe_3O_4@fmSiO_2 yolk–shell NCs, guided by external magnetic fields, was demonstrated to effectively reduce β-actin expression in HeLa cells without exhibiting toxicity typical of PEI [165].

7.2.1.3 CNTs

In an effort to reduce the toxicity and extend the blood circulation period, CNTs were also functionalized with PEI. An example was the non-covalent functionalization of SWCNTs with succinated polyethylenimine (PEI-SA), which delivered siRNA in melanoma-bearing C57BL/6 mice [166]. Gene silencing and significant cellular internalization were found for fluorescent Cy3-labeled siRNA specific to Braf (siBraf). Further, the 25-d application of IS/C/siBraf resulted in a decrease in tumor volume [166]. Wu et al. grafted the multi-walled carbon nanotubes (MWCNTs) with PEI, followed by conjugation with fluorescein isothiocyanate (FITC) and prostate stem cell antigen (PSCA) monoclonal antibody (mAb). The CNT-PEI(FITC)-mAb complex exhibited improved biocompatibility when tested *in vitro* and *in vivo*. Furthermore, ultrasound (US) imaging validated their ability as a contrast agent. In PC-3 tumor-bearing mice, CNT-PEI(FITC)-mAb was found to significantly inhibit tumor growth, demonstrating their vast potential both as contrast agents and drug carriers [167].

7.2.1.4 Au NPs

Especially in cancer therapy, there was a pressing need for

nanoscale gene delivery vehicles to distribute siRNAs. The research group led by Lee et al. demonstrated the controlled production of PEI-coated Au NPs utilizing catechol-conjugated PEI (PEI-C) for siRNA delivery. In aqueous conditions, PEI-C generated spherical multicore micelles, which functioned as reductive templates for the formation and fabrication of spherical Au NPs with tailorable particle size and surface potential due to the reductive nature and hydrophobicity of the conjugated catechol groups. With crosslinking, PEI-C was firmly attached to the surface of crystalline Au seeds, resulting in cationic Au NPs. As a result of the PEI coating on Au NPs, stable siRNA-Au NP complexes were formed, which exhibited a profound effect on suppressing gene expression on tumor cells. The internalization and siRNA unpacking and the effectiveness of gene silencing were observed to depend heavily on the particle size and surface potential of the Au NPs. As a result of the low density of primary amine groups and the lack of uncomplexed PEI fraction in water, the cytotoxicity of PEI-coated AuNPs was exceedingly low [168].

To better understand the effect of particle size on cell transfection efficiency, Au NPs were coupled with PEI, resulting in two sets of PEI-coated Au NPs with particle diameters centered at around 6 nm (< 10 nm Au-PEI NPs) and 70 nm (< 100 nm Au-PEI NPs), respectively. During Au-PEI NPs/DNA complex preparation, plasmids encoding reporter genes or suicide genes were attached to Au-PEI NPs. Human osteosarcoma Saos-2 cells were used to assess the Au-PEI NPs' ability to function as transfection vectors in serum-enriched media. Both Au-PEI NP types were found to be negatively charged in DNA conjugates. Cell uptake was seen for both types of Au-PEI NPs, despite the electrostatic repulsion that exists between the plasmid-conjugated NPs and the cell surface. Complexes formed from < 10 nm Au-PEI NPs transfected cells well; however, complexes derived from < 100 nm Au-PEI NPs did not. The efficacy of the smaller Au-PEI NPs as transfection vectors was connected to their reduced aggregation in cells and DNA escape from endosomes. At the same time, large clumps of NPs associated with DNA were identified in endocytic vesicles incubated with < 100 nm Au-PEI NPs [169].

7.2.1.5 Graphene oxide (GO) NPs

The fact that siRNA silences specific proteins entailed that it could drastically reduce cancer cell's MDR. Among the most prominent anti-apoptotic defense proteins, Bcl-2, was strongly linked to cancer cells' MDR [165]. Using Bcl-2-targeted siRNA to inhibit the expression of Bcl-2 proteins in cancer cells would successfully combat cancer cells' MDR and enable them to be treated more effectively [165]. Zhang et al. delivered Bcl-2-targeted siRNA and the anticancer drug DOX in a sequential manner by functionalizing PEI with graphene oxide (PEI-GO). The PEI-GO was reported to be an ideal nanocarrier for the delivery of siRNA and small molecule drugs. Furthermore, PEI-GO's sequential siRNA and DOX delivery into cancer cells rendered a synergistic impact, resulting in dramatically improved chemotherapeutic efficacy [170].

7.2.2 Interaction with cationic chitosan modified NPs

Among the many therapeutic uses [171–172], chitosan (a polymer with native amine groups derived from chitin) is an attractive candidate for cancer treatment. In light of its intrinsic properties (such as biocompatibility, structural variability, mucoadhesion, biodegradability, non-toxicity, and electrostatic effect, allowing it to combine easily with anionic biomacromolecules such as DNA [173–175]), many studies have been focused on using it with inorganic carriers.

7.2.2.1 MSNs

The study by Gurka et al. regarding the functionalization of MSNs and urokinase plasminogen activator ligand (UPA) with chitosan highlighted their effectivity as a pH-sensitive nanocarrier, delivering the drugs to the tumor's acidic microenvironment [176]. In this study, chitosan was used to enhance drug loading efficiency, and UPA as a plasminogen activator receptor overexpressed in pancreatic cancer cells [176].

Murugan et al. developed a nano-carrier by loading MSN with the topotecan (TPT) drug conjugated with quercetin (QT) on the surface. The poly(acrylic acid) (PAA) and chitosan were used to coat the drug-loaded MSNs, which were attached to arginine-glycine-aspartic acid (cRGD) to target cancer cells, especially breast cancer cells, through integrin receptor-mediated endocytosis. In this study, the disintegration of chitosan elicited the drug release due to the inter-tissue/intracellular pH [177].

The approach of "tumor-triggered targeting" allowed

the development of dual-pH-sensitive anticancer nanocarriers based on chitosan (CHI/MSN) to improve drug efficacy and minimize adverse effects. MSN was loaded with DOX and modified with benzimidazole (Bz). Next, as a "gatekeeper," chitosan-graft-β-cyclodextrin (CHI-g-CD) served to coat the MSN by virtue of the host-guest interaction between β-CD and Bz. Methoxy poly(ethylene glycol) benzaldehyde (mPEG-CHO) was grafted onto CHI via the pH-sensitive benzoic imine bond and subsequently coated with the targeting adamantane-glycine-arginine-glycine-aspartic acid-serine (Ad-GRGDS) peptide. Since PEG provided dynamic protection at pH 7.4, the resultant carriers were considered "stealthy", which was able to expose the shielded targeting peptide and the positive charge of CHI under weakly acidic conditions, resulting in "tumor-triggered targeting". The association between the β-CD and Bz groups within tumor cells could be disrupted by the reduced pH, causing DOX to be released. The tumor-bearing BALB/c mice were randomly assigned to five groups and intravenously treated with PBS (control), DOX, DOX@MSN-CHI-RGD, DOX@MSN-CHI-PEG, and DOX@MSN-CHI-RGD-PEG, respectively, thrice on days 0, 2, and 4. The DOX@MSN-CHI-RGD-PEG containing the targeting peptide inhibited tumor growth more effectively than DOX@MSN-CHI-PEG alone. The mice in the DOX@MSN-CHI-RGD-PEG groups showed the best decreased tumor sizes, with an average tumor weight of around 18.0% than the PBS group. The DOX@MSN-CHI-RGD-PEG was shown to promote apoptosis in cancer cells, reduce tumor development, and diminish DOX cytotoxicity toward normal cells in both *in vitro* and *in vivo* investigations. Thus, the DOX@MSN-CHI-RGD-PEG system was considered to be a viable cancer treatment option [178].

7.2.2.2 Selenium NPs

Due to the short half-life and lethal side effects of TNF-α, its therapeutic usage was significantly curtailed. Yan and colleagues constructed a stable nano-drug named TNF-α-derived polypeptide (P16) coupled, chitosan (CTS)-modified selenium NPs (SC), denoted as SCP, where SC as a slow-release carrier was attached to P16. SCP reduced the proliferation of several types of tumor cells, including DU145 prostate cancer cells. However, RWPE-1 human prostate epithelial cells were not inhibited by SCP. SCP was more potent than P16 and TNF-α in inducing G0/G1 cell-cycle arrest and apoptosis in DU145 cells. SCP demonstrated substantially greater anticancer effects in xenograft models bearing DU145 tumor than P16 or estramustine (a prostate cancer therapeutic drug), with fewer adverse side effects. Additionally, in DU145 xenograft tumors, SCP suppressed cell growth and increased apoptosis. Moreover, SCP's anticancer effects were mediated through p38 MAPK/JNK pathway activation, leading to arrest in G0/G1 cell cycle, along with caspase-responsive cell death, as evidenced by mechanistic investigations. According to these findings, SCP might be a viable method of treating prostate cancer [179].

7.2.2.3 Zinc sulfide (ZnS) NPs

For *in vivo* imaging of oral epithelial carcinoma, the study by Jayasree et al. employed chitosan zinc sulfide:Mn functionalized with mannose (CS-M-ZnS). Physico-chemically stable doped ZnS nanocrystals were exploited as cyto-friendly nanocomplexes with excellent uptake efficiency in cancer regions because of their physico-chemical stability, highly adjustable spectra, and extremely stable fluorescence, which were superior to other heavy metals. The bioconjugated particles were found to be sufficiently stable, with an average size of around 150 nm. The chitosan improved the nanocrystals' biocompatibility and supplied adequate mannosylation functionality. *In vitro* cytotoxicity testing on mouse fibroblast (L929) and oral epithelial carcinoma (KB) cells validated their cytocompatibility. As revealed by KB cells overexpressing mannose receptors, mannose biocon-jugation conferred specificity and selective cellular labeling properties. The combination of these nanocrystals with CS-M resulted in many benefits, including passivating the fluorescent nanocrystals' surface defects, increasing fluorescence emission, and enhancing cancer cell internalization with improved biocompatibility in cancer imaging and human serum, potentially improving cancer diagnosis and prognosis [180].

7.2.2.4 Au NPs

As shown in a study by Manivasagan et al., paclitaxel-loaded-thiol chitosan-layered silica/gold nanoshells conjugated with anti-epidermal growth factor receptor antibodies (anti-EGFR-PTX-TCS-GNSs) were established as theranostics in fluorescence/photoacoustic dual-modal

imaging-guided chemophotothermal synergistic therapy. The resultant nano-complex was 152 nm and had a surface potential of 49 mV. This nano-complex possessed properties including biodegradability, high stability of serum, biosafety, extended circulation, high NIR absorption, excellent photothermal stability, enhanced drug entrapment, effective targeting, and controlled release of drug in cancerous sites when exposed to the laser, providing an ideal platform for NIR laser triggered drug release during combined chemophotothermal therapy with photoacoustic imaging (PAI). In an acidic environment, the nano-complex released drugs three times faster after 48 h of exposure to NIR laser at 808 nm than under normal conditions. The anti-EGFR-PTX-TCS-GNSs + laser irradiation group resulted in 81.9% apoptosis. In comparison, it was 25.45%, 17.15%, and 13.27% for free PTX, PTX-TCSGNSs, and anti-EGFR-PTX-TCS-GNSs, respectively, expressing a significant photothermal therapeutic potency. As compared to all other groups, the anti-EGFR-PTX-TCS-GNSs + laser irradiation group had a 100% survival rate over 34 d. Additionally, after 5 h of treatment with nano-complexes, antibody-decorated conjugate internalization was about four times that of the non-targeted sample, indicating that anti-EGFR-PTX-TCS-GNS was highly internalized via receptors. The intravenous treatment of nano-complexes in breast tumor-bearing nude mice revealed an elevated PA signal (532 nm) of hemoglobin level at the tumor after 6 h in response to intense NIR absorption and dense blood vessels, showing the impressive ability of the nano-complex to aid in tumor detection [181].

7.2.2.5 CaP NPs

In a recent study, a siRNA-loaded chitosan-coated calcium phosphate NP (CS/CaP/siRNA NP) was designed as part of the treatment for cervical cancer. Notably, the nano-precipitation approach was used to generate the CS/CaP/siRNA NPs. The resulting NPs were homogeneously spherical, exhibited a diameter and zeta potential of approximately 194 nm and +27 mV, respectively. It was demonstrated that siEGFR could successively be delivered into Hela cells employing these NPs, resulting in a dramatic reduction of EGFR expression, which was likely due to improved cell adherence of chitosan, allowing greater time for cellular uptake. The internalized CS/CaP/siRNA NPs subsequently displayed pH-responsive NP disintegration, resulting in increased siRNA release and rapid lysosomal escape into the cytoplasm. Furthermore, *in vivo* anticancer studies revealed that the CS/CaP/siRNA NPs could effectively inhibit tumor growth following intratumoral injection in Hela tumor-induced nude mice models, resulting in no significant difference in body weight throughout the experiment. As a result of these findings, the CS/CaP/siRNA NPs offered great potential for mucosal delivery of siRNA in cervical cancer treatment [182].

In another study, Roy et al. used alginate enclosed chitosan-coated calcium phosphate (AEC-CP) nanocarriers to encapsulate Fe_3O_4-bLf (Fe_3O_4-saturated lactoferrin) (NCs). Using xenografts of colon cancer stem cells, the nanoformulation was administered orally to mice injected with triple positive (EpCAM, CD133, CD44) sorted colon cancer stem cells. Tumor regression was found in 70% of mice fed non-targeted (NT) NCs, with 30% of mice experiencing cancer recurrence following 30 d of treatment. However, the reappearance of the tumor was only observed in 10% of mice given Tar (AEC-CP-Fe_3O_4-bLf) NCs, resulting in considerably higher survivability [183].

7.3 Interaction with cationic lipid modified NPs

Cationic lipids are amphiphilic compounds with positive charge that forms positively charged liposomes spontaneously in aqueous solutions, occasionally in conjunction with a neutral helper lipid. These liposomes are primarily used in gene therapy or immunization trials as efficient carriers of DNA, RNA, or proteins [184]. Cationic liposomes, as opposed to neutral or negatively charged liposomes, can effectively interact with negatively charged molecules (for instance, plasmids, mRNAs, nucleic acids, proteins, oligonucleotides, and peptides) primarily through electrostatic attraction [185–187] to promote cellular uptake as well as facilitate nucleic acid delivery [188] and the release of the therapeutics at the desired sites [189]. In addition, these theranostic liposomes can entrap inorganic NPs and can incorporate the nucleic acid therapeutics or drugs inside the hydrophilic core or embed them in the lipophilic bilayer outside [188,190–193]. Figure 7 illustrates the incorporation of drugs or nucleic acids conjugated NPs in liposomes.

By far, the most prominent lipid-based nanocarriers that deliver siRNAs are cationic liposomes. The electrostatic interaction between negatively charged siRNA and

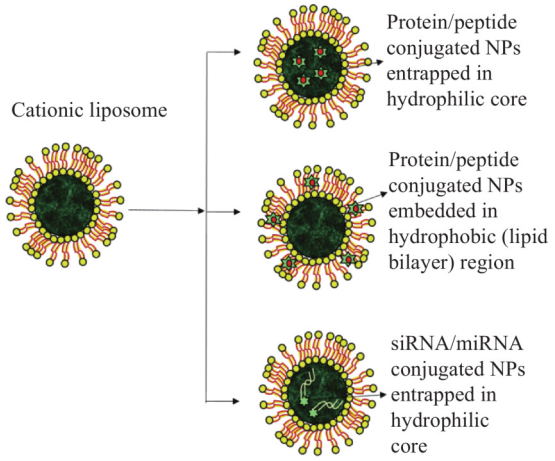

Fig. 7 Incorporation of drugs or nucleic acid conjugated NPs in liposomes. The cationic liposomes can entrap inorganic NPs loaded therapeutics inside the hydrophilic core or embed them in the lipophilic bilayer outside.

cationic lipids is primarily responsible for the loading of siRNA into cationic liposomes. The cationic lipids aid in the penetration within cells and facilitate the escape of particles from endosomes. Some cationic liposomes, such as 1,2-dioleoyl-3-trimethylammonium propane (DOTAP) siRNA, N-(1-[2,3-dioleyloxy]-propyl)-N,N,N-trimethylammonium chloride–siRNA, and Lipofectamine® 2000 (Life Technologies, MD, USA)–siRNA complexes, are frequently employed as delivery vehicles for siRNA [194–195]. However, these complexes generally have a significant charge density at their surfaces, making them interact readily with serum proteins and provoke an immune response, causing their rapid removal from the blood [196].

7.3.1 CaP NPs

Numerous studies have shown that cationic lipid conjugated inorganic drug delivery platforms can effectively treat a variety of cancers. For example, nanosized CaP core coated with a layer of cationic lipid (DOTAP (±)-N,N,N-trimethyl-2,3-bis(z-octadec-9-eneoyloxy)-1-propanaminium chloride), followed by grafting the surface with PEG and anisamide (AA) ligands, played an essential function in particle size and agglomeration control [197]. As a result, a high targetability for sigma receptor-expressing B16F10 melanoma cells was achieved. The respective NPs possessed an average particle size of 40 nm and a surface potential of 25 mV. The CaP core was found to disintegrate and release the entrapped siRNA at lower pH of the endosomes, while the PEG coating improved the gene silencing activity both *in-vitro* and *in-vivo* by protecting genetic materials from nuclease attack. A single intravenous injection of antiluciferase siRNA (0.12 mg siRNA/kg) loaded lipid calcium phosphate (LCP) NPs reduced transcription of the luciferase gene by 78% in metastatic lung tumor-bearing C57BL/6 mice [197]. Interestingly, when siRNAs were formulated against MDM2 (murine double minute 2-oncogene which negatively regulates p53 tumor suppressor protein), c-myc, and vascular endothelial growth factor (VEGF) in the targeted LCP NPs, oncogenes were silenced in metastatic nodules. On treatment, the respective siRNA-loaded NPs significantly dwindled lung metastases by 70%–80% at a relatively low dose (0.36 $mg \cdot kg^{-1}$). In contrast, the control group had no noticeable effect. Furthermore, these targeted LCP NPs were non-toxic, and a 27.8% improvement in the average survival time of the animals was detected when compared with the control group [197]. Reinhardt et al. developed silica NPs exposed quaternary ammonium groups (NPQ+) through chemical surface functionalization and evaluated them in terms of diffuse reflectance infrared Fourier transform (DRIFT), 1H NMR spectroscopies, ζ potential, and light scattering measurements (colloidal stability analysis). A co-sedimentation assay was used to demonstrate the enhanced efficacy of DNA delivery bound to NPQ+ at basic pH. Cryo-electron microscopic (cryo-EM) images demonstrated that in NPQ+/DNA/cationic lipids [1,2-dioleoyl-3-trimethylammonium propane (DOTAP)] ternary complexes, the DNA strands were sandwiched between the NPQ+ surface and the cationic lipid bilayer. The unusual electrostatic colloidal stability of NPQ+ and enhanced DNA binding affinity at high salt concentrations led to the development of a ternary assembly that could modulate these complexes' stability and delivery properties in a physiological environment [198].

7.3.2 Quantum dots (QDs)

Al-Jamal and colleagues investigated the pharmacokinetics of newly designed vesicles containing liposomes and quantum dots (L-QDs) after systemic treatment in nude mice. Hybrid vesicles' serum stability was assessed by measuring turbidity and carboxyfluorescein release following the addition of hydrophobic QDs into various bilayer compositions. Additionally, elements (cadmium) were analyzed in order to determine the blood profile and

tissue accumulation of LQD hybrids. Based on the L-QD lipid bilayer properties, distinct tissue distribution patterns and affinities were detected after intravenous injection. It was found that cationic (DOTAP/DOPE/Chol) hybrids were promptly eliminated from the blood while readily accumulated in lung tissues, but adding PEG to the surface of zwitterionic vesicles considerably extended their blood circulation half-life following systemic distribution. Overall, the L-QD hybrid vesicle system was thought to be a promising platform for QD distribution to various tissues due to the ease with which the hybrid vesicle properties could be modulated. Furthermore, by combining drugs and QDs within the distinct compartments of a single vesicle, L-QD opened up several possibilities for the development of dual therapeutic and imaging (theranostic) approaches [199]. The same research group also demonstrated the fabrication of L-QD bilayer vesicles by incorporating the CdSe/ZnS QDs in the smallest size (2 nm core diameter) into cationic 1,2-dioleoyl-3-trimethylammonium-propane lipid bilayers, which self-assembled into small unilamellar vesicles. The inclusion of QDs occurred as a result of the self-association of hydrophobic molecules within biomembranes, according to the structural characterization of hybrid bilayers containing L-QDs by cryogenic electron microscopy. In lung epithelial cells (A549), L-QD vesicles were found to attach and internalize, as well as evidence of intracellular trafficking was detected by confocal laser scanning microscopy. Furthermore, cationic L-QD vesicles were treated intratumorally in human cervical cancer (C33a) xenografts, improving retention rates. The hybrid L-QD bilayer vesicles were expected to be an effective delivery platform, allowing an extensive range of therapeutic and diagnostic agents to be delivered to cancerous cells [200].

In another study, QDs were functionalized with PEG, then loaded into the hydrophilic core of lipids. The produced cationic f-QD-L was found to heighten cellular internalization in cancer cells. It was revealed that f-QD-L could penetrate deeper into the 3D multicellular spheroids on modification with lipid by layer. Moreover, on intratumoral injection in solid tumor models, f-QD-L stained tumor cells more effectively than f-QD. Thereby, f-QD-L could be regarded as a reliable tumor tracking and imaging agent, both *in vitro* and *in vivo* [201]. Interestingly, Wang et al. developed a multi-functional liposome consisting of a liposome carrier, constituting hydrophilic iron oxide in the inner core, hydrophobic CdSe QDs in phospholipid bilayer, lipid-PEG derivative on the surface, and cRGDyk peptide attached to the distal ends of the lipid-PEG derivative. The *in vitro* analysis of lipid-PEG derivatives demonstrated low toxicity, increased stability, improved phagocytosis resistance, enhanced detection signal, and good tumor targetability. Furthermore, an increase in multi-functional liposome accumulation in the tumor and the liver revealed their efficacy in dual-modality imaging [202].

7.3.3 Iron oxide NPs

In an effort to develop magnetic NP-supported lipid bilayers (SLBs), hydroxylated cationic oxime ether lipid was conjugated with core–shell Fe_3O_4–SiO_2 NPs (SNPs). The following NPs were loaded with DOX or an amphiphilic analog to investigate the efficacy of the respective cationic SLBs in MCF-7 cells. The SLB-drug conjugates (with a dose of 50 μg of SNP/> 5×10^4 cells) could confer extreme toxicity in MCF-7 cells after 2 h of exposure and could readily internalize and accommodate in the cancer cells, thus signifying their ability to act as a magnetic drug carrier [203].

7.3.4 Au NPs

For the intracellular delivery of siRNAs, Kong et al. generated cationic lipid-coated Au NPs (L-AuNP/siRNA). The initial hydrodynamic diameter was slightly higher for L-AuNP/siRNA ((77.3 ± 4.2) nm) as opposed to L-AuNPs ((62.3 ± 7.9) nm). However, a dramatic decrease was observed in the surface potential of L-AuNP/siRNA ((32.2 ± 3.3) mV) compared to L-AuNP ((59.4 ± 4.5) mV), indicating that complexation with siRNA significant mitigated the surface charge. Furthermore, the resultant L-AuNP/siRNA conjugates had less aggregated spherical morphology, as confirmed by atomic force microscopy (AFM) height images. Thus, L-AuNP/siRNA complexes were stable polyelectrolytes generated through electrostatic interactions, which could facilitate their internalization within cells, enhance gene silencing, and impart less toxic effects than PEI (polycationic carrier). Thus, L-AuNPs might be used as a safe and effective intracellular carrier for siRNAs [204].

7.4 Interaction with amine group modified inorganic NPs

Surface modification with amine/amide could catalyze the successful delivery of drugs in the tumor. In particular, the

functionalization of inorganic NPs with amino acids holds great promise. In single amino acids, both the amino- and carboxy-terminals are available for conjugation. In addition to their biocompatibility, they are designed to address the problems that arise with off-target distribution, morphology, size, and uptake by immune cells [205].

7.4.1 Au NPs

Biswas and coworkers reported on the indirect attachment of Thomsen Friedenreich (TF) antigens to Au NPs by conjugating them with two amino acids, serine and threonine [206]. An anti-apoptotic protein known as Gal3 (galectin-3) was bound to the TF antigen. Apoptosis was four times greater in threonine-modified particles compared with serine in Gal3 positive cancer. Possibly, this might be due to the higher threonine conjugation compared to serine [206].

7.4.2 Silver (Ag) NPs

Shi et al. developed citrate-coated AgNPs in the presence of histidine, glycine, and l-cysteine to evaluate the biological fate and toxicity of these NPs [207]. Glycine, which binds Ag^+ with the lowest energy, however, had no discernible impact on transformations and toxicity. The size of AgNPs and the release of Ag^+ were clearly higher when histidine bound to Ag^+ with greater binding energy. The formation of the Ag-histidine complex contributed to a decrease in AgNP cytotoxicity. Additionally, l-cysteine, which had the highest binding energy to Ag^+, completely transformed AgNPs into $[Ag(Cys)_n]^+$ and Ag_2S precipitates, thereby causing the most significant reduction in AgNP toxicity. Consequently, the particles' reduced size and shape cause them to internalize more rapidly, resulting in apoptosis in cancer cells. Hence, NP size and morphology proved to affect the activation of the extrinsic apoptosis pathway [207].

7.4.3 CNTs

To mitigate the adverse effects of DOX and enhance the antitumor effect of DOX-loaded CNTs, DOX-loaded thermo-sensitive liposomes and lysine-modified SWCNTs were used as a drug carriers. The DOX-lysine/SWCNTs exhibited improved drug binding efficacy (86.5% ± 3.7%). The DOX-lysine/SWCNTs could pass through the cell membranes efficiently and exhibited an enhanced antitumor effect on human hepatic cancer (SMMC-7721) cells. The tumor volume was significantly reduced in sarcoma 180-bearing mice with thermo-sensitive liposomes and DOX groups. The inhibition of tumor growth on SMMC-7721 cells and the sarcoma 180-bearing mice was significantly enhanced after treatment with near-infrared laser light at 808 nm. A dramatic rise in body weight, food and water intake, and mental state was noticed in sarcoma 180 tumor-induced mice on DOX-lysine/SWCNTs treatment compared to free DOX. Therefore, DOX-lysine/SWCNTs could be exploited as a potential drug delivery vehicle when coupled with laser irradiation [208].

7.4.4 Se NPs

According to one study, selenium (Se) NPs modified with valine, lysine, and aspartic acid have a more potent anticancer effect [209]. These particles were tested against MCF-7, HeLa, and Hep G2 cells. In comparison to serine and aspartic acid, SeNPs decorated by lysine had greater antitumor potency. The lysine-modified Se particles activated both caspase 8 and caspase 9, resulting in Fas and mitochondria-mediated apoptosis. The rise in ROS might be responsible for activating caspases. Notably, ROS can be induced by lysine, which has two times as many amino functional groups. An increase in apoptosis was also observed when MCF-7 cells were treated with Se modified aspartic acid NPs. Moreover, ROS overproduction induced by Se modified aspartic acid NPs in cancer cells might be responsible for caspase activation and mitochondrial dysfunction. It should be noted that after internalization, the particles resided on the acidic lysosomes, where the amino acids undergo protonation as a result of the acidic pH, generating ROS [209].

7.4.5 Iron oxide NPs

In one study, Yang and colleagues modified iron oxide NPs with histidine-conjugated magnetic poly(amino acid) NPs (H-MPNs) for DOX delivery [210]. The TEM images of H-MPNs and MPNs displayed particle sizes between 40 and 80 nm, respectively. However, according to DLS, the average diameter and the zeta potential of H-MPNs were (99.4 ± 1.6) nm and (+13.6 ± 1.04) mV at pH 7.4, and (133.7 ± 3.7) nm and (+30.9 ± 2.31) mV at pH 5.2, respectively, revealing that conjugated histidine moieties could increase swelling at pH 5.2. The acidic pH in endosomes induced histidine ionization, which released

the DOX. These findings paved the way for further improvement because only 6.8 wt.% of DOX was loaded. To assess the biocompatibility of H-MPNs and the therapeutic effectiveness of DOX-loaded H-MPNs, MTT assays were performed using HeLa cells. H-MPNs and MPNs were treated to HeLa cells with various concentrations, ranging from 0.0625 to 0.25 $mg \cdot mL^{-1}$, and incubated for 24 h. Interestingly, due to their poly(amino acid) shell, neither H-MPNs nor MPNs exhibited toxic effects in high quantities, disclosing their non-toxicity and biocompatibility. However, compared to the DOX-loaded MPNs, the increased cytotoxicity of DOX-loaded H-MPNs was attributed to the greater nuclear penetration of DOX provided by H-MPNs' endosomal escape. Consequently, DOX-loaded H-MPNs were found to be more effective than DOX-loaded MPNs.

Importantly, in GBM, antiangiogenic therapy could cause acute tumor regression, but no improvement in patient survival has been reported. Agemy et al. designed a nanosystem with three properties (CGKRK peptide, ($D[KLAKLAK]_2$) peptide, and iron oxide component), intended to be delivered to the tumor's vascular system. In mice, the iron oxide component of the NPs allowed imaging of GBM tumors. In one GBM mouse model, systemic treatment with NPs effectively prevented tumor development while dramatically slowing tumor growth in another. Additionally, the tumor penetrating peptides injected with the NPs was observed to increase their therapeutic efficacy [211].

7.4.6 Gadolinium oxide nanoparticles (GONs)

To ensure GBM therapeutics with high efficiency (i.e., high-contrast MRI and radiosensitivity of GBM), Shen et al. developed nanomaterials (14 nm) that were highly transportable across the blood-brain barrier (BBB). This was achieved by modifying poly(acrylic acid) (PAA) stabilized extremely small gadolinium oxide nanoparticles (ES-GONs) with reductive bovine serum albumin (rBSA), producing ES-GON-rBSA (which was generated in the water phase initially). RGD dimer (RGD2, Glu-$\{Cyclo[Arg\text{-}Gly\text{-}Asp\text{-}(D\text{-}Phe)\text{-}Lys]\}_2$) and lactoferrin (LF) were then conjugated to ES-GON-rBSA, thereby generating ES-GON-rBSA-LF-RGD2 composite. To demonstrate the BBB transportability, ES-GON-rBSA3-LF-RGD2 was compared with Magnevist via T_1-weighted MR images. It was strongly evident that ES-GON-rBSA3-LF-RGD2 crossed the BBB *in vivo* and had access to brain-enhancing MRI contrast, but Magnevist barely accumulated in the brain at this Gd concentration. Further, ES-GON-rBSA3-LF-RGD2 was investigated *in vivo* for its efficacy against glioblastoma using T_1-weighted MRI. In nude mice bearing U-87 MG tumor, ES-GON-rBSA3-LF-RGD2 was intravenously administered, followed by T_1-weighted MR imaging at different time points after injection. Before intravenous injection, the tumors' MRI signals were very weak, but improved after intravenous administration, peaking 12 h after injection with ES-GON-rBSA3-LF-RGD2. The ES-GON-rBSA-LF-RGD2 was highly biocompatible and could cross the BBB of mice owing to its small size (13.4 nm), as well as LFDD receptor-mediated transcytosis. The results of orthotopic GBM studies confirmed that ES-GON-rBSA3-LF-RGD2 could accumulate in GBM and boost radiotherapy as a radio-sensitizer [212].

7.4.7 MSNs

Taratula et al. modified the MSN surface by conjugating luteinizing hormone-releasing hormone (LHRH, a hormonal decapeptide that releases gonadotropin) through PEG spacer, incorporating the anticancer drugs (DOX and cisplatin), with two forms of siRNA as suppressors of the pump and non-pump cellular resistance. The orthotopic mouse models were used to test the capacity of the MSN-based DDS to achieve local inhalation lung delivery of active components. The local administration of the MSN-based DDS by inhalation resulted in the preferred accumulation of nano-carriers in the lung (73%), which was 14.6 times greater compared to i.v. injection (5%). Thus, MSNs were prevented from entering the systemic circulation and from accumulating in other tissues. Overall, MSN-based DDS per organ was most abundant in the liver (73%), kidneys (15%), and spleen (15%) following i.v. injection (7%). In contrast, the percentage of MSN-based DDS in the liver, kidneys, and spleen after a single inhalation was 17%, 9%, and 1%, respectively [213].

Notably, NPs could be endowed with improved pharmacokinetic profiles when conjugated with peptides motifs. For example, Fei et al. reported on constructing an Arg-Gly-Asp (RGD)-conjugated liposome-hollow silica hybrid (RGD-LP-CHMSN) to deliver and release arsenic trioxide (ATO), whose tumor-targeting effect was hindered by the dose-limited toxicity and pharmacokinetics. In MCF-7, HepG2, and LO2 cells, RGD-LP-CHMSN

exhibited minimal toxicity and excellent biocompatibility. RGD-LP-CHMSN-ATO displayed increased cellular uptake. Moreover, the hybrid demonstrated a reduction in the half-maximal inhibitory concentration (IC_{50}). Based on the pharmacokinetic analysis, the RGD-LP-CHMSN-ATO group demonstrated a 1.7-times increase in half-life and a 2.4-fold rise in area under the curve, compared with the ATO group. Additionally, these nano-vehicles had enhanced the targeting potential of ATO in the H22 tumor xenograft model [214]. Currently, (trialkoxy) silanes with functional groups are commonly used to modify MSN surfaces for attaching various molecules, including siRNAs, target ligands for peptides, and polymers. For example, MSNs modified with (3-mercaptopropyl) trimethoxysilane, treated with 2,2-dipyridyl disulfide, and conjugated with triphenylphosphonium (TPP) antibiotics peptide (KLAKLAK)2 (TPep) were used to produce the desired MSN-TPep [215]. Topotecan (TPT, a topoisomerase inhibitor) in hydrochloride solution could be incorporated into MSN-TPep in PBS by stirring overnight at room temperature to combat ovarian cancer, lung cancer, and others. Micrographs taken by SEM and TEM revealed that the MSNs used in the study exhibited an average particle size of 120 nm and had a monodisperse distribution. DLS data, however, showed a slightly larger particle size with a narrow particle size distribution. With tumor acid-sensitive PEGlated anionic polymer, positively charged MSN-TPep NPs demonstrated rapid entry into the cells (as a result of their attraction to the negatively charged cell membrane), fast elimination from the bloodstream, and enhanced accumulation in tumor [216]. Following that, the NPs were anchored to the poly(ethylene glycol)-blocked-2,3-dimethyl maleic anhydride-modified poly(L-lysine) (PEG-PLL(DMA)) to produce MSN-TPep/PEG-PLL(DMA) NP via electrostatic interactions [215]. The produced MSN-TPep/PEGPLL(DMA) NP demonstrated a surface potential of 212.4 mV. Additionally, the MSN-TPep/PEGPLL(DMA) NPs displayed increased tumor cell internalization, enhanced mitochondrial damage capability, and excellent antitumor efficiency *in vitro*. In addition, conjugation with TPT led to profound tumor growth inhibition [215].

8 Efficacy of drug-loaded inorganic nanocarriers against free drugs

Inorganic NPs are very effective in the treatment of cancer, as demonstrated in the previous sections. Chemotherapeutic agents can be delivered through inorganic NPs, allowing for more efficient drug or gene delivery, while surpassing the limits of chemotherapy [217]. Active and passive targeting, for example, have enhanced the accumulation of drug-loaded nanocarriers in cancer cells rather than in healthy tissues. The modification of inorganic nanocarriers through different strategies and interactions to load therapeutics and imaging agents enhances their effectiveness against cancer cells. Table 1 summarizes the efficacy of a few drugs-loaded inorganic nanocarriers against free drugs [54,58,60,67,69,87,90,96,105,113–114,123,135,138,140, 142, 148,150–151,163,181,208,218–236].

9 Conclusions and future prospects

Advances made to combat the challenges associated with inorganic NPs (including off-target drug distribution, sequential biological barriers, instability in the blood) leverage their use in cancer therapy. The delivery of therapeutic cargos, from proteins to small molecules, peptides and nucleic acids, using inorganic NPs has dramatically improved the translation of emerging therapeutics. Conversely, different interactions or strategies (physical entrapment, ionic interactions, covalent bonding, affinity-based interactions, and intercalation) used to develop and optimize NP-based therapeutic platforms have been adapted to enhance their efficacy in new and pre-existing drug delivery systems. Based on these interactions and approaches, inorganic NP-based therapeutic platforms can have an assortment of modifiable features (including surface properties, size, morphology, and responsiveness) that can be tailored to optimize their performance for targeted delivery. Numerous research is still being conducted on the preconceived ideas of developing different drug delivery systems by modifying inorganic NPs with different conjugates through various interactions. As compared to other interactions, an extremely high affinity is achieved with the affinity (biotin-avidin) interaction as it consists of several hydrogen-hydrophilic bonds. Importantly, ionic interactions to load drugs can pose difficulties in the development of formulations. Drug molecules having $-NH_2$ group, for example, may bind with a $-COOH$ group to produce huge aggregates. Moreover, ionic interactions can be affected by pH, making them unstable in the acidic

Table 1 Comparison of efficacy between drugs and drugs-loaded inorganic nanocarriers

Nanocarrier	Drug	Results with drug loaded nanocarriers *vs.* free drugs	Refs.
PEI/PEG/MSNs	Trastuzumab	In trastuzumab-resistant HCC1954 xenografts, single dosage of siHER2–NPs significantly decreased (60%) HER2 protein levels. Treatment with multiple intravenous doses over three weeks resulted in a marked reduction in tumor growth. Trastuzumab (10 $mg \cdot kg^{-1}$) administered intraperitonially, trastuzumab (5 $mg \cdot kg^{-1}$) injected via tail vein, and trastuzumab (5 $mg \cdot kg^{-1}$) and paclitaxel (3.1 $mg \cdot kg^{-1}$) injected via tail vein showed a reduced efficacy in suppressing tumor progression in HCC1954 tumor-bearing mice.	[54]
C60@Au-PEG	DOX	1. In contrast to the DOX group, C60@Au-PEG/DOX (amide bond), and C60@Au-PEG/DOX (hydrazone bond) exhibited significant levels of DOX in the blood after injection, suggesting that C60@Au-PEG/DOX (amide bond) and C60@Au-PEG/DOX (hydrazone bond) prolonged DOX circulation time in the blood in S180 tumor-induced female BALB/*c* mice. 2. In comparison to DOX, C60@Au-PEG/DOX (amide bond) and C60@Au-PEG/DOX (hydrazone bond) markedly lowered the accumulation of DOX in the heart and spleen, decreasing the adverse effects of DOX on heart and spleen. 3. The relative tumor volume (V/V_0) of DOX was 2.7±0.26 compared to 1.9±0.21 for C_{60}@Au-PEG/DOX, indicating that more DOX could potentially enter the tumor site with C_{60}@Au-PEG.	[69]
PEI-PEG-MSNs	DOX	Dox and P-gp siRNA loaded PEI-PEG-MSNs complex in MCF-7/MDR tumor-bearing xenograft model demonstrated greater accumulation in the tumor as a result of prolonged blood circulation, leading to 80% of tumor growth suppression in comparison to free DOX (17%), MSN-DOX (62%) and P-gp siRNA (0%).	[60]
CPNPs	Cer_{10}	MTS cytotoxicity assay demonstrating dosage responsive cytotoxic actions of Cer_{10}-CPNPs compared to control CPNPs which exhibit modest cytotoxicity at the highest particle number concentration and Cer_{10} in UACC 903 melanoma cells.	[67]
MSN@Gelatin	DOX	For DOX/MSN@Gelatin, a dose-dependent cytotoxicity was recorded (IC_{50} = (17.27±0.63) $\mu g \cdot mL^{-1}$) in Hep-G2 cells, which was higher than that of free DOX. On the contrary, minimal toxicity (IC_{50} > 100 $\mu g \cdot mL^{-1}$) was observed for MSN@Gelatin.	[58]
PEG-SWCNTs	PTX	*In vitro* PTX-PEG-SWCNTs showed higher efficacy in suppressing tumor growth compared to PTX alone in a murine 4T1 breast cancer model, owing to prolonged blood circulation and 10-fold higher tumor PTX uptake by SWNT delivery through enhanced permeability and retention (EPR).	[123]
MSNs-capped MMP9	Cisplatin, Bz	1. Cisplatin and Bz-loaded MSNs capped with MMP9 were found to cause significant cell apoptosis in human tumor cells and mouse and human lung tumors. The lowest cisplatin dose (2 $\mu mol \cdot L^{-1}$) had the most enhanced cytotoxicity, increasing by over 35% in the presence of Bz. It represents an increase in cytotoxic potency of 5- to 10-fold for nontoxic doses of a single drug. These findings demonstrated that cisplatin and Bz delivered together via NPs were additively cytotoxic, enabling a reduction in drug dosage. 2. Kras mutant mouse 3D-LTC treated with free (nonencapsulated) drug(s) induced apoptosis with no distinction between tumorous and nontumorous tissues.	[87]
PEG-CA and biotinylated PEG-fibronectin-CA	Gemcitabine, anastrozole	1. HPLC revealed that cellular uptake of gemcitabine and anastrozole was higher in breast cancer cells for the surface-modified NPs than CA and free drugs. 2. In the cytotoxicity study, surface modified NPs showed greater toxicity than unmodified CA NPs and free gemcitabine and anastrozole. 3. Tumor regression study using surface-modified gemcitabine-encapsulated NPs revealed dramatic shrinkage of tumors compared to free gemcitabine.	[90]
LDH	MTX	The antitumor effects of intact MTX (30 $mg \cdot kg^{-1}$) and MTX-LDH (75 $mg \cdot kg^{-1}$ was equivalent to 30 $mg \cdot kg^{-1}$ MTX) using HOS-bearing xenograft mice models demonstrated that MTX-LDH treated tumors were considerably smaller than intact MTX.	[105]
LDH	5-Fu	The 5-fluorouracil-LDH (5-Fu–LDH) revealed sustained release, prolonged half-life, and increased distribution of 5-Fu in tumors in comparison to free 5-Fu.	[96]
LDH	Mercaptoundecahydro-closo-dodecaborate (BSH) anionic molecules	In biodistribution experiments with xenografted mice, the tumor-to-blood ratio of BSH in the BSH-LDH (boron delivery system) treated group was shown to be 4.4 times greater than in the intact BSH treated group 2 h after drug administration.	[113]
Ferrous ions doped MgAl-LDH (Fe-LDH)	DOX	Tumor growth in 4T1 bearing mice was suppressed following treatment of PTT and chemotherapy with Fe-LDH/DOX compared to free DOX.	[114]
Pt-PEG-GNRs	Cisplatin	In comparison to free cisplatin, cytotoxicity analyses (MTT assay) revealed increased toxicity for cervical cancer HeLa cells, human lung carcinoma A549 cells and human breast adenocarcinoma MCF-7 cells, with IC_{50} values around 9 to 65 fold lower.	[135]
TCL-SPION	DOX	*In vivo* studies showed more significant tumor growth suppression with DOX@TCL-SPIONs than mice treated with 5% glucose, TCL-SPION, DOX (0.64 $mg \cdot kg^{-1}$), and DOX (5 $mg \cdot kg^{-1}$).	[138]
$CaCO_3$	DOX	The *in vitro* chemosensitivity test utilizing MTT, modified neutral red/trypan blue assay, and LDH were used to demonstrate that $CaCO_3$/DOX nanocrystals could mitigate tumor cell growth more than free DOX.	[140]
Mesoporous $CaCO_3$	Etoposide	The MTT assay showed that etoposide-loaded mesoporous $CaCO_3$ inhibited SGC-7901 cells more effectively and lessened the toxic effects of etoposide in HEK 293 T cells compared with free etoposide.	[142]
α-Ketoglutaric acid-modified CA	AZ628 (Raf-kinase inhibitor)	The MTT assay on MCF-7 and 4T1 cells showed that the %cytotoxicity of AZ628-loaded α-KAMCA NPs was substantially greater than that of AZ628-loaded CA NPs, and only AZ628 at similar doses. In MCF-7 and 4T1 cells, AZ628-loaded α-KAMCA NPs displayed around 9% and 12% higher cytotoxicity, respectively, than AZ628-loaded CA NPs, and a 30% greater cytotoxic efficacy compared to free drugs.	[150]
Citrate-modified CA and α-ketoglutaric acid-modified CA	CYP, DOX	1. Compared with CYP alone, the antitumor efficacy of the group treated with CYP-loaded α-ketoglutaric acid-modified CA NPs showed a five-fold reduction in tumor growth in murine breast cancer models. In addition, the CYP-loaded NPs accumulated more in the tumor than free CYP. 2. Biodistribution studies showed less accumulation of DOX-loaded NPs in the heart than free DOX, suggesting their effectiveness in attenuating cardiotoxicity in mice. These findings indicated that both citrate-modified CA and α-ketoglutaric acid-modified CA carriers could prolong the circulation time, increase the antitumor effect, and abate the toxicity of the chemotherapeutic drugs in healthy tissues.	[148]

(*continued*)

Nanocarrier	Drug	Results with drug loaded nanocarriers *vs.* free drugs	Refs.
Citrate-modified CA	DOX	In MCF-7 cells, citrate-modified CA enhanced the cellular uptake and had a half-maximal inhibitory concentration 1000 times lower than free DOX.	[151]
Fe-PEI NPs	Cisplatin	Fe-PEI NPs loaded cisplatin could more effectively suppress cancer cell growth (*in vitro* and *in vivo*) than free cisplatin.	[163]
Anti-EGFR-TCS-GNSs	PTX	In MDA-MB-231 cells, the anti-EGFR-PTX-TCS-GNSs + laser irradiation group induced 81.9% apoptosis. In comparison, the photothermal therapeutic potencies of free PTX, PTX-TCSGNSs, and anti-EGFR-PTX-TCS-GNSs were 25.45%, 17.15%, and 13.27%, respectively. The anti-EGFR-PTX-TCS-GNSs + laser irradiation group demonstrated a 100% survival rate over a period of 34 d, compared to all other groups. In addition, antibody-decorated conjugates uptake was four times than that of non-targeted samples after 5 h of treatment, demonstrating the receptor-mediated internalization of anti-EGFR-PTX-TCS-GNS.	[181]
Lysine/SWCNTs	DOX	The inhibition of tumor growth on SMMC-7721 cells and the sarcoma 180-bearing mice was significantly enhanced after treatment with DOX-lysine/SWCNTs in near-infrared laser light at 808 nm. A dramatic rise in body weight, food and water intake, and mental state was noticed in sarcoma 180 tumor-induced mice on DOX-lysine/SWCNTs treatment compared to free DOX.	[208]
Mn@$CaCO_3$-loaded PD-L1-targeting siRNA	ICG	In Lewis lung cancer cells, Mn@$CaCO_3$/ICG-loaded PD-L1-targeting siRNA increased the PDT effect *in vitro*. Furthermore, *in vivo* tests revealed that this nanoplatform was capable of transporting the cargos to the tumor and inhibit tumor growth more efficiently than free ICG.	[218]
PEI/PEG/MSNs	DOX	Using near-infrared fluorescence imaging and elemental Si analysis, the human squamous carcinoma xenografts in nude mice after intravenous injection revealed passive accumulation of 12% of the tail vein-injected PEI/PEG/MSNs at the tumour site, indicating successful cellular internalization and DOX delivery to KB-31 cells. The resultant NPs showed apoptosis and tumor shrinkage that was greater than that of free DOX.	[219]
F-FMSNs	CPT	In tumor regression study using nude mice induced with MCF-7 cells, administration of CPT suppressed tumor growth by 14% at the end of the study (the 68th day) compared to control, indicating that it is an efficient tumor-suppressing agent when dissolved in DMSO. In contrast, from day 48 on, the average tumor volumes in groups treated with CPT-loaded FMSN or CPT-loaded F-FMSN continued to decrease at a faster rate.	[220]
ZnO-Au-PLA-GPPS-FA-1 and ZnO-Au-PLA-GPPS-FA-2	CPT	The CPT-loaded nanocarriers were more cytotoxic to Hela cells at the same concentration of up to 75 $\mu g \cdot mL^{-1}$ for ZnO-Au-PLA-GPPS-FA-1 and ZnO-Au-PLA-GPPS-FA-2 nanocarriers, containing about 4.7 and 6.5 $\mu g \cdot mL^{-1}$ free CPT in both systems, respectively. Despite the same levels of CPT, the inhibition rates of the CPT-loaded nanocarriers were greater than those of the free CPT.	[221]
ZnO	DOX	The cytotoxicity study showed that DOX-loaded ZnO NPs had a greater anticancer effect than either blank ZnO NPs or DOX alone.	[222]
LDH	RH	The MTT assay reveals that RH-LDHs delivered drugs more effectively to cancer cells cancer cells compared to pure RH due to pure RH's poor bioavailability.	[223]
LDH	MTX	The half maximal inhibitory concentration of MTX-LDH (48 h) suggested that MTX-LDH had improved efficacy and sensitivity in human colon cancer cells HCT-116. In comparison, naked MTX took 72 h to achieve similar outcomes.	[224]
Carboxylate-modified MgAl LDH	Cisplatin	The anti-proliferative effect of cisplatin-conjugated carboxylate-modified MgAl LDH on colon cancer cell lines was stronger than that of the free drug, according to *in vivo* data.	[225]
NaCa-LDH	DAC	On malignant (A-375) melanoma and breast cancer (MCF-7) cell lines, the anticancer activity of DAC-NaCa-LDH is higher than that of free DAC.	[226]
PLGA-coated MgAl LDH (PLGA-LDH)	MTX	Greater therapeutic efficacy was observed with PLGA-LDH-MTX than that of the bare MTX, according to *in vitro* and *in vivo* experiments.	[227–228]
FA-modified nanocarrier based on the self-assembly of delaminated CoAl LDH and MnO_2	DOX, PTX	Based on both *in vitro* cytotoxicity studies and a xenograft tumor model of hepatoma, this nanocarrier was more effective in fighting cancer than either the free drugs alone or the corresponding cocktail solutions.	[229]
GE11-Se NPs	Ori	GE11-Ori-Se NPs caused a larger level of ROS in KYSE-150 cells than oridonin or Chi-Se NPs, implying that the combination of Chi-Se NPs and oridonin synergistically increased intracellular ROS levels in KYSE-150 cells, increasing the anticancer activity.	[230]
FA-QD	DOX	1. Fluorescence microscopy and the MTT assay revealed that the folate-targeted DOX-QD NPs exhibit greater toxic effects than non-targeted NPs and the free DOX, demonstrating their preferential accumulation in 4T1 and MCF-7 cells *in vitro*. 2. The *in vivo* tumor inhibitory impact of FA-QD-DOX NPs revealed that the targeted formulation outperformed the non-targeted formulation and free DOX in terms of therapeutic efficacy.	[231]
Herceptin coupled Au-Fe_3O_4 NPs (Au-Fe_3O_4-Herceptin)	Cisplatin	The platin-Au-Fe_3O_4-Herceptin NPs serve as nanocarriers for the targeted delivery of platin into Her2-positive breast cancer cells (Sk-Br3). The half-maximal inhibitory concentration (IC_{50}) of platin-Au-Fe_3O_4-Herceptin NPs against Sk-Br3 cells is 1.76 μg of Pt/mL, which is significantly less than the 3.5 $\mu g \cdot mL^{-1}$ required for cisplatin.	[232]
Au NPs with a PEG spacer linked via an acid-labile linkage (DOX-Hyd@AuNPs)	DOX	When compared to free DOX, DOX-Hyd@AuNPs boosted drug accumulation and retention in multidrug-resistant MCF-7/ADR cancer cells, resulting in higher toxicity and greater apoptosis in MCF-7/ADR cancer cells.	[233]
MSA-capped gold nanoconstructs loaded with SMI#9 (Rad6 protein inhibitor)	Cisplatin	*In vitro*, the effective dose of cisplatin required to suppress the development of 50% of cancer cells (4.9 $\mu mol \cdot L^{-1}$) was about five times lower than free cisplatin (> 25 $\mu mol \cdot L^{-1}$).	[234]
Calcium phosphate-polymer hybrid with inhibitors for microRNA-221 and microRNA-222	pac	MTS assay was used to evaluate the cytotoxic efficacy of pac-encapsulated NPs (NP(pac)), co-delivery NPs (NP(pac/miRi) or NP(pac/miRi NC)), and free pac in MDA-MB-231 cells after 72 h. The difference between the encapsulated form (NP(pac)) and the free form of pac in terms of cell viability was small. At a high dosage of 0.67 $\mu g \cdot mL^{-1}$, pac reduced cell viability by 40%. At the same dosage of 0.67 $\mu g \cdot mL^{-1}$, the cell viability of NP(pac/miRi) decreased by 80%. The cytotoxicity evaluation at a broader range of concentrations demonstrated that the NP(pac/miRi) only needed 1% of the pac in the free form to produce the same cytotoxicity (around 80%).	[235]

(*continued*)

Nanocarrier	Drug	Results with drug loaded nanocarriers *vs.* free drugs	Refs.
PEGylated Au NP	Pc 4	The *in vivo* drug delivery period for PDT has been lowered to less than 2 h with the Au NP-Pc 4 conjugates, compared to 2 d with the free Pc 4 conjugates.	[236]

tumor microenvironment. Despite these shortcomings, ionic interactions involving surface modification of NPs with amine/amide groups, cationic macromolecules (polymers, lipids), or Ca-doped, CaP, $CaCO_3$ particles for complexation of therapeutics provide the impetus for targeted drug delivery. Incorporating therapeutics into porous NPs or intercalating NP-based platforms through co-precipitation or anion-exchange reactions (e.g., LDHs) can improve gene and drug delivery. As opposed to physical encapsulation, covalent bonding offers manifest advantages, including the ability to increase therapeutic efficacy, enhance drug residence in the body, improve biodistribution, decrease release times, and alleviate systemic toxicity. Therefore, the covalent functionalization of NPs plays an imperative role in delivering and releasing payloads at the site of the lesion. Even though surface charge on cationic polymer-based or lipid-based NPs may enhance their uptake by cells [154], these drug delivery systems tend to aggregate, lose stability and become toxicity-prone and are eliminated by MPS. It is believed that the need for large dosages of drug-loaded particles to render therapeutic doses is the primary determinant for the distribution of positively charged NPs in MPS organs, leading to the clustering of cationic NPs. It is true that cationic polymer or lipid-based NPs themselves do not pose any harm, but they are capable of causing emboli in the lungs when agglomerated [154]. The superior interaction between negatively charged biological membranes and cationic polymer or lipid-based NPs may prove to be inconvenient since the particles and erythrocyte membrane exhibit the same pronounced affinity [237]. Notably, a related event is the accelerated opsonization and macrophage absorption of cationic particles in the circulation [238–239]. To ensure extended circulation, it is essential that the particles must be as tiny and neutral as feasible.

In order to effectively deliver therapeutic and imaging molecules to the site of action, more *in vitro* research and explanations, as well as accurate noninvasive monitoring (over time), are required for the efficacy of the NP platforms (prepared through these approaches or interactions). Therefore, a more in-depth analysis of NP design based on these approaches or interactions, and a more detailed investigation on the NPs' fate within the body, is necessary to improve the specificity of these claims. In addition, small animal models are often the primary preclinical models for clinical studies, which further complicates this issue since they cannot accurately represent humans. Therefore, it is imperative to address and overcome these limitations and evaluate safety profiles, screen therapeutic efficacy, and apply stringent controls during the development phase of clinical trials in cancer treatment.

As highlighted in this review, the unprecedented effects of different strategies or interactions (such as physical entrapment into porous/hollow nanostructures, ionic interactions with native and surface-modified NPs, covalent bonding, affinity-based interactions, and intercalation through co-precipitation or anion exchange reaction) to load therapeutics in modified/unmodified inorganic NPs have shown distinct advantages over other conventional NP-based drug delivery systems. Moreover, the change of physicochemical characteristics resulting from these approaches is the mainstay for improved pharmacokinetic parameters (such as reduced indiscriminate tissue distributions, longer blood-residence times, lower drug-related toxicity, etc.), which elucidate the designing of innovative drug delivery platforms for site-specific delivery. Although most of the pre-existing NP-based drug delivery platforms have been unsuccessful in their clinical translation, there is still hope of establishing new promising platforms in the near future for treating cancer.

Authors' contributions S.T.H. performed the writing of the manuscript, designing of figures, and prepared the initial draft of the manuscript; M.M.B.H. reviewed and edited the manuscript; E.H.C. provided valuable guidance and edited the manuscript. All authors have read and agreed to the final version of the manuscript.

Disclosure of potential conflicts of interests The authors declare no conflict of interest in the content of this work.

Funding note Open Access funding enabled and organized by CAUL and its Member Institutions.

References

[1] Wang G, Chen Y, Wang P, et al. Preferential tumor accumulation and desirable interstitial penetration of poly(lactic-co-glycolic acid) nanoparticles with dual coating of chitosan oligosaccharide and polyethylene glycol-poly(D,L-lactic acid). Acta Biomaterialia, 2016, 29: 248–260

[2] Laha D, Pramanik A, Chattopadhyay S, et al. Folic acid modified copper oxide nanoparticles for targeted delivery in *in vitro* and *in vivo* systems. RSC Advances, 2015, 5(83): 68169–68178

[3] Williams J, Lansdown R, Sweitzer R, et al. Nanoparticle drug delivery system for intravenous delivery of topoisomerase inhibitors. Journal of Controlled Release, 2003, 91(1–2): 167–172

[4] Leroux J C, Allémann E, De Jaeghere F, et al. Biodegradable nanoparticles — from sustained release formulations to improved site specific drug delivery. Journal of Controlled Release, 1996, 39(2–3): 339–350

[5] Gupta S, Gupta M K. Possible role of nanocarriers in drug delivery against cervical cancer. Nano Reviews & Experiments, 2017, 8(1): 1335567

[6] Nguyen K T. Targeted nanoparticles for cancer therapy: promises and challenge. Journal of Nanomedicine & Nanotechnology, 2011, 2(5): 103e

[7] Ky K. Nanotechnology platforms and physiological challenges for cancer therapeutic. Nanomedicine, 2007, 3: 103–110

[8] Foroozandeh P, Aziz A A. Insight into cellular uptake and intracellular trafficking of nanoparticles. Nanoscale Research Letters, 2018, 13(1): 339

[9] Haque S T, Islam R A, Gan S H, et al. Characterization and evaluation of bone-derived nanoparticles as a novel pH-responsive carrier for delivery of doxorubicin into breast cancer cells. International Journal of Molecular Sciences, 2020, 21(18): 6721

[10] Moghimi S M, Hunter A C, Murray J C. Long-circulating and target-specific nanoparticles: theory to practice. Pharmacological Reviews, 2001, 53(2): 283–318

[11] Huang H C, Barua S, Sharma G, et al. Inorganic nanoparticles for cancer imaging and therapy. Journal of Controlled Release, 2011, 155(3): 344–357

[12] Haque S T, Chowdhury E H. Recent progress in delivery of therapeutic and imaging agents utilizing organic-inorganic hybrid nanoparticles. Current Drug Delivery, 2018, 15(4): 485–496

[13] Haque S T, Karim M E, Othman I, et al. Mitigating off-target distribution and enhancing cytotoxicity in breast cancer cells with alpha-ketoglutaric acid-modified Fe/Mg-CA nanoparticles. Journal of Pharmaceutical Investigation, 2022, 52(3): 367–386

[14] Anselmo A C, Mitragotri S. Nanoparticles in the clinic: an update. Bioengineering & Translational Medicine, 2019, 4(3): e10143

[15] Mitchell M J, Billingsley M M, Haley R M, et al. Engineering precision nanoparticles for drug delivery. Nature Reviews Drug Discovery, 2021, 20(2): 101–124

[16] Chen Y, Xue Z, Zheng D, et al. Sodium chloride modified silica nanoparticles as a non-viral vector with a high efficiency of DNA transfer into cells. Current Gene Therapy, 2003, 3(3): 273–279

[17] Xu Z P, Zeng Q H, Lu G Q, et al. Inorganic nanoparticles as carriers for efficient cellular delivery. Chemical Engineering Science, 2006, 61(3): 1027–1040

[18] Garnett M C. Gene-delivery systems using cationic polymers. Critical Reviews™ in Therapeutic Drug Carrier Systems, 1999, 16(2): 147–207

[19] Wang F, Li C, Cheng J, et al. Recent advances on inorganic nanoparticle-based cancer therapeutic agents. International Journal of Environmental Research and Public Health, 2016, 13(12): 1182

[20] Jokerst J V, Lobovkina T, Zare R N, et al. Nanoparticle PEGylation for imaging and therapy. Nanomedicine, 2011, 6(4): 715–728

[21] Byrne J D, Betancourt T, Brannon-Peppas L. Active targeting schemes for nanoparticle systems in cancer therapeutics. Advanced Drug Delivery Reviews, 2008, 60(15): 1615–1626

[22] Yang G, Sun X, Liu J, et al. Light-responsive, singlet-oxygen-triggered on-demand drug release from photosensitizer-doped mesoporous silica nanorods for cancer combination therapy. Advanced Functional Materials, 2016, 26(26): 4722–4732

[23] Zhang Z, Wang J, Nie X, et al. Near infrared laser-induced targeted cancer therapy using thermoresponsive polymer encapsulated gold nanorods. Journal of the American Chemical Society, 2014, 136(20): 7317–7326

[24] Ye Y Q, Yang F L, Hu F Q, et al. Core-modified chitosan-based polymeric micelles for controlled release of doxorubicin. International Journal of Pharmaceutics, 2008, 352(1–2): 294–301

[25] Ye Y Q, Yang F L, Hu F Q, et al. Core-modified chitosan-based polymeric micelles for controlled release of doxorubicin.

International Journal of Pharmaceutics, 2008, 352(1–2): 294–301

[26] Maier-Hauff K, Ulrich F, Nestler D, et al. Efficacy and safety of intratumoral thermotherapy using magnetic iron-oxide nanoparticles combined with external beam radiotherapy on patients with recurrent glioblastoma multiforme. Journal of Neuro-Oncology, 2011, 103(2): 317–324

[27] Berry C C, Wells S, Charles S, et al. Dextran and albumin derivatised iron oxide nanoparticles: influence on fibroblasts *in vitro*. Biomaterials, 2003, 24(25): 4551–4557

[28] Gupta A K, Curtis A S. Lactoferrin and ceruloplasmin derivatized superparamagnetic iron oxide nanoparticles for targeting cell surface receptors. Biomaterials, 2004, 25(15): 3029–3040

[29] Gupta A K, Gupta M. Cytotoxicity suppression and cellular uptake enhancement of surface modified magnetic nanoparticles. Biomaterials, 2005, 26(13): 1565–1573

[30] Masood F. Polymeric nanoparticles for targeted drug delivery system for cancer therapy. Materials Science and Engineering C, 2016, 60: 569–578

[31] Drummond D C, Meyer O, Hong K, et al. Optimizing liposomes for delivery of chemotherapeutic agents to solid tumors. Pharmacological Reviews, 1999, 51(4): 691–743

[32] Shmeeda H, Amitay Y, Tzemach D, et al. Liposome encapsulation of zoledronic acid results in major changes in tissue distribution and increase in toxicity. Journal of Controlled Release, 2013, 167(3): 265–275

[33] Hadjipanayis C G, Machaidze R, Kaluzova M, et al. EGFRvIII antibody-conjugated iron oxide nanoparticles for magnetic resonance imaging-guided convection-enhanced delivery and targeted therapy of glioblastoma. Cancer Research, 2010, 70(15): 6303–6312

[34] El-Sayed I H, Huang X, El-Sayed M A. Surface plasmon resonance scattering and absorption of anti-EGFR antibody conjugated gold nanoparticles in cancer diagnostics: applications in oral cancer. Nano Letters, 2005, 5(5): 829–834

[35] Khan M A, Singh D, Ahmad A, et al. Revisiting inorganic nanoparticles as promising therapeutic agents: a paradigm shift in oncological theranostics. European Journal of Pharmaceutical Sciences, 2021, 164: 105892

[36] Scicluna M C, Vella-Zarb L. Evolution of nanocarrier drug-delivery systems and recent advancements in covalent organic framework-drug systems. ACS Applied Nano Materials, 2020, 3(4): 3097–3115

[37] Bharti C, Nagaich U, Pal A K, et al. Mesoporous silica nanoparticles in target drug delivery system: a review. International Journal of Pharmaceutical Investigation, 2015, 5(3): 124–133

[38] Song S W, Hidajat K, Kawi S. Functionalized SBA-15 materials as carriers for controlled drug delivery: influence of surface properties on matrix-drug interactions. Langmuir, 2005, 21(21): 9568–9575

[39] Varga N, Benkő M, Sebők D, et al. Mesoporous silica core–shell composite functionalized with polyelectrolytes for drug delivery. Microporous and Mesoporous Materials, 2015, 213: 134–141

[40] Wang Y, Zhao Q, Han N, et al. Mesoporous silica nanoparticles in drug delivery and biomedical applications. Nanomedicine: Nanotechnology, Biology, and Medicine, 2015, 11(2): 313–327

[41] Xiong L, Du X, Shi B, et al. Tunable stellate mesoporous silica nanoparticles for intracellular drug delivery. Journal of Materials Chemistry B: Materials for Biology and Medicine, 2015, 3(8): 1712–1721

[42] Karimi M, Zangabad P S, Ghasemi A, et al. Chapter 7: Nanotoxicology and future scope for smart nanoparticles. In: Karimi M, Zangabad P S, Ghasemi A, et al., eds. Smart External Stimulus-Responsive Nanocarriers for Drug and Gene Delivery. Morgan & Claypool Publishers, 2015

[43] Asefa T, Tao Z. Biocompatibility of mesoporous silica nanoparticles. Chemical Research in Toxicology, 2012, 25(11): 2265–2284

[44] Wang N, Cheng X, Li N, et al. Nanocarriers and their loading strategies. Advanced Healthcare Materials, 2019, 8(6): 1801002

[45] Lu J, Liong M, Zink J I, et al. Mesoporous silica nanoparticles as a delivery system for hydrophobic anticancer drugs. Small, 2007, 3(8): 1341–1346

[46] Tang L, Cheng J. Nonporous silica nanoparticles for nanomedicine application. Nano Today, 2013, 8(3): 290–312

[47] Corbalan J J, Medina C, Jacoby A, et al. Amorphous silica nanoparticles aggregate human platelets: potential implications for vascular homeostasis. International Journal of Nanomedicine, 2012, 7: 631–639

[48] Chen F, Hong H, Zhang Y, et al. *In vivo* tumor targeting and image-guided drug delivery with antibody-conjugated, radiolabeled mesoporous silica nanoparticles. ACS Nano, 2013, 7(10): 9027–9039

[49] Karimi M, Eslami M, Sahandi-Zangabad P, et al. pH-Sensitive stimulus-responsive nanocarriers for targeted delivery of therapeutic agents. Wiley Interdisciplinary Reviews: Nanomedicine and Nanobiotechnology, 2016, 8(5): 696–716

[50] Karimi M, Sahandi-Zangabad P, Ghasemi A, et al. Temperature-responsive smart nanocarriers for delivery of therapeutic agents: applications and recent advances. ACS Applied Materials & Interfaces, 2016, 8(33): 21107–21133

[51] Rosenholm J M, Meinander A, Peuhu E, et al. Targeting of porous hybrid silica nanoparticles to cancer cells. ACS Nano,

2009, 3(1): 197–206

[52] Karaman D S, Desai D, Senthilkumar R, et al. Shape engineering vs organic modification of inorganic nanoparticles as a tool for enhancing cellular internalization. Nanoscale Research Letters, 2012, 7(1): 358

[53] Xia T, Kovochich M, Liong M, et al. Polyethyleneimine coating enhances the cellular uptake of mesoporous silica nanoparticles and allows safe delivery of siRNA and DNA constructs. ACS Nano, 2009, 3(10): 3273–3286

[54] Ngamcherdtrakul W, Morry J, Gu S, et al. Cationic polymer modified mesoporous silica nanoparticles for targeted siRNA delivery to HER2+ breast cancer. Advanced Functional Materials, 2015, 25(18): 2646–2659

[55] Wang Y, Cui Y, Huang J, et al. Redox and pH dual-responsive mesoporous silica nanoparticles for site-specific drug delivery. Applied Surface Science, 2015, 356: 1282–1288

[56] Radu D R, Lai C Y, Jeftinija K, et al. A polyamidoamine dendrimer-capped mesoporous silica nanosphere-based gene transfection reagent. Journal of the American Chemical Society, 2004, 126(41): 13216–13217

[57] Kar M, Tiwari N, Tiwari M, et al. Poly-L-arginine grafted silica mesoporous nanoparticles for enhanced cellular uptake and their application in DNA delivery and controlled drug release. Particle & Particle Systems Characterization, 2013, 30(2): 166–179

[58] Zou Z, He D, He X, et al. Natural gelatin capped mesoporous silica nanoparticles for intracellular acid-triggered drug delivery. Langmuir, 2013, 29(41): 12804–12810

[59] Park I Y, Kim I Y, Yoo M K, et al. Mannosylated polyethylenimine coupled mesoporous silica nanoparticles for receptor-mediated gene delivery. International Journal of Pharmaceutics, 2008, 359(1–2): 280–287

[60] Meng H, Mai W X, Zhang H, et al. Codelivery of an optimal drug/siRNA combination using mesoporous silica nanoparticles to overcome drug resistance in breast cancer *in vitro* and *in vivo*. ACS Nano, 2013, 7(2): 994–1005

[61] Jang M, Yoon Y I, Kwon Y S, et al. Trastuzumab-conjugated liposome-coated fluorescent magnetic nanoparticles to target breast cancer. Korean Journal of Radiology, 2014, 15(4): 411–422

[62] Sun Q, You Q, Wang J, et al. Theranostic nanoplatform: triple-modal imaging-guided synergistic cancer therapy based on liposome-conjugated mesoporous silica nanoparticles. ACS Applied Materials & Interfaces, 2018, 10(2): 1963–1975

[63] Wei W, Ma G H, Hu G, et al. Preparation of hierarchical hollow $CaCO_3$ particles and the application as anticancer drug carrier. Journal of the American Chemical Society, 2008, 130(47): 15808–15810

[64] Ueno Y, Futagawa H, Takagi Y, et al. Drug-incorporating calcium carbonate nanoparticles for a new delivery system. Journal of Controlled Release, 2005, 103(1): 93–98

[65] Chen S, Zhao D, Li F, et al. Co-delivery of genes and drugs with nanostructured calcium carbonate for cancer therapy. RSC Advances, 2012, 2(5): 1820–1826

[66] Wang J, Chen J S, Zong J Y, et al. Calcium carbonate/carboxymethyl chitosan hybrid microspheres and nanospheres for drug delivery. The Journal of Physical Chemistry C, 2010, 114(44): 18940–18945

[67] Kester M, Heakal Y, Fox T, et al. Calcium phosphate nanocomposite particles for *in vitro* imaging and encapsulated chemotherapeutic drug delivery to cancer cells. Nano Letters, 2008, 8(12): 4116–4121

[68] Bae K H, Lee K, Kim C, et al. Surface functionalized hollow manganese oxide nanoparticles for cancer targeted siRNA delivery and magnetic resonance imaging. Biomaterials, 2011, 32(1): 176–184

[69] Shi J, Chen Z, Wang L, et al. A tumor-specific cleavable nanosystem of PEG-modified C60@Au hybrid aggregates for radio frequency-controlled release, hyperthermia, photodynamic therapy and X-ray imaging. Acta Biomaterialia, 2016, 29: 282–297

[70] Chen S, Zhao X, Chen J, et al. Mechanism-based tumor-targeting drug delivery system. Validation of efficient vitamin receptor-mediated endocytosis and drug release. Bioconjugate Chemistry, 2010, 21(5): 979–987

[71] Pardridge W M, Boado R J. Enhanced cellular uptake of biotinylated antisense oligonucleotide or peptide mediated by avidin, a cationic protein. FEBS Letters, 1991, 288(1–2): 30–32

[72] Zeng X, Sun Y X, Zhang X Z, et al. Biotinylated disulfide containing PEI/avidin bioconjugate shows specific enhanced transfection efficiency in HepG2 cells. Organic & Biomolecular Chemistry, 2009, 7(20): 4201–4210

[73] Wojda U, Goldsmith P, Miller J L. Surface membrane biotinylation efficiently mediates the endocytosis of avidin bioconjugates into nucleated cells. Bioconjugate Chemistry, 1999, 10(6): 1044–1050

[74] Rosebrough S F. Pharmacokinetics and biodistribution of radiolabeled avidin, streptavidin and biotin. Nuclear Medicine and Biology, 1993, 20(5): 663–668

[75] Schechter B, Silberman R, Arnon R, et al. Tissue distribution of avidin and streptavidin injected to mice — effect of avidin carbohydrate, streptavidin truncation and exogenous biotin. European Journal of Biochemistry, 1990, 189(2): 327–331

[76] Yao Z, Zhang M, Sakahara H, et al. Avidin targeting of intraperitoneal tumor xenografts. Journal of the National Cancer Institute, 1998, 90(1): 25–29

[77] González M, Argaraña C E, Fidelio G D. Extremely high thermal stability of streptavidin and avidin upon biotin binding. Biomolecular Engineering, 1999, 16(1–4): 67–72

[78] Elia G. Biotinylation reagents for the study of cell surface proteins. Proteomics, 2008, 8(19): 4012–4024

[79] Jain A, Cheng K. The principles and applications of avidin-based nanoparticles in drug delivery and diagnosis. Journal of Controlled Release, 2017, 245: 27–40

[80] Hoya K, Guterman L R, Miskolczi L, et al. A novel intravascular drug delivery method using endothelial biotinylation and avidin-biotin binding. Drug Delivery, 2001, 8(4): 215–222

[81] Singh N P, Yolcu E S, Askenasy N, et al. ProtEx: a novel technology to display exogenous proteins on the cell surface for immunomodulation. Annals of the New York Academy of Sciences, 2005, 1056(1): 344–358

[82] Nguyen T T, Sly K L, Conboy J C. Comparison of the energetics of avidin, streptavidin, neutrAvidin, and anti-biotin antibody binding to biotinylated lipid bilayer examined by second-harmonic generation. Analytical Chemistry, 2012, 84(1): 201–208

[83] Artemov D, Mori N, Okollie B, et al. MR molecular imaging of the Her-2/neu receptor in breast cancer cells using targeted iron oxide nanoparticles. Magnetic Resonance in Medicine, 2003, 49(3): 403–408

[84] Yan C, Wu Y, Feng J, et al. Anti-αvβ3 antibody guided three-step pretargeting approach using magnetoliposomes for molecular magnetic resonance imaging of breast cancer angiogenesis. International Journal of Nanomedicine, 2013, 8: 245–255

[85] Barve A, Jain A, Liu H, et al. An enzyme-responsive conjugate improves the delivery of a PI3K inhibitor to prostate cancer. Nanomedicine: Nanotechnology, Biology, and Medicine, 2016, 12(8): 2373–2381

[86] Steinbach J M, Seo Y E, Saltzman W M. Cell penetrating peptide-modified poly(lactic-co-glycolic acid) nanoparticles with enhanced cell internalization. Acta Biomaterialia, 2016, 30: 49–61

[87] van Rijt S H, Bölükbas D A, Argyo C, et al. Protease-mediated release of chemotherapeutics from mesoporous silica nanoparticles to *ex vivo* human and mouse lung tumors. ACS Nano, 2015, 9(3): 2377–2389

[88] Oliveri V, D'Agata R, Giglio V, et al. Cyclodextrin-functionalised gold nanoparticles via streptavidin: a supramolecular approach. Supramolecular Chemistry, 2013, 25(8): 465–473

[89] Barth B M, Sharma R, Altinoğlu E I, et al. Bioconjugation of calcium phosphosilicate composite nanoparticles for selective targeting of human breast and pancreatic cancers *in vivo*. ACS Nano, 2010, 4(3): 1279–1287

[90] Mozar F S, Chowdhury E H. Surface-modification of carbonate apatite nanoparticles enhances delivery and cytotoxicity of gemcitabine and anastrozole in breast cancer cells. Pharmaceutics, 2017, 9(2): 21

[91] Bajaj P, Mikoryak C, Wang R, et al. A carbon nanotube-based Raman-imaging immunoassay for evaluating tumor targeting ligands. Analyst, 2014, 139(12): 3069–3076

[92] Lai G, Wu J, Ju H, et al. Streptavidin-functionalized silver-nanoparticle-enriched carbon nanotube tag for ultrasensitive multiplexed detection of tumor markers. Advanced Functional Materials, 2011, 21(15): 2938–2943

[93] Cotí K K, Belowich M E, Liong M, et al. Mechanised nanoparticles for drug delivery. Nanoscale, 2009, 1(1): 16–39

[94] Ladewig K, Xu Z P, Lu G Q. Layered double hydroxide nanoparticles in gene and drug delivery. Expert Opinion on Drug Delivery, 2009, 6(9): 907–922

[95] Choi S J, Choy J H. Layered double hydroxide nanoparticles as target-specific delivery carriers: uptake mechanism and toxicity. Nanomedicine, 2011, 6(5): 803–814

[96] Choi S J, Oh J M, Choy J H. Biocompatible nanoparticles intercalated with anticancer drug for target delivery: pharmacokinetic and biodistribution study. Journal of Nanoscience and Nanotechnology, 2010, 10(4): 2913–2916

[97] Choy J H, Jung J S, Oh J M, et al. Layered double hydroxide as an efficient drug reservoir for folate derivatives. Biomaterials, 2004, 25(15): 3059–3064

[98] Oh J M, Choi S J, Lee G E, et al. Inorganic metal hydroxide nanoparticles for targeted cellular uptake through clathrin-mediated endocytosis. Chemistry: An Asian Journal, 2009, 4(1): 67–73

[99] Nel A, Xia T, Mädler L, et al. Toxic potential of materials at the nanolevel. Science, 2006, 311(5761): 622–627

[100] Choi S J, Oh J M, Choy J H. Safety aspect of inorganic layered nanoparticles: size-dependency *in vitro* and *in vivo*. Journal of Nanoscience and Nanotechnology, 2008, 8(10): 5297–5301

[101] Oh J M, Biswick T T, Choy J H. Layered nanomaterials for green materials. Journal of Materials Chemistry, 2009, 19(17): 2553–2563

[102] Panyam J, Labhasetwar V. Biodegradable nanoparticles for drug and gene delivery to cells and tissue. Advanced Drug Delivery Reviews, 2003, 55(3): 329–347

[103] Oh J M, Choi S J, Kim S T, et al. Cellular uptake mechanism of an inorganic nanovehicle and its drug conjugates: enhanced efficacy due to clathrin-mediated endocytosis. Bioconjugate Chemistry, 2006, 17(6): 1411–1417

[104] Oh J M, Park M, Kim S T, et al. Efficient delivery of anticancer

drug MTX through MTX-LDH nanohybrid system. Journal of Physics and Chemistry of Solids, 2006, 67(5–6): 1024–1027

[105] Choi S J, Oh J M, Chung H E, et al. *In vivo* anticancer activity of methotrexate-loaded layered double hydroxide nanoparticles. Current Pharmaceutical Design, 2013, 19(41): 7196–7202

[106] Javaid A, Bone M, Stanley C. Effect of fenbufen on the quality of life of patients with pain from squamous-cell carcinoma of the bronchus. In: Proceedings of the Thorax, 1988: 244

[107] Li B, He J, Evans D G, et al. Inorganic layered double hydroxides as a drug delivery system — intercalation and *in vitro* release of fenbufen. Applied Clay Science, 2004, 27(3–4): 199–207

[108] Ambrogi V, Fardella G, Grandolini G, et al. Intercalation compounds of hydrotalcite-like anionic clays with antiinflammatory agents — I. Intercalation and *in vitro* release of ibuprofen. International Journal of Pharmaceutics, 2001(1–2): 23–32

[109] Whilton N T, Vickers P J, Mann S. Bioinorganic clays: synthesis and characterization of amino-andpolyamino acid intercalated layered double hydroxides. Journal of Materials Chemistry, 1997, 7(8): 1623–1629

[110] Xue Y H, Zhang R, Sun X Y, et al. The construction and characterization of layered double hydroxides as delivery vehicles for podophyllotoxins. Journal of Materials Science: Materials in Medicine, 2008, 19(3): 1197–1202

[111] Park D H, Cho J, Kwon O J, et al. Biodegradable inorganic nanovector: passive versus active tumor targeting in siRNA transportation. Angewandte Chemie International Edition in English, 2016, 55(14): 4582–4586

[112] Li L, Qian Y, Sun L, et al. Albumin-stabilized layered double hydroxide nanoparticles synergized combination chemotherapy for colorectal cancer treatment. Nanomedicine: Nanotechnology, Biology, and Medicine, 2021, 34: 102369

[113] Choi G, Jeon I R, Piao H, et al. Highly condensed boron cage cluster anions in 2d carrier and its enhanced antitumor efficiency for boron neutron capture therapy. Advanced Functional Materials, 2018, 28(27): 1704470

[114] Guo Z, Xie W, Lu J, et al. Ferrous ions doped layered double hydroxide: smart 2D nanotheranostic platform with imaging-guided synergistic chemo/photothermal therapy for breast cancer. Biomaterials Science, 2021, 9(17): 5928–5938

[115] Xu T, Liu J, Sun L, et al. Enhancing tumor accumulation and cellular uptake of layered double hydroxide nanoparticles by coating/detaching pH-triggered charge-convertible polymers. ACS Omega, 2021, 6(5): 3822–3830

[116] Baek M, Kim I S, Yu J, et al. Effect of different forms of anionic nanoclays on cytotoxicity. Journal of Nanoscience and Nanotechnology, 2011, 11(2): 1803–1806

[117] Xu Z P, Niebert M, Porazik K, et al. Subcellular compartment targeting of layered double hydroxide nanoparticles. Journal of Controlled Release, 2008, 130(1): 86–94

[118] Hong R, Han G, Fernández J M, et al. Glutathione-mediated delivery and release using monolayer protected nanoparticle carriers. Journal of the American Chemical Society, 2006, 128(4): 1078–1079

[119] Fadel T R, Fahmy T M. Immunotherapy applications of carbon nanotubes: from design to safe applications. Trends in Biotechnology, 2014, 32(4): 198–209

[120] Villa C H, Dao T, Ahearn I, et al. Single-walled carbon nanotubes deliver peptide antigen into dendritic cells and enhance IgG responses to tumor-associated antigens. ACS Nano, 2011, 5(7): 5300–5311

[121] Dyke C A, Stewart M P, Tour J M. Separation of single-walled carbon nanotubes on silica gel. Materials morphology and Raman excitation wavelength affect data interpretation. Journal of the American Chemical Society, 2005, 127(12): 4497–4509

[122] Lee K M, Li L, Dai L. Asymmetric end-functionalization of multi-walled carbon nanotubes. Journal of the American Chemical Society, 2005, 127(12): 4122–4123

[123] Liu Z, Chen K, Davis C, et al. Drug delivery with carbon nanotubes for *in vivo* cancer treatment. Cancer Research, 2008, 68(16): 6652–6660

[124] Sobhani Z, Behnam M A, Emami F, et al. Photothermal therapy of melanoma tumor using multiwalled carbon nanotubes. International Journal of Nanomedicine, 2017, 12: 4509–4517

[125] Sacchetti C, Rapini N, Magrini A, et al. *In vivo* targeting of intratumor regulatory T cells using PEG-modified single-walled carbon nanotubes. Bioconjugate Chemistry, 2013, 24(6): 852–858

[126] Lee J S, Green J J, Love K T, et al. Gold, poly(β-amino ester) nanoparticles for small interfering RNA delivery. Nano Letters, 2009, 9(6): 2402–2406

[127] Li L, Nurunnabi M, Nafiujjaman M, et al. A photosensitizer-conjugated magnetic iron oxide/gold hybrid nanoparticle as an activatable platform for photodynamic cancer therapy. Journal of Materials Chemistry B: Materials for Biology and Medicine, 2014, 2(19): 2929–2937

[128] Cheng Y, Doane T L, Chuang C H, et al. Near infrared light-triggered drug generation and release from gold nanoparticle carriers for photodynamic therapy. Small, 2014, 10(9): 1799–1804

[129] Massich M D, Giljohann D A, Schmucker A L, et al. Cellular response of polyvalent oligonucleotide-gold nanoparticle conjugates. ACS Nano, 2010, 4(10): 5641–5646

[130] Huschka R, Zuloaga J, Knight M W, et al. Light-induced release of DNA from gold nanoparticles: nanoshells and

nanorods. Journal of the American Chemical Society, 2011, 133(31): 12247–12255

[131] Chen C C, Lin Y P, Wang C W, et al. DNA-gold nanorod conjugates for remote control of localized gene expression by near infrared irradiation. Journal of the American Chemical Society, 2006, 128(11): 3709–3715

[132] Dhar S, Gu F X, Langer R, et al. Targeted delivery of cisplatin to prostate cancer cells by aptamer functionalized Pt(IV) prodrug-PLGA-PEG nanoparticles. Proceedings of the National Academy of Sciences of the United States of America, 2008, 105(45): 17356–17361

[133] Dhar S, Liu Z, Thomale J, et al. Targeted single-wall carbon nanotube-mediated Pt(IV) prodrug delivery using folate as a homing device. Journal of the American Chemical Society, 2008, 130(34): 11467–11476

[134] Dhar S, Daniel W L, Giljohann D A, et al. Polyvalent oligonucleotide gold nanoparticle conjugates as delivery vehicles for platinum(IV) warheads. Journal of the American Chemical Society, 2009, 131(41): 14652–14653

[135] Min Y, Mao C, Xu D, et al. Gold nanorods for platinum based prodrug delivery. Chemical Communications, 2010, 46(44): 8424–8426

[136] Ding W, Guo L. Immobilized transferrin Fe_3O_4@SiO_2 nanoparticle with high doxorubicin loading for dual-targeted tumor drug delivery. International Journal of Nanomedicine, 2013, 8: 4631–4639

[137] Kresse M, Wagner S, Pfefferer D, et al. Targeting of ultrasmall superparamagnetic iron oxide (USPIO) particles to tumor cells *in vivo* by using transferrin receptor pathways. Magnetic Resonance in Medicine, 1998, 40(2): 236–242

[138] Yu M K, Jeong Y Y, Park J, et al. Drug-loaded superparamagnetic iron oxide nanoparticles for combined cancer imaging and therapy *in vivo*. Angewandte Chemie International Edition in English, 2008, 47(29): 5362–5365

[139] Som A, Raliya R, Tian L, et al. Monodispersed calcium carbonate nanoparticles modulate local pH and inhibit tumor growth *in vivo*. Nanoscale, 2016, 8(25): 12639–12647

[140] Kamba A S, Ismail M, Ibrahim T A T, et al. A pH-sensitive, biobased calcium carbonate aragonite nanocrystal as a novel anticancer delivery system. BioMed Research International, 2013, 2013: 587451

[141] Hammadi N I, Abba Y, Hezmee M N M, et al. Formulation of a sustained release docetaxel loaded cockle shell-derived calcium carbonate nanoparticles against breast cancer. Pharmaceutical Research, 2017, 34(6): 1193–1203

[142] Peng H, Li K, Wang T, et al. Preparation of hierarchical mesoporous $CaCO_3$ by a facile binary solvent approach as anticancer drug carrier for etoposide. Nanoscale Research Letters, 2013, 8(1): 321

[143] Li J, Yang Y, Huang L. Calcium phosphate nanoparticles with an asymmetric lipid bilayer coating for siRNA delivery to the tumor. Journal of Controlled Release, 2012, 158(1): 108–114

[144] Wu Z, Chen J, Sun Y, et al. Tumor microenvironment-response calcium phosphate hybrid nanoparticles enhanced siRNAs targeting tumors *in vivo*. Journal of Biomedical Nanotechnology, 2018, 14(10): 1816–1825

[145] Dong Y, Liao H, Fu H, et al. pH-sensitive shell–core platform block DNA repair pathway to amplify irreversible DNA damage of triple negative breast cancer. ACS Applied Materials & Interfaces, 2019, 11(42): 38417–38428

[146] Qiu C, Wei W, Sun J, et al. Systemic delivery of siRNA by hyaluronan-functionalized calcium phosphate nanoparticles for tumor-targeted therapy. Nanoscale, 2016, 8(26): 13033–13044

[147] Haque S T, Karim M E, Abidin S A Z, et al. Fe/Mg-modified carbonate apatite with uniform particle size and unique transport protein-related protein corona efficiently delivers doxorubicin into breast cancer cells. Nanomaterials, 2020, 10(5): 834

[148] Hossain S M, Zainal Abidin S A, Chowdhury E H. Krebs cycle intermediate-modified carbonate apatite nanoparticles drastically reduce mouse tumor burden and toxicity by restricting broad tissue distribution of anticancer drugs. Cancers, 2020, 12(1): 161

[149] Mozar F S, Chowdhury E H. PEGylation of carbonate apatite nanoparticles prevents opsonin binding and enhances tumor accumulation of gemcitabine. Journal of Pharmaceutical Sciences, 2018, 107(9): 2497–2508

[150] Hossain S M, Shetty J, Tha K K, et al. α-Ketoglutaric acid-modified carbonate apatite enhances cellular uptake and cytotoxicity of a Raf-kinase inhibitor in breast cancer cells through inhibition of MAPK and PI-3 kinase pathways. Biomedicines, 2019, 7(1): 4

[151] Hossain S M, Chowdhury E H. Citrate- and succinate-modified carbonate apatite nanoparticles with loaded doxorubicin exhibit potent anticancer activity against breast cancer cells. Pharmaceutics, 2018, 10(1): 32

[152] Verma G, Barick K, Shetake N G, et al. Citrate-functionalized hydroxyapatite nanoparticles for pH-responsive drug delivery. RSC Advances, 2016, 6(81): 77968–77976

[153] Rodríguez-Ruiz I, Delgado-López J M, Durán-Olivencia M A, et al. pH-responsive delivery of doxorubicin from citrate-apatite nanocrystals with tailored carbonate content. Langmuir, 2013, 29(26): 8213–8221

[154] Bilensoy E. Cationic nanoparticles for cancer therapy. Expert Opinion on Drug Delivery, 2010, 7(7): 795–809

[155] Slita A, Egorova A, Casals E, et al. Characterization of

modified mesoporous silica nanoparticles as vectors for siRNA delivery. Asian Journal of Pharmaceutical Sciences, 2018, 13(6): 592–599

[156] Zakeri A, Kouhbanani M A J, Beheshtkhoo N, et al. Polyethylenimine-based nanocarriers in co-delivery of drug and gene: a developing horizon. Nano Reviews & Experiments, 2018, 9(1): 1488497

[157] Vaidyanathan S, Chen J, Orr B G, et al. Cationic polymer intercalation into the lipid membrane enables intact polyplex DNA escape from endosomes for gene delivery. Molecular Pharmaceutics, 2016, 13(6): 1967–1978

[158] Benjaminsen R V, Mattebjerg M A, Henriksen J R, et al. The possible "proton sponge" effect of polyethylenimine (PEI) does not include change in lysosomal pH. Molecular Therapy, 2013, 21(1): 149–157

[159] Wang X, Niu D, Hu C, et al. Polyethyleneimine-based nanocarriers for gene delivery. Current Pharmaceutical Design, 2015, 21(42): 6140–6156

[160] Zhang T, Xue X, He D, et al. A prostate cancer-targeted polyarginine-disulfide linked PEI nanocarrier for delivery of microRNA. Cancer Letters, 2015, 365(2): 156–165

[161] Li X, Chen Y, Wang M, et al. A mesoporous silica nanoparticle–PEI–fusogenic peptide system for siRNA delivery in cancer therapy. Biomaterials, 2013, 34(4): 1391–1401

[162] Shen J, Kim H C, Su H, et al. Cyclodextrin and polyethylenimine functionalized mesoporous silica nanoparticles for delivery of siRNA cancer therapeutics. Theranostics, 2014, 4(5): 487–497

[163] Tutuianu R, Popescu L M, Preda M B, et al. Evaluation of the ability of nanostructured PEI-coated iron oxide nanoparticles to incorporate cisplatin during synthesis. Nanomaterials, 2017, 7(10): 314

[164] Liu G, Xie J, Zhang F, et al. N-Alkyl-PEI-functionalized iron oxide nanoclusters for efficient siRNA delivery. Small, 2011, 7(19): 2742–2749

[165] Zhang L, Wang T, Li L, et al. Multifunctional fluorescent-magnetic polyethyleneimine functionalized Fe_3O_4–mesoporous silica yolk–shell nanocapsules for siRNA delivery. Chemical Communications, 2012, 48(69): 8706–8708

[166] Siu K S, Chen D, Zheng X, et al. Non-covalently functionalized single-walled carbon nanotube for topical siRNA delivery into melanoma. Biomaterials, 2014, 35(10): 3435–3442

[167] Wu H, Shi H, Zhang H, et al. Prostate stem cell antigen antibody-conjugated multiwalled carbon nanotubes for targeted ultrasound imaging and drug delivery. Biomaterials, 2014, 35(20): 5369–5380

[168] Lee Y, Lee S H, Kim J S, et al. Controlled synthesis of PEI-coated gold nanoparticles using reductive catechol chemistry for siRNA delivery. Journal of Controlled Release, 2011, 155(1): 3–10

[169] Cebrián V, Martín-Saavedra F, Yagüe C, et al. Size-dependent transfection efficiency of PEI-coated gold nanoparticles. Acta Biomaterialia, 2011, 7(10): 3645–3655

[170] Zhang L, Lu Z, Zhao Q, et al. Enhanced chemotherapy efficacy by sequential delivery of siRNA and anticancer drugs using PEI-grafted graphene oxide. Small, 2011, 7(4): 460–464

[171] Sheng J, Han L, Qin J, et al. N-trimethyl chitosan chloride-coated PLGA nanoparticles overcoming multiple barriers to oral insulin absorption. ACS Applied Materials & Interfaces, 2015, 7(28): 15430–15441

[172] Şenel S, McClure S J. Potential applications of chitosan in veterinary medicine. Advanced Drug Delivery Reviews, 2004, 56(10): 1467–1480

[173] Kean T, Thanou M. Biodegradation, biodistribution and toxicity of chitosan. Advanced Drug Delivery Reviews, 2010, 62(1): 3–11

[174] Lin J, Li Y, Li Y, et al. Drug/dye-loaded, multifunctional PEG–chitosan–iron oxide nanocomposites for methotraxate synergistically self-targeted cancer therapy and dual model imaging. ACS Applied Materials & Interfaces, 2015, 7(22): 11908–11920

[175] Mao S, Sun W, Kissel T. Chitosan-based formulations for delivery of DNA and siRNA. Advanced Drug Delivery Reviews, 2010, 62(1): 12–27

[176] Gurka M K, Pender D, Chuong P, et al. Identification of pancreatic tumors *in vivo* with ligand-targeted, pH responsive mesoporous silica nanoparticles by multispectral optoacoustic tomography. Journal of Controlled Release, 2016, 231: 60–67

[177] Murugan C, Rayappan K, Thangam R, et al. Combinatorial nanocarrier based drug delivery approach for amalgamation of anti-tumor agents in breast cancer cells: an improved nanomedicine strategy. Scientific Reports, 2016, 6: 34053

[178] Liao T, Liu C, Ren J, et al. A chitosan/mesoporous silica nanoparticle-based anticancer drug delivery system with a "tumor-triggered targeting" property. International Journal of Biological Macromolecules, 2021, 183: 2017–2029

[179] Yan Q, Chen X, Gong H, et al. Delivery of a TNF-α-derived peptide by nanoparticles enhances its antitumor activity by inducing cell-cycle arrest and caspase-dependent apoptosis. FASEB Journal, 2018, 32(12): 6948–6964

[180] Jayasree A, Sasidharan S, Koyakutty M, et al. Mannosylated chitosan-zinc sulphide nanocrystals as fluorescent bioprobes for targeted cancer imaging. Carbohydrate Polymers, 2011, 85(1): 37–43

[181] Manivasagan P, Nguyen V T, Jun S W, et al. Anti-EGFR antibody conjugated thiol chitosan-layered gold nanoshells for

dual-modal imaging-guided cancer combination therapy. Journal of Controlled Release, 2019, 311–312: 26–42

[182] Li P, Yan Y, Zhang H, et al. Treatment of cervical cancer by siRNA-loaded chitosan-coated calcium phosphate nanoparticles. Journal of Chinese Pharmaceutical Sciences, 2018, 27(8): 517–529

[183] Roy K, Kanwar R K, Kanwar J R. LNA aptamer based multimodal, Fe_3O_4-saturated lactoferrin (Fe_3O_4-bLf) nanocarriers for triple positive (EpCAM, CD133, CD44) colon tumor targeting and NIR, MRI and CT imaging. Biomaterials, 2015, 71: 84–99

[184] Lonez C, Vandenbranden M, Ruysschaert J M. Cationic liposomal lipids: from gene carriers to cell signaling. Progress in Lipid Research, 2008, 47(5): 340–347

[185] Caplen N J. Nucleic acid transfer using cationic lipids. Methods in Molecular Biology, 2000, 133: 1–19

[186] Zhu N, Liggitt D, Liu Y, et al. Systemic gene expression after intravenous DNA delivery into adult mice. Science, 1993, 261(5118): 209–211

[187] Lindner L H, Brock R, Arndt-Jovin D, et al. Structural variation of cationic lipids: minimum requirement for improved oligonucleotide delivery into cells. Journal of Controlled Release, 2006, 110(2): 444–456

[188] Pillai G, Cox A, Yuen L. The science and technology of cancer theranostic nanomedicines: a primer for clinicians and pharmacists. SOJ Pharmacy and Pharmaceutical Sciences, 2018, 5(2): 1–7

[189] Mudshinge S R, Deore A B, Patil S, et al. Nanoparticles: emerging carriers for drug delivery. Saudi Pharmaceutical Journal, 2011, 19(3): 129–141

[190] Al-Jamal W T, Al-Jamal K T, Tian B, et al. Lipid-quantum dot bilayer vesicles enhance tumor cell uptake and retention *in vitro* and *in vivo*. ACS Nano, 2008, 2(3): 408–418

[191] Leung S J, Romanowski M. Light-activated content release from liposomes. Theranostics, 2012, 2(10): 1020–1036

[192] Torchilin V P. Recent advances with liposomes as pharmaceutical carriers. Nature Reviews. Drug Discovery, 2005, 4(2): 145–160

[193] Nie Y, Ji L, Ding H, et al. Cholesterol derivatives based charged liposomes for doxorubicin delivery: preparation, *in vitro* and *in vivo* characterization. Theranostics, 2012, 2(11): 1092–1103

[194] Sørensen D R, Leirdal M, Sioud M. Gene silencing by systemic delivery of synthetic siRNAs in adult mice. Journal of Molecular Biology, 2003, 327(4): 761–766

[195] Zhang S, Zhao B, Jiang H, et al. Cationic lipids and polymers mediated vectors for delivery of siRNA. Journal of Controlled Release, 2007, 123(1): 1–10

[196] Tao W, Mao X, Davide J P, et al. Mechanistically probing lipid-siRNA nanoparticle-associated toxicities identifies Jak inhibitors effective in mitigating multifaceted toxic responses. Molecular Therapy, 2011, 19(3): 567–575

[197] Yang Y, Li J, Liu F, et al. Systemic delivery of siRNA via LCP nanoparticle efficiently inhibits lung metastasis. Molecular Therapy, 2012, 20(3): 609–615

[198] Reinhardt N, Adumeau L, Lambert O, et al. Quaternary ammonium groups exposed at the surface of silica nanoparticles suitable for DNA complexation in the presence of cationic lipids. The Journal of Physical Chemistry B, 2015, 119(21): 6401–6411

[199] Al-Jamal W T, Al-Jamal K T, Cakebread A, et al. Blood circulation and tissue biodistribution of lipid-quantum dot (L-QD) hybrid vesicles intravenously administered in mice. Bioconjugate Chemistry, 2009, 20(9): 1696–1702

[200] Al-Jamal W T, Al-Jamal K T, Tian B, et al. Lipid-quantum dot bilayer vesicles enhance tumor cell uptake and retention *in vitro* and *in vivo*. ACS Nano, 2008, 2(3): 408–418

[201] Al-Jamal W T, Al-Jamal K T, Bomans P H, et al. Functionalized-quantum-dot-liposome hybrids as multimodal nanoparticles for cancer. Small, 2008, 4(9): 1406–1415

[202] Wang F, Chen Z, Zhu L. cRGD-conjugated magnetic-fluorescent liposomes for targeted dual-modality imaging of bone metastasis from prostate cancer. Journal of Liposome Research, 2015, 25(2): 89–100

[203] Mattingly S J, O'Toole M G, James K T, et al. Magnetic nanoparticle-supported lipid bilayers for drug delivery. Langmuir, 2015, 31(11): 3326–3332

[204] Kong W H, Bae K H, Jo S D, et al. Cationic lipid-coated gold nanoparticles as efficient and non-cytotoxic intracellular siRNA delivery vehicles. Pharmaceutical Research, 2012, 29(2): 362–374

[205] Chakraborty A, Boer J C, Selomulya C, et al. Amino acid functionalized inorganic nanoparticles as cutting-edge therapeutic and diagnostic agents. Bioconjugate Chemistry, 2018, 29(3): 657–671

[206] Biswas S, Medina S H, Barchi J J Jr. Synthesis and cell-selective antitumor properties of amino acid conjugated tumor-associated carbohydrate antigen-coated gold nanoparticles. Carbohydrate Research, 2015, 405: 93–101

[207] Shi J, Sun X, Zou X, et al. Amino acid-dependent transformations of citrate-coated silver nanoparticles: impact on morphology, stability and toxicity. Toxicology Letters, 2014, 229(1): 17–24

[208] Zhu X, Xie Y, Zhang Y, et al. Thermo-sensitive liposomes loaded with doxorubicin and lysine modified single-walled carbon nanotubes as tumor-targeting drug delivery system. Journal of Biomaterials Applications, 2014, 29(5): 769–779

[209] Feng Y, Su J, Zhao Z, et al. Differential effects of amino acid surface decoration on the anticancer efficacy of selenium nanoparticles. Dalton Transactions, 2014, 43(4): 1854–1861

[210] Yang H M, Lee H J, Park C W, et al. Endosome-escapable magnetic poly(amino acid) nanoparticles for cancer diagnosis and therapy. Chemical Communications, 2011, 47(18): 5322–5324

[211] Agemy L, Friedmann-Morvinski D, Kotamraju V R, et al. Targeted nanoparticle enhanced proapoptotic peptide as potential therapy for glioblastoma. Proceedings of the National Academy of Sciences of the United States of America, 2011, 108(42): 17450–17455

[212] Shen Z, Liu T, Yang Z, et al. Small-sized gadolinium oxide based nanoparticles for high-efficiency theranostics of orthotopic glioblastoma. Biomaterials, 2020, 235: 119783

[213] Taratula O, Garbuzenko O B, Chen A M, et al. Innovative strategy for treatment of lung cancer: targeted nanotechnology-based inhalation co-delivery of anticancer drugs and siRNA. Journal of Drug Targeting, 2011, 19(10): 900–914

[214] Fei W, Zhang Y, Han S, et al. RGD conjugated liposome-hollow silica hybrid nanovehicles for targeted and controlled delivery of arsenic trioxide against hepatic carcinoma. International Journal of Pharmaceutics, 2017, 519(1–2): 250–262

[215] Luo G F, Chen W H, Liu Y, et al. Multifunctional enveloped mesoporous silica nanoparticles for subcellular co-delivery of drug and therapeutic peptide. Scientific Reports, 2014, 4: 6064

[216] Yang X Z, Du J Z, Dou S, et al. Sheddable ternary nanoparticles for tumor acidity-targeted siRNA delivery. ACS Nano, 2012, 6(1): 771–781

[217] Jin K T, Lu Z B, Chen J Y, et al. Recent trends in nanocarrier-based targeted chemotherapy: selective delivery of anticancer drugs for effective lung, colon, cervical, and breast cancer treatment. Journal of Nanomaterials, 2020, 2020: 9184284

[218] Liu Y, Pan Y, Cao W, et al. A tumor microenvironment responsive biodegradable $CaCO_3$/MnO_2-based nanoplatform for the enhanced photodynamic therapy and improved PD-L1 immunotherapy. Theranostics, 2019, 9(23): 6867–6884

[219] Meng H, Xue M, Xia T, et al. Use of size and a copolymer design feature to improve the biodistribution and the enhanced permeability and retention effect of doxorubicin-loaded mesoporous silica nanoparticles in a murine xenograft tumor model. ACS Nano, 2011, 5(5): 4131–4144

[220] Lu J, Liong M, Li Z, et al. Biocompatibility, biodistribution, and drug-delivery efficiency of mesoporous silica nanoparticles for cancer therapy in animals. Small, 2010, 6(16): 1794–1805

[221] Chen T, Zhao T, Wei D, et al. Core–shell nanocarriers with ZnO quantum dots-conjugated Au nanoparticle for tumor-targeted drug delivery. Carbohydrate Polymers, 2013, 92(2): 1124–1132

[222] Sharma H, Kumar K, Choudhary C, et al. Development and characterization of metal oxide nanoparticles for the delivery of anticancer drug. Artificial Cells, Nanomedicine, and Biotechnology, 2016, 44(2): 672–679

[223] Senapati S, Thakur R, Verma S P, et al. Layered double hydroxides as effective carrier for anticancer drugs and tailoring of release rate through interlayer anions. Journal of Controlled Release, 2016, 224: 186–198

[224] Chakraborty J, Roychowdhury S, Sengupta S, et al. Mg–Al layered double hydroxide-methotrexate nanohybrid drug delivery system: evaluation of efficacy. Materials Science and Engineering C, 2013, 33(4): 2168–2174

[225] Kuo Y M, Kuthati Y, Kankala R K, et al. Layered double hydroxide nanoparticles to enhance organ-specific targeting and the anti-proliferative effect of cisplatin. Journal of Materials Chemistry B: Materials for Biology and Medicine, 2015, 3(17): 3447–3458

[226] Asiabi H, Yamini Y, Alipour M, et al. Synthesis and characterization of a novel biocompatible pseudo-hexagonal NaCa-layered double metal hydroxides for smart pH-responsive drug release of dacarbazine and enhanced anticancer activity in malignant melanoma. Materials Science and Engineering C, 2019, 97: 96–102

[227] Ray S, Joy M, Sa B, et al. pH dependent chemical stability and release of methotrexate from a novel nanoceramic carrier. RSC Advances, 2015, 5(49): 39482–39494

[228] Ray S, Mishra A, Mandal T K, et al. Optimization of the process parameters for the fabrication of a polymer coated layered double hydroxide-methotrexate nanohybrid for the possible treatment of osteosarcoma. RSC Advances, 2015, 5(124): 102574–102592

[229] Wen J, Lv Y, Xu Y, et al. Construction of a biodegradable, versatile nanocarrier for optional combination cancer therapy. Acta Biomaterialia, 2019, 83: 359–371

[230] Pi J, Jiang J, Cai H, et al. GE11 peptide conjugated selenium nanoparticles for EGFR targeted oridonin delivery to achieve enhanced anticancer efficacy by inhibiting EGFR-mediated PI3K/AKT and Ras/Raf/MEK/ERK pathways. Drug Delivery, 2017, 24(1): 1549–1564

[231] Alibolandi M, Abnous K, Sadeghi F, et al. Folate receptor-targeted multimodal polymersomes for delivery of quantum dots and doxorubicin to breast adenocarcinoma: *in vitro* and *in vivo* evaluation. International Journal of Pharmaceutics, 2016, 500(1–2): 162–178

[232] Xu C, Wang B, Sun S. Dumbbell-like Au-Fe_3O_4 nanoparticles

for target-specific platin delivery. Journal of the American Chemical Society, 2009, 131(12): 4216–4217

[233] Wang F, Wang Y C, Dou S, et al. Doxorubicin-tethered responsive gold nanoparticles facilitate intracellular drug delivery for overcoming multidrug resistance in cancer cells. ACS Nano, 2011, 5(5): 3679–3692

[234] Haynes B, Zhang Y, Liu F, et al. Gold nanoparticle conjugated Rad6 inhibitor induces cell death in triple negative breast cancer cells by inducing mitochondrial dysfunction and PARP-1 hyperactivation: synthesis and characterization. Nanomedicine: Nanotechnology, Biology, and Medicine, 2016, 12(3): 745–757

[235] Zhou Z, Kennell C, Lee J Y, et al. Calcium phosphate-polymer hybrid nanoparticles for enhanced triple negative breast cancer treatment via co-delivery of paclitaxel and miR-221/222 inhibitors. Nanomedicine: Nanotechnology, Biology, and Medicine, 2017, 13(2): 403–410

[236] Cheng Y, Samia A C, Meyers J D, et al. Highly efficient drug delivery with gold nanoparticle vectors for *in vivo* photodynamic therapy of cancer. Journal of the American Chemical Society, 2008, 130(32): 10643–10647

[237] Zelphati O, Uyechi L S, Barron L G, et al. Effect of serum components on the physico-chemical properties of cationic lipid/oligonucleotide complexes and on their interactions with cells. Biochimica et Biophysica Acta, 1998, 1390(2): 119–133

[238] Passirani C, Benoit J P. Complement activation by injectable colloidal drug carriers. In: Mahato R I, ed. Biomaterials for Delivery and Targeting of Proteins and Nucleic Acids. Boca Raton, FL, USA: CRC Press, 2005

[239] Brigger I, Dubernet C, Couvreur P. Nanoparticles in cancer therapy and diagnosis. Advanced Drug Delivery Reviews, 2002, 54(5): 631–651